Deliverable D1 - Technical Report NF-PERSEUS 2023

Charbel Abdel Nour, Cédric Adjih, Karine Amis, Xavier Begaud, Matthieu Crussière, Antoine Durant, Marco Di Renzo, Catherine Douillard, Hajar El Hassani, Joumana Farah, et al.

RÉPUBLIQUE FRANÇAISE
Liberté
Égalité
Fraternité

anr agence nationale de la recherche

FRANCE 2030 PROGRAMME DE RECHERCHE RÉSEAUX DU FUTUR

Grant agreement ANR-22-PEFT-0004

Deliverable D1
Technical Report NF-PERSEUS 2023
Power-Efficient Radio interface for Sub-7GHz distributEd massive MIMO infrastrUctureS

Période du 01/05/2023 au 31/12/2023

Delivery date	30/04/2024
Version	1
Authors (listed in alphabetical order)	Charbel Abdel Nour (IMT Atlantique), Cédric Adjih (INRIA), Karine Amis (IMT Atlantique), Xavier Bégaud (Télécom Paris), Matthieu Crussière (IETR), Antoine Durant (CEA), Marco di Renzo (L2S), Catherine Douillard (IMT Atlantique), Hajar El Hassan (ETIS), Joumana Farah (IETR), Inbar Fijalkow (ETIS), Davy Gaillot (IETR), Jean-Marie Gorce (INRIA), Claire Goursaud (INSA Lyon), Maxime Guillaud (INRIA), Didier Le Ruyet (CNAM), Asma Mabrouk (CEA), Pascal Pagani (CEA), Germain Dang-Kien Pham (Télécom Paris), Balakrishna Prabhu (LAAS), Ghaya Rekaya (Télécom Paris), Eric Simon (IEMN), Rafik Zayani (CEA).
Dissemination	Public
Keywords	Cell-free networks, massive MIMO, use cases, reconfigurable intelligent surfaces, hardware impairments, waveform, non-orthogonal multiple access, resource allocation, grant-free access, quantum detection, interference management.

Executive summary

This is deliverable D1 "Technical Report NF-PERSEUS 2023". This document provides an overview of the progress of the studies undertaken in NF-PERSEUS project and their progress by the end of 2023.

Chapter 1 delves into the advantages of cell-free architectures and their pivotal role in shaping the future of 6G wireless networks. Cell-free architectures, which move away from the traditional cellular network model, offer several compelling benefits that make them a promising solution for the next generation of mobile communication.

Chapter 2 describes the main use cases identified for the NF-PERSEUS project and their KPI, providing an inventory of use case specifications, representative deployment scenarios and technical requirements. It presents also the MAMIMOSA sounder which will be employed to perform massive MIMO channel measurments for the considered NF-PERSEUS scenarios.

Chapter 3 examines and discusses relevant reference scenarios based on RIS. This analysis sheds light on the technical challenges involved and the potential performance that can be achieved.

Chapter 4 provides an in-depth analysis of the performance metrics used to evaluate cell-free network architectures. It presents the studies and research activities undertaken within Work Package 3 (WP3) and summarizes the progress made by the end of 2023. It presents some potential PHY layer solutions studied in the framework of NF-PERSEUS project. These solutions comprise advanced precoding/combing schemes and multi-carrier waveforms which are adequate for cell-free architectures.

Chapter 5 provides an overview of the progress of the studies undertaken in WP4 and their progress by the end of 2023. WP4 deals with radio resource management and aims at introducing novel multi-user access schemes and resource allocation algorithms dedicated to distributed antenna systems, with an emphasis on achieving power and spectrum efficient massive access in scalable B5G sub-7GHz networks.

Chapter 6 presents an overview of electromagnetically consistent communication models for Reconfigurable Intelligent Surfaces (RISs). These models aim to describe the communication mechanisms and performance characteristics of RISs, which are emerging technologies that can dynamically control the propagation of electromagnetic waves. The chapter then goes on to showcase preliminary results obtained based on a communication model for RISs that is grounded in multiport network theory. Multiport network theory provides a framework for analyzing the electromagnetic behavior of complex systems, which is particularly relevant for understanding the operation and capabilities of RISs.

Chapter 7 summarizes the studies undertaken in WP2 related to Radio-Frequency Front-End Modules, Reconfigurable antennas and RIS aspects of the project NF-PERSEUS. Specifically, it provides details about the design and manufacturing of Hybrid PA architecture, design and manufacturing of highly efficient miniature and reconfigurable antennas using in particular agile metamaterials and/or biosourced technologies.

Chapter 8 gives the conclusion.

Table of content

Chapter 1 : Introduction

The advent of 6G wireless technology is expected to provide notably augmented data rates and traffic capacities in comparison to its predecessors, accompanied by a significant reduction in data connection latency. Nevertheless, these advancements are mainly achieved for User Equipment (UEs) situated in proximity to the cell centres. Besides, the persistent issues of inter-cell interference and handover problems, inherent to the cellular framework, continue to impose limitations on performance at the cell peripheries. Therefore, large variations of data rates are witnessed throughout the cells, with high peaks at cell centres and a low Quality-Of-Service (QoS) at cell-edges. To alleviate these issues, beyond 5G networks necessitate a transition towards a cell-free paradigm, wherein the absence of cellular boundaries can efficiently mitigate the inter-cell interference and handover issues, albeit introducing several new challenges.
The alternative structure of cell-free massive multiple input multiple output (CF-mMIMO) [21, 57] consists in distributing an important number of access points (APs) over the deployment area. These APs cooperate to serve UEs optimally, by exploiting the massive macro-diversity gain. Each of these densely deployed APs is equipped with a small number of antennas and is generally connected to a central processing unit (CPU) via fronthaul links constituted by high-capacity coaxial cables, fiber optics or wireless links. By doing so, the average distance between each UE and its serving APs is reduced compared to the classical cellular configurations and shadow fading is also combatted by the spatial diversity.
In the following we cite some of the particularities, challenges, and open issues in CF-mMIMO as identified in the recent litterature and studied in the NF-PERSEUS project.

Channel estimation and pilot assignment

Using Time Division Duplexing (TDD), channel estimation (CE) is performed in uplink [14], where APs can compute local channel estimates using pilots transmitted by the UEs. Regardless of the choice of the CE method, pilot contamination appears in CF-mMIMO, just as in any large-scale communication system, due to pilot reuse. However, it tends to be a lesser concern when compared to the context of cellular massive MIMO, especially when each AP is equipped with a limited number of antennas and serves only a moderate number of UEs.
Nonetheless, the precision of CE in CF-mMIMO has a direct impact on inter-user interference, a factor that gains increasing prominence as the network attains higher levels of density. Pilot contamination both reduces the CE quality, which hinders coherent transmission, and makes it harder to reject interference between pilot-sharing UEs. To limit these negative effects, proper pilot assignment techniques [19, 142] need to be implemented, particularly in a massive access scenario where the number of UEs is close to that of APs. This last challenge is of great concern as it poses heavy constraints on the scalability of CF-mMIMO systems.

AP selection

Two distinct transmission scenarios are used in CF-mMIMO [26]. In the first one, all the APs across the network collaboratively serve each UE; this scenario is referred to as the 'ALL' framework. However, it is both impractical and energy-inefficient in expansive geographical areas, where each UE maintains physical proximity to only a subset of APs.

Consequently, a more commonly employed framework, known as Dynamic Cooperation Clustering (DCC), is preferred. Under DCC, each UE is exclusively served by a pre-selected set of APs, thus necessitating the division of APs into partially overlapping subsets when serving the UEs. AP clustering schemes were studied in [19,26] based on large-scale channel parameters. However, it remains essential to adapt such selection schemes to high mobility scenarios such as in Vehicle-to-Infrastructure (V2I) communications.

Centralized and distributed deployment scenarios

Centralized and distributed architectures have been explored in the context of CF-mMIMO [26]. In uplink, when using the centralized approach, the pilot and data signals received at all serving APs are gathered through the fronthaul links at the CPU, which performs channel estimation and data detection. Therefore, optimal (but unscalable) or suboptimal scalable centralized receive combining methods can be applied at the CPU. In this scenario, APs only act as remote-radio heads or relays.
In the uplink distributed operation, local estimates of the UE channel response and data are computed at the APs. They are then gathered and combined at the CPU which computes a weighted average of the local estimates and then proceeds to the final detection. The distributed operation requires that APs be equipped with powerful processors but enables an ultra-dense deployment of APs. Therefore, the CPU capabilities become dimensioned based on the number of UEs, but largely unaffected by the number of APs. This brings the possibility to add new APs to the network without having to upgrade the CPUs. Two additional advantages of the distributed scenario are the drastic reduction in fronthaul signalling compared to the centralized operation and the avoidance of the fronthaul quantization distortion (inevitable in the transmission of signalling information).
Considering downlink, with the centralized operation, the CPU selects the precoding vectors and computes the signals to be transmitted, while the APs only take in charge the physical transmission. This scenario enables centralized precoding where the signals transmitted from multiple APs can be coherently received at desired UEs while also suppressing the undesired UEs signals.
In the distributed operation of downlink, each AP receives the data from the CPU and designs the locally transmitted signal using local precoding based on the locally available channel estimates. The signals transmitted from the serving APs are coherently received at the desired UE, but the interference suppression capability is reduced compared to the centralized operation since each AP can only suppress the interference that itself is generating. This is a limiting factor since APs are envisioned to have only few antennas.
As a result, in both uplink and downlink, centralized operation can achieve substantially higher spectral efficiency (SE) than the distributed operation. However, it poses many implementation challenges, as already mentioned. This is an open issue that deserves a deep analysis.

Power allocation/control

In addition to signal detection (in uplink) and precoding (in downlink), power allocation (or control in uplink) needs to be properly designed. Some previous works [17,26] have introduced optimization techniques that aim to maximize a network-wide utility function, typically SE, energy efficiency (EE) or max-min fairness. While allowing to reach quasi-optimal solutions, such strategies necessitate heavy computations that hinder their applicability in low-latency contexts. Therefore, heuristic power allocation (PA) techniques [26, 60] were proposed in this context, such as fractional power control. Such methods rely on pre-defined precoding schemes like maximal ratio (MR), zero-forcing (ZF) or minimum mean-squared error (MMSE). However, while being scalable, they provide solutions that are far from the optimal. Given the importance of optimizing the energy usage of networks and maximizing the terminals battery life, further investigations are essential in this prospect.

Provisioning of backhaul links

As the density of APs distributed across the coverage area grows, it becomes evident that the burden on the backhaul (connecting APs to the core network) of the cell-free system will quickly surpass that of conventional cellular

networks. Employing wired solutions like optical fiber can prove to be cost-prohibitive in wide areas. The wireless solution, while being more viable, introduces its own set of challenges [143], encompassing issues like spectrum availability and the reliability of delivering high data rates over wireless links.
In order to pave the way for realistic implementations of cell-free networks, innovative strategies for backhaul provisioning are needed, that can be inspired from the methods used in Cloud Radio Access Network (C-RAN). A possible solution [143] to tackle the problem entails conducting research to minimize backhaul requirements by decentralizing processing as much as possible and employing heavy signal quantization for data transmitted over the backhaul.
Inband backhauling [130] can also constitute an alternative solution, where data transmission over the backhaul links occurs within the same spectral bands as those utilized for the access links (connecting APs to users). The objective behind this reuse is to optimize the overall system SE, provided that the interference generated is properly managed by well-designed resource and power allocation techniques.

Reconfigurable Intelligent Surfaces in cell-free

Despite the considerable gains in SE offered by massive MIMO in general and more particularly by CF-mMIMO, concerns exist regarding the implementation costs and EE of multi-antenna systems [143]. Indeed, it has been demonstrated that significantly increasing the number of antennas is not the best solution to enhance the EE of future networks. This is due to the fact that the total energy consumption rises linearly with the number of RF chains needed by the active components, while data rates exhibit logarithmic growth. One potential approach to reach a spectrally and energy-efficient system while keeping hardware costs to a minimum is by embracing the concept of passive MIMO, specifically in the form of reconfigurable intelligent surfaces (RIS). The latter are composed of numerous small elements that can reflect incoming signals in a controllable manner. In contrast to CF-mMIMO and cooperative relays, which rely on active hardware components to enhance signal propagation conditions, RISs are believed to require only minimal operational power.
In fact, the purpose of the RIS technology is not to supplant or compete with traditional massive MIMO or CF-mMIMO but to complement it. It can be deployed in a flexible manner to address coverage gaps or to enhance capacity in areas where it is required.
One of the main challenges in this context is the joint optimization of the transmit beamforming vectors and RIS parameters [55, 76] that needs to be performed in a way to maximize the network metric by solving a non-convex optimization problem. Obtaining globally optimal solutions entails a high computational complexity, even for systems of moderate size. Several other open issues that need to be studied in RIS-empowered systems include channel estimation, transmission of RIS control information, optimal RIS deployment positions, to name a few.

Chapter 2 : Use cases of NF-PERSEUS

2.1 Introduction

This chapter describes the main use-cases identified for the NF-PERSEUS project and their respective KPIs. The technical requirements and the deployment scenarios are described reporting the main deployment opportunities for cell-free networks and the use-cases identified. It presents also the MAMIMOSA sounder which will be employed to perform massive MIMO channel measurments for the considered NF-PERSEUS scenarios.

2.2 Tbps experienced data rates for ultra-dense areas [S1]

2.2.1 Description and technical requirements

Table 2.2.1 illustrates the description of the first use case and its technical requirements and challenges.

2.2.2 Measurement scenario(s)

This measurement campaign will be carried out on the Cité Scientifique campus in Villeneuve d'Ascq, in an area measuring $160m \times 280m$, as shown in Figure 2.1. We plan to carry out this campaign in June 2024, depending on weather conditions. We plan to take $L = 20$ different positions for the Tx, and $K = 40$ different positions for the Rx, which will correspond to a cell-free network with 20 access points (APs) and 40 users. User positions will be measured both indoors and outdoors, to match a real cell-free network use case. We plan to take 15 measurement points in the P3 building, spread over two different floors, 3 in P4 on the ground floor, 3 in P7 on the ground floor, and the rest outdoors. The Rx positions will be distributed over the area to be covered. By way of illustration, we have placed 10 possible Tx positions on the figure.

2.2.3 Technical setup and radio configuration

The measurements will be performed using the maMIMOSA (massive Multiple Input Multiple Output Sounder Architecture) channel sounder, the technical specifications of which can be found in Chapter 6. To summarize, the channel sounder operates at a frequency of 5.89 GHz with a bandwidth of 80 MHz. The data are modulated using orthogonal frequency-division multiplexing (OFDM) with 8192 subcarriers and a subcarrier spacing of 12.21 kHz prior to transmission. A pilot transmission scheme is employed at the Tx antennas to achieve a frequency spacing of 97.66 kHz between consecutive measured subcarriers on a single antenna. The Tx is equipped with a linear array of 8 vertically polarized patch antennas. The Rx will be equipped with two linear arrays of 4 omnidirectional antennas each, placed at either end of the carriage and separated by 1.5m. In this way, one recording will correspond to two different users situated 1.5m apart. This enables us to double the number of user positions. The measurement frame corresponds to 100 consecutive OFDM symbols. This will enable us to obtain the large-scale parameters by averaging over these 100 symbols.

The following table summarizes the parameters:

General description	In order to expand network capacity and align with exponentially growing traffic demand, we consider a wide deployment of access points (APs) at a cell-free network. It will result in high network densification in dense urban area (e.g. campus, airports, stadiums, ...), where inter-AP distances could be less than 100 meters.	
Scenario	High data rates for dense population areas (crowded outdoor area (square), ...)	
	Environment Coverage range Service	Outdoor/Indoor 500 m^2/ 1 km^2 Video streaming, Extended/Augmented reality, video downloading, social networking, ...
	Mobility Link visibility	Static LoS/NLoS
	Frequency band Bandwidth Tx power TDD	5,89 GHz TDD Up to 80 MHz 20-30 dBm both UL and DL
	Waveform	OFDM or post-OFDM, ICS 12.2 kHz (u=0), FFTsize = 1024, 818 active subcarriers, 103 subcarriers as GuardBand at each side
Technical challenges	- Massive number of simultaneous connections and high traffic volume - Deployment in wide open area	

Table 2.1: Use case 1. Description and technical requirements

Number of APs	20
Number of antennas per AP	8
Number of user positions	80
Number of antennas per user	4
bandwidth	80 MHz
Central frequency	5.89 GHz
Doppler	No Doppler measured

Table 2.2: Campus scenario parameters

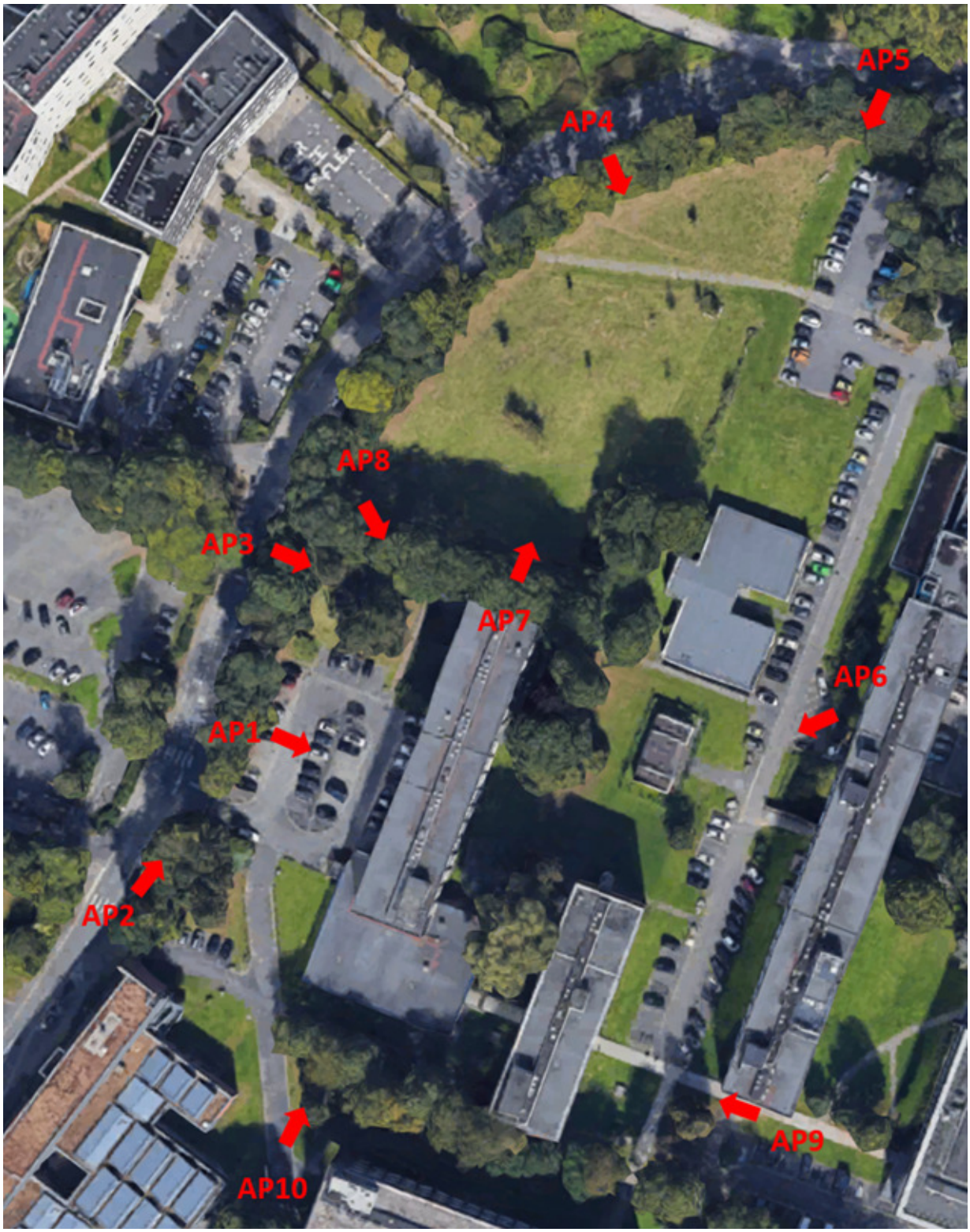

Figure 2.1: Cité Scientifique campus in Villeneuve d'Ascq.

2.3 Smart factory [S2]

2.3.1 Description and technical requirements

Table 2.3.1 illustrates the description of the second use case and its technical requirements and challenges.

General description	Digital Twins have been shown to significantly impact the transformation of industries, such as factories' automation. In this use case, we focus on monitoring and control of digital twins related real-time processes bu using the CF-mMIMO technology. This latter can ensure the bidirectional communication between the digital and physical twins, as well as to send control signals. Through this use case, we will show the capability of CF-mMIMO technology to provide extremely high reliability and low latency for for a large massive number of devices, with an emphasis on enhancing the energy efficiency.	
Scenario	Robotized factories, warehouses and logistics	
	Environment	Outdoor/Indoor
	Coverage range	60 000 m^2/ 10 000 m^2
	Service Mobility Link visibility	Control, monitoring, digital twin Static LoS/NLoS
	Frequency band Bandwidth Tx power TDD	2.4 or 3.8 GHz TDD Up to 20 MHz 20-30 dBm both UL and DL
	Waveform	OFDM or post-OFDM, OFDM 5GNR, Fs=61.44MHz, ICS 15/30KHz (u=0,1)
Technical challenges	- Extremely high reliability and low latency - Massive number of simultaneous devices - High accuracy synchronization in case of sporadic traffic - High energy-efficiency (sensors under batteries)	

Table 2.3: Use case 2 description and technical requirements

2.3.2 Deployment scenario(s)

Deployment characteristic(s)

In this scenario, we will study the performance of a communication system for a small factory environment. Typically, a small factory or, equivalently, a workshop or storage area, consists of an indoor environment located in a fairly large building (of the order of 20,000 to 160,000 m²). Such an area can be arranged with ceiling of different heights (up to 25 m), and can be organised with a highly variable density of furniture or partitions. Depending on the height and density of the machinery and furniture, different types of clutter can arise, with different clutter sizes, typically from 2 m to 10 m.

Strong shadowing and a high probability of LOS obstruction is expected in the Small Factory Environment. Regarding the channel multipath structure, the large number of possible scatterers are expected to yield large delay and angular spreads.

Deploying a dense cell-free topology has several benefits, among which the enhancement of radio conditions and link availability due to the increased LOS coverage. The reliability should also be significantly increased by the useful combination of various radio links. For positioning purposes, a dense radio infrastructure can also be very helpful.

Regarding channel modelling, the large size of this indoor environment along with the nature of the surrounding material (flat metallic and/or plastic or wooden structures) will probably make it possible to model the channel using empirical propagation models and simplified ray tracing/launching type of modelling.

Environment description(s)

For the PERSEUS project, the Small Factory environment was not intended as a priority scenario regarding experimental investigations, and therefore no dedicated channel sounding campaign is planned within the course of the project. The project will nonetheless benefit from experimental data, through collaboration with an external partner who will complementarily provide a set of measured channel responses and make it available to the PERSEUS project for further analysis and processing.

The measurements will take place in a factory of size 21,000 m², as shown in Figure 2.2. The factory is composed of three main zones each with different shapes, sizes, materials, and clutter density. Zone A is composed of metallic machines and metallic storage containers. Zone B is almost empty for the purpose of movement of factory workers transporting factory loads. Zone C contains metallic lockers and wooden benches and some metallic housing units. The data collected during this measurement campaign will be provided to the PERSEUS project in the first quarter of 2024.

2.3.3 Technical setup and radio configuration

General system parameters

The Small Factory use case will be addressed using the C-band (between 3.7 and 4.2 GHz), which is a well suited band for high capacity and reliability demanding scenario as it will provide more spectrum availability. The parameters considered in this scenario are summarized in Table 2.4.

Frequency band (MHz)	3700-4200
Duplexing mode	TDD
DL/UL ratio	Symmetric (1:1)
Bandwidth (MHz)	100

Table 2.4: Small Factory general system parameters.

Access point configuration

The APs are equipped with up to 16 antenna elements and transmits a max power between 20 and 30 dBm. In terms of directivity, different types of antennas can be used, depending on the installation conditions, varying from an omni-directional antennas down to 60° aperture antennas.

UE configuration

In this scenario, the simplest UE devices like sensors are equipped with a low-complexity low-power radio-end comprising from 1 to 2 antenna elements. Higher end UEs may be equipped with a maximum of 4 antenna elements.

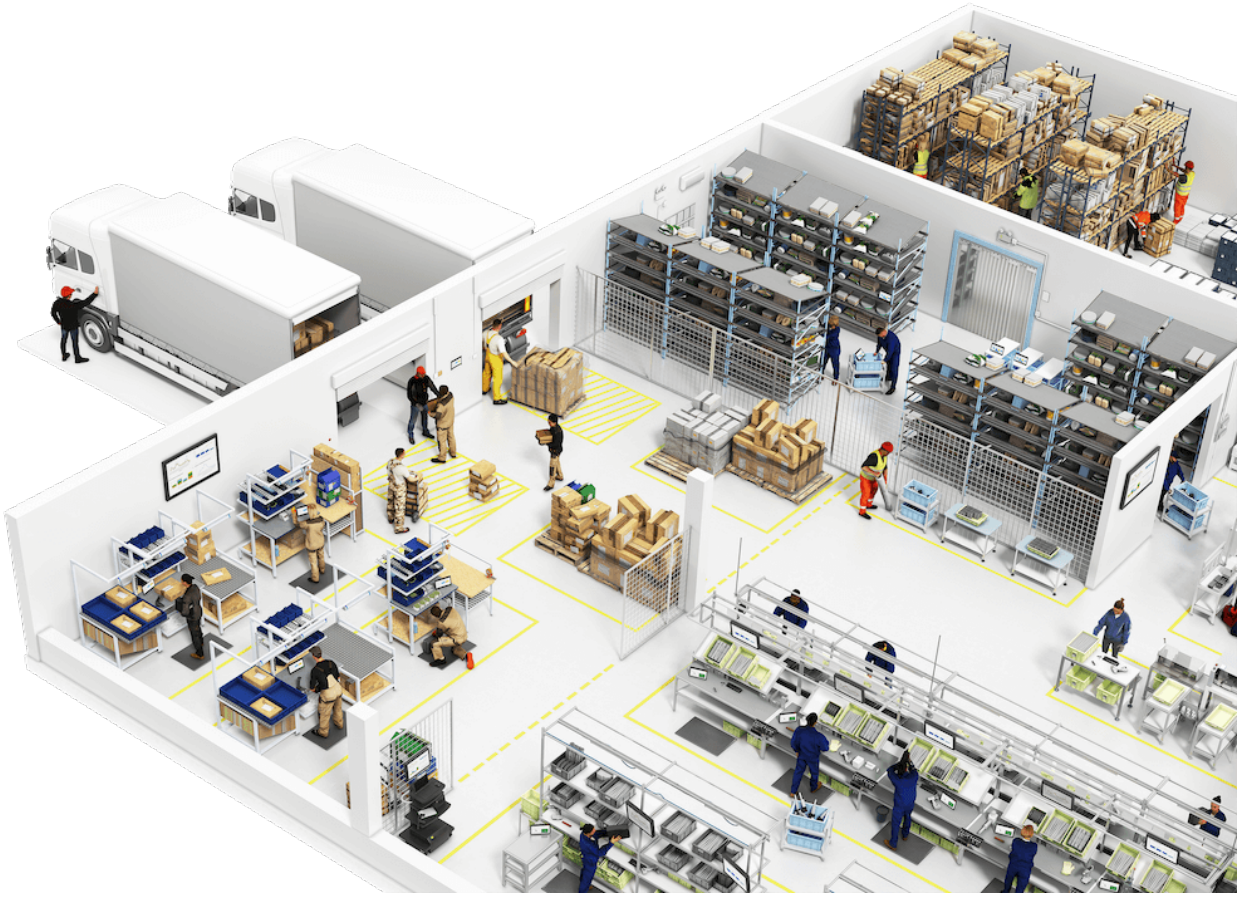

Figure 2.2: Small Factory example environment.

Finally, various mobility levels up to 30 km/h can be integrated in the simulation scenarios. In particular, three levels are considered : Fixed sensor (0 km/h), Pedestrian (from 0 to 3 km/h), and Automated Guided Vehicles with speeds up to 30 km/h.

2.3.4 System services & required KPIs

Service requirements

The reliable communications and possible localization requirements corresponding to the activity of Small Factories will put strong constraints on the system. The communication systems will need a high reliability, with low latency, in particular to make it possible for both operators and autonomous vehicles to work simultaneously in a safe environment.

The traffic may also be sporadic, which means that the required throughput demand can be irregular from almost zero communication to the challenging situation of a large number of devices transmitting large amounts of data simultaneously.

Finally, the number of communicating devices in a Small Factory scenario can be massive, with hundreds of connected objects. This constraints along with the fact that most devices will be battery-operated also raises the requirement of low-energy communication systems.

Main KPIs

The communication network in the factory scenario is expected to offer different types of

- Telepresence and mixed reality applications where high capacity and data rates are required.
- Remote control of robots and UAVs where low latency and high reliability are mandatory.
- Sensors: high availability requirement and high density of connected equipment but with sporadic traffic and low required data rates.

The corresponding KPI requirements are illustrated in Table 2.5

Use Case	Telepresence and mixed reality	Remote Control	Sensors
Peak Data Rate (Mbps)	1000	100	0.1
Experienced Data Rate (Mbps)	50	10	0.01
Reliability (%)	99.9	99.9999	99.99
Availability (%)	99.9	99.9999	99.99

Table 2.5: KPI requirements for the Small Factory scenario.

2.4 V2I in sub-urban environment [S3]

2.4.1 Description and KPIs

Table 2.4.1 illustrates the description of use cas S3 and the technical requirements and challenges.

2.4.2 Measurement scenario(s)

For these measurements, we will use the lab's van for the Rx, fitted with antennas on the roof. Three measurement scenarios are planned: 1 straight line, 1 crossroads, 1 roundabout. This campaign will extend the preliminary results of vehicular cell-free channel sounding described in [113]. In [113], no Doppler has been measured, and just one drive was considered. The campaign will also take place on the Cité Scientifique campus. Precise locations have not yet been defined.

2.4.3 Technical setup & radio configuration

At Tx, the antennas are patches, mounted in a horizontal linear array. 4 configurations are planned: 1 AP with 8 antennas, 2 APs with 4 antennas, 4 APs with 2 antennas, 8 APs with 1 antenna. The Rx consists of 4 omnidirectional antennae spread across the van roof. We have configured the system for a maximum speed of 90 km/h, i.e. a maximum Doppler frequency of 495 Hz. The frame is shown in Figure 2.3:

This frame provides 1.6 Hz of Doppler resolution, with a range of $+/-512.6$ Hz. In summary, the parameters are as follows:

2.5 Massive MIMO Radio Channel Sounder: MaMIMOSA

To this end, a massive MIMO radio channel sounder operating between 2 and 12 GHz with 80 MHz bandwidth has been jointly developed by the University of Lille (IEMN CNRS) and Ghent (Belgium) for 5G mobility scenarios such as V2X communications. The architecture relies on the physical and reconfigurable software radio channel sounder MIMOSA [73] which is capable of performing real-time measurements at 1.35 GHz like reported in [136] to

General description	The advancements of wireless communication technologies has promoted the rapid development of vehicular communications and intelligent transport systems (ITS). As an important part of vehicular communications, vehicle-to-infrastructure (V2I) is used for the huge data transmission between vehicles and roadside units. The CF-mMIMO technology has the potential to offer an effective solution to the challenges of managing vehicular communications and ensuring consistent signal quality across all areas. This is achieved through the use of multiple antennas and spatial processing techniques, which can enhance signal reception and mitigate interference between various users or devices within the network.	
Scenario	Autonomous vehicle	
	Environment	Outdoor/Indoor
	Coverage range	500 m^2/ 1 km^2
	Service	Control, monitoring
	Mobility	30-70 km/h
	Link visibility	LoS/NLoS
	Frequency band	5,89 GHz TDD
	Bandwidth	Up to 80 MHz
	Tx power	20-30 dBm
	TDD	both UL and DL
	Waveform	OFDM or post-OFDM, ICS 12.2 kHz (u=0), FFTsize = 1024, 818 active subcarriers, 103 subcarriers as GuardBand at each side
Technical challenges	- Extremely high reliability and low latency required for accuracy control - Handover management	

Table 2.6: use case 3: description and technical requirements

Number of APs	1-8
Number of antennas per AP	1-8
Number of user positions	1 moving user
Number of antennas per user	4
bandwidth	80 MHz
Central frequency	5.89 GHz
Doppler	Doppler resolution of 1.6 Hz, range +/- 512.6 Hz

Table 2.7: V2I scenario parameters

analyze the stationarity of V2I radio channel in a Suburban Environment. MaMIMOSA has been designed to fulfill all the constraints identified in time-varying massive MIMO channels such as high Doppler resolution with a large Doppler span, spatial antenna selection, compactness, energy consumption, etc. The sounding parameters of the developed massive system can be freely selected depending on the studied environment resulting in the measured massive MIMO radio channel without the need for additional tedious post-processing. As of now, MaMIMOSA is

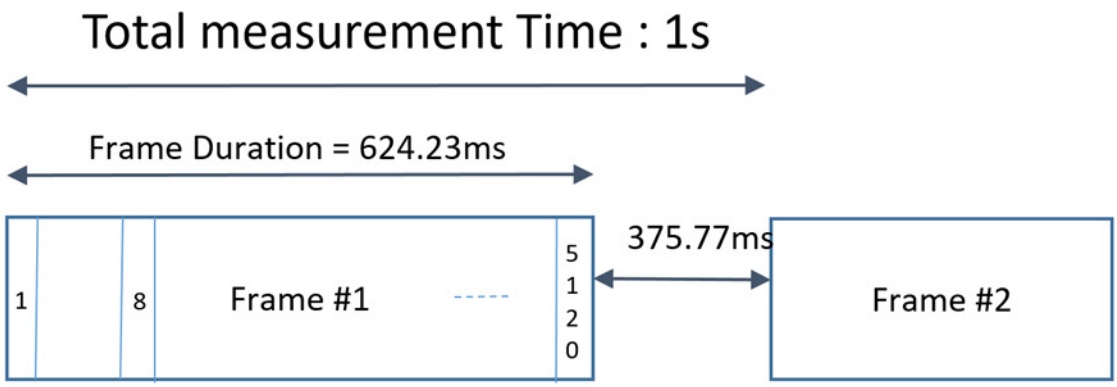

Figure 2.3: Frame measurement in V2I scenario.

being setup to perform 64 x 16 massive radio channel measurements at 5.89 GHz for V2X communications. The 1.3 GHz frequency of MIMOSA is used as an intermediate frequency (IF) to transpose the baseband signal to RF at 5.89 GHz with 80 MHz bandwidth.

2.5.1 MaMIMOSA Architecture

Frame Structure

The basic 64×16 Massive MIMO transmitting frame structure consists in one $51.2\mu s$ preamble subsequently followed by 8 OFDM symbols of $121.92\mu s$ including the cyclic prefix as illustrated in Fig. 1. Hence, the total OFDM sequence to measure a full 64×16 massive MIMO matrix is 1 µms. The preamble provides the time synchronization of the frame such that the OFDM symbols can be decoded. Each OFDM symbol corresponds to an 8-antenna subarray out of 64 and the OFDM sequence (i.e. subarray sequence) can be selected by the user. The time duration between consecutive frames can be manually set from 1 ms to any larger values depending on the desired maximum Doppler shift. As initially developed for MIMOSA [73], the total number of transmitted OFDM subcarriers per symbol N_t is 8192 which can be uniformly distributed on each antenna element using interleaved OFDM. For instance, the frequency space δF between the subcarriers of a single antenna is 97.66 kHz, meanwhile the frequency space of between subcarriers is 12.21 kHz. The automatic gain control (ACG) is performed with the cyclic prefix for each symbol and is used to correct the measured MIMO matrix.

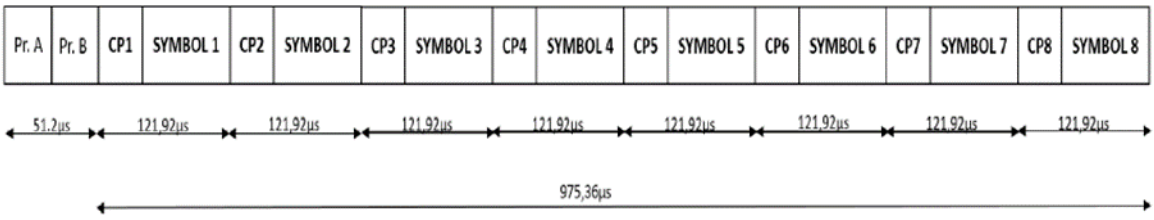

Figure 2.4: MaMIMOSA Frame Structure.

Transmitter and Receiver Unit

The MaMIMOSA transmitter (Tx) chain is presented in Fig. 2. It is composed of 4 parts: 1) ”time and position” records information such as the GPS position and 3D position of the antenna array (yaw, pitch, roll). The reference rubidium clock is also found to synchronize all Tx signals. 2) The signal manager is organized thanks to a computer

embedded into a chassis which also includes the FPGA-based digital processing cards to generate and send the signals. 3) The baseband signals are first mixed at 1.3 GHz as an intermediate frequency (IF). It is then transposed to any frequencies between 2 and 12 GHz with a second mixer. The different mixing stages are all synchronized with the 10 MHz local oscillator (LO). The operating central frequency of the sounder is selected by the user and depends on the RF filters and antennas. The maximum bandwidth is 100 MHz with output power values which can be selected between 0.01 W to 0.5 W per RF chain (maximum power of 4 W for the 8 outputs).

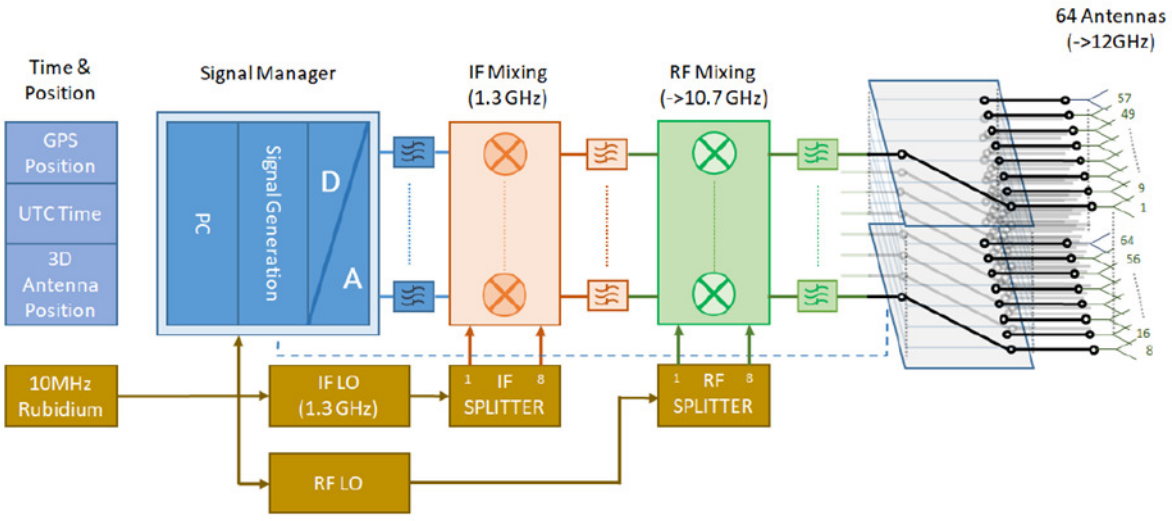

Figure 2.5: MaMIMOSA Tx Chain.

Figure 3 presents a front and back picture of MaMIMOSA highlighting the compactness of the sounder. The two bottom chassis form the basis of MIMOSA (operating at 1.35 GHz) whereas the two top chassis extend it to a massive system. The top chassis is the switching box with 8 inputs (back) and 64 outputs (front) which are controlled via the FPGA. The insertion losses are 1.7 dB with a switching time of 100ns and 40 dB isolation between ports. The chassis beneath includes the filters and second RF mixer. A tablet can be used with a keyboard and mouse to configure the unit and visualize the selected transfer functions or power delay profiles for example.

Similarly, the Rx chain is composed of several parts (Fig. 4). The RF module transposes the received signals to the IF module and then to baseband. The AGC adjusts the signal strength to optimize the signals at the input of the analog-to-digital converter (ADC). The different mixing stages are all synchronized with the 10 MHz LO. The digital signals are then processed by the digital processing unit to compute in real-time the complex transfer function H(f,t) via the FPGA cards. The data is sent to an embedded PC either for display or record on a 300 GB hard drive. The GPS position and 3D antenna array orientation are tagged along the data. A rubidium reference clock synchronizes all signals like for Tx. The receiver has 16 inputs such that the processing is performed in parallel. The bandwidth is 100 MHz and the AGC dynamic is 64 dB with 0.5 dB step. Both Tx and Rx units can be powered with Li-ion batteries that provide up to 8 hours of continuous measurements.

Calibration Procedure

The calibration procedure is automatically performed in eight consecutive steps by using an 8×1 combiner placed after the Tx output switches connected to a 1×16 splitter placed before the Rx inputs. Each step corresponds to an 8×1 subarray of the Massive array. The measurement cables are also included into the procedure to remove their contribution from the radio channel. The splitter transfer functions are also measured and removed. The measured 64 x 16 system transfer function is recorded in a single file. It is then used dynamically to calibrate the radio channel transfer function each time it is measured. This calibration procedure is possible because the signal sent to each emitting port is mapped to a specific set of frequencies thanks to frequency-division multiplexing.

(a) (b)

Figure 2.6: Picture of the MaMIMOSA Tx Unit from the (a) front and (b) back.

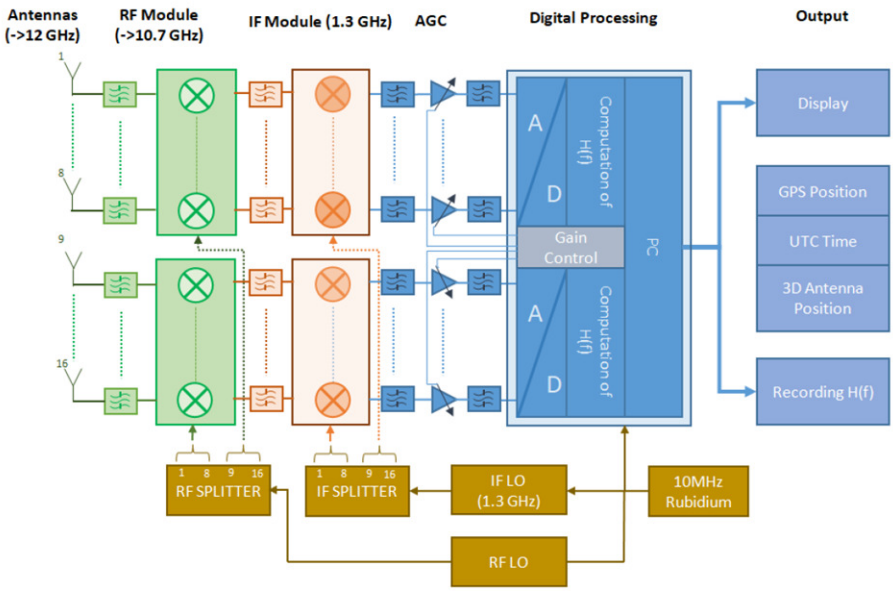

Figure 2.7: MaMIMOSA Rx Chain.

Massive antenna array and receiving antenna Since the target application is V2X communications, a dedicated massive antenna array operating at 5.89 GHz with 80 MHz bandwidth is considered. The array can sit on a tripod as an example and will primarily be used as a static access point for V2I scenarios. The MaMIMOSA antenna array will be a vertical planar array of 10×10 antennas and is currently being designed and built by the University of Ghent. Since 64 elements of the array can be connected via SMA coaxial cables to the Tx unit, the remaining antennas (array perimeter) will be used as dummies and connected to 50Ω loads to attenuate the finite array side effects. The elementary element is a vertically polarized patch (duroid 5880) with 250 MHz bandwidth at -10 dB around 5.89 GHz. This bandwidth much larger than the available 100 MHz bandwidth of the sounder is needed to obtain sufficient bandwidth for the final array due to coupling effects. The plots were simulated with Sim4Life (ZMT, Zurich, Switzerland), a full-wave 3D multiphysics simulation platform. The finite-difference time-domain (FDTD) technique was used to simulate $S11$ and $S21$.

Fig. 5 presents the 10×10 array with the radome in transparency and support cables on the back. Since all patches of the array are mono-polarized, a 90° rotation of the array will allow selecting either the vertical or horizontal polarization. Finally, all 16 antennas that will be used at the Rx side consist in the same patch antenna than for Tx. Each antenna can be integrated into a dedicated support that can be safely attached to a high-speed moving vehicle or simply set on a table.

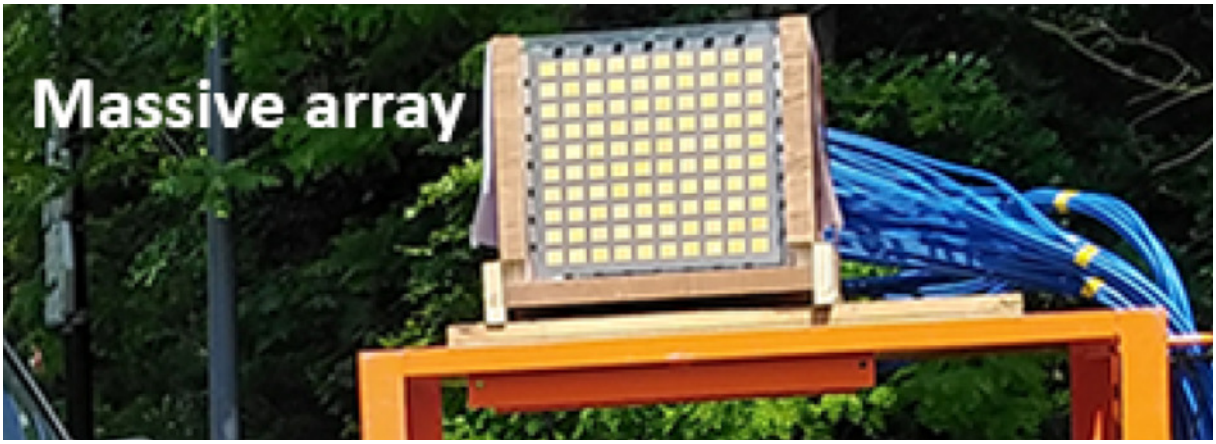

Figure 2.8: MaMIMOSA Tx Massive Array.

2.5.2 Cell-free MaMIMOSA Upgrade

A new network architecture without the concept of cells appeared a few years ago: the cell-free mobile network [58] [36]. In the cell-free context, an important number of access points (APs) distributed over a large geographical area cooperate to optimally serve the users (UE). These APs are equipped with a small number of antennas and are connected to a central processing unit (CPU) via a wired or wireless backhaul link. The cell-free concept encompasses the 5G massive MIMO technique wherein many antennas are densely distributed over the area. As a result, cell-free massive MIMO can be viewed as a generalization of 5G massive MIMO. Due to the proximity and diversity of APs, it offers a far more uniform coverage and increased connectivity. In particular, critical life-safety services considered in upcoming vehicular networks specifically rely on a highly uniform QoS. Although the cell-free massive MIMO has recently received a lot of attention at the theoretical level, the validation of this approach for outdoor vehicular applications was only demonstrated with the currently discussed sounder [113]. This was done by upgrading the real-time channel sounder MaMIMOSA to measure channels in such distributed configurations. In particular, it was recently set up to measure the time-varying 64×16 radio channel at 5.89 GHz with an 80 MHz bandwidth as presented earlier. The upgrade consists in geographically distributing the transmit antennas using up to 500 meter-long RF-over-fiber (RoF) links. This enables the real-time channel between a vehicle and a network of distributed antennas to be measured. The current MaMIMOSA configuration supports up to 8 single-antenna APs or L APs equipped each with a N–antenna array, with $L \times N = 8$. Based on the measurements,

the performance of the different topologies are compared in terms of the achievable mean SNR, delay spread, and path loss characteristics.

For the time being, eight 500 meter-long RoF links with 1 dB/km attenuation loss are connected to MaMIMOSA and TX as shown in Fig. 6 and 7. The RF-optical converters integrate a power amplifier to compensate for the insertion losses at the expense of a 27 dB noise figure. The output power was set to 0 dBm for each RF chain and a 15 dB gain power amplifier was placed in between the optical/RF module and antenna to reach a 15 dBm transmit power signal with 40 dB SNR. The length of all coaxial cables was 2.5 m. A hybrid calibration procedure using one of the RoF links was performed since both RoF and coaxial links are used.

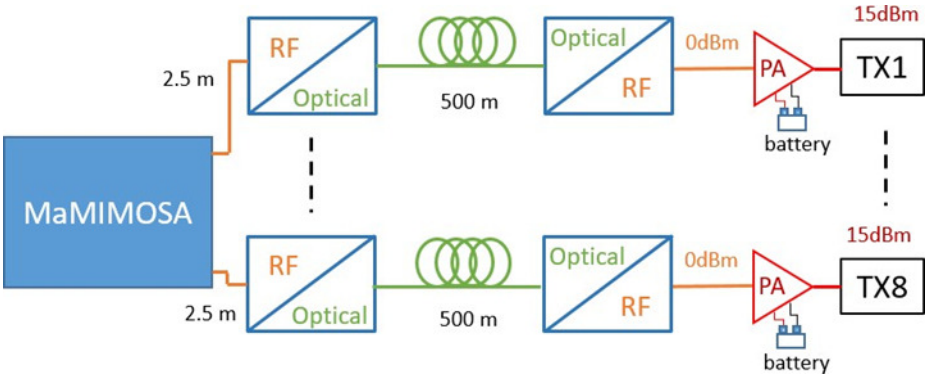

Figure 2.9: Cell-free sounding architecture using 8 RoF links and one coaxial link.

Figure 2.10: MaMIMOSA transmission system with the 500m long RoF links.

2.5.3 Doppler characteristics of the system

Critical features of multidimensional radio channel sounders designed to assess Doppler characteristics are the Doppler span and resolution. The former defines the maximum Doppler shift of the multipath components (MPC) whereas the latter defines the observable minimum Doppler difference between MPC. The Doppler resolution is inversely proportional to the capability of the system to treat the received signals and record the processed data on the physical hard drive. Depending on the massive MIMO radio channel configuration desired by the user and investigated vehicular scenario, the system has been designed to be as flexible as possible to select the best Doppler parameters without significant intercarrier interference. Basically, the recording time can be increased by either increasing the interframe time, intersymbol time in a frame, or decreasing the number of Rx users. The configuration parameters can be set by the user for different mobility scenarios and Doppler resolution values. Overall, the system is limited by the 100 Mo/s data transfer from the FPGA cards to the hard drive. Evidently, the

recording is also bounded by the hard drive capacity. As an example, for an urban scenario where the regulated speed is typically 50 km/h (± 277 Hz maximum Doppler shift), a massive 64×16 MIMO channel can be measured during 120 seconds with a 1 Hz Doppler resolution and 300 Hz Doppler span. This only requires 15 GB on the hard drive and the measurement can be repeated to entirely fill the remaining space.

Chapter 3 : RIS-Empowered Scenarios and Use Cases

3.1 Introduction

Reconfigurable Intelligent Surfaces (RIS) corresponds to a planar surface composed of unit-cells, whose properties can be controlled dynamically to 'tune' the incident wireless signals through reflection, refraction, focusing, collimation, modulation or absorption. RIS can be potentially deployed for both indoor and outdoor usage, including offices, airports, shopping centres, lamp posts and advertising billboards, and may take any shape or be integrated onto objects. Its characteristics may also result in low energy consumption, making RIS a sustainable technology solution. RIS can be configured to operate at any part of the radio spectrum, including frequencies from below 6 GHz to THz, and may harness tools from Artificial Intelligence (AI) and Machine Learning (ML) to enable systems operation and optimization.

As RIS is envisaged to be a new enabling candidate wireless technology for the control of the radio signals between a transmitter and a receiver in a dynamic and goal-oriented way, turning the wireless environment into a service. This has motivated a host of potential new use cases targeting at: i) the enhancement of various system key-performance-indicators (KPIs), and ii) the support of new wireless technology applications and capabilities.

These include enhancements to the capacity, coverage, positioning, security, and sustainability, as well as the support of further sensing, wireless power transfer, and ambient backscattering capabilities.

The European Telecommunications Standards Institute (ETSI) started in 2021 an Industry Specification Group (ISG), which is in charge of defining this technology and to identify promising use cases and application scenarios. The aspects are discussed in this chapter.

3.2 Definition and General Structure

RIS is considered a key candidate wireless technology trend for future networks. RIS corresponds to a new network node composed of an arrangement of scattering elements called unit-cells, whose properties can be dynamically controlled to change its electromagnetic behaviour. The response of RIS can be controlled dynamically and/or semi-statically through control signalling such as to tune the incident wireless signals through reflection, refraction, focusing, collimation, modulation, absorption or any combination of these. As a new network node dynamically and/or semi-statically configured by the RIS controller, turning the wireless environment from a passive to an intelligent actor such that the channel becomes programmable. This trend will expand basic wireless system design paradigms, creating innovation opportunities which will progressively impact the evolution of wireless system architecture, access technologies, and networking protocols (see Figure 3.1).

RIS can be implemented using mostly passive components without requiring high-cost active components such as power amplifiers, resulting in low implementation cost and energy consumption. This allows easy and flexible deployment of RIS, with the possibility of RIS taking any shape and to be integrated onto objects (e.g. walls, buildings, lamp posts, etc.). RIS are supposed to run as nearly-passive devices and hence are unlikely to increase exposure to EMF, and in fact, they can potentially be used to reduce EM pollution in legacy deployments. These associated characteristics suggest RIS may be considered as a sustainable environmentally friendly technology solution. RIS may have different structures with considerations of cost, form factor, design and integration.

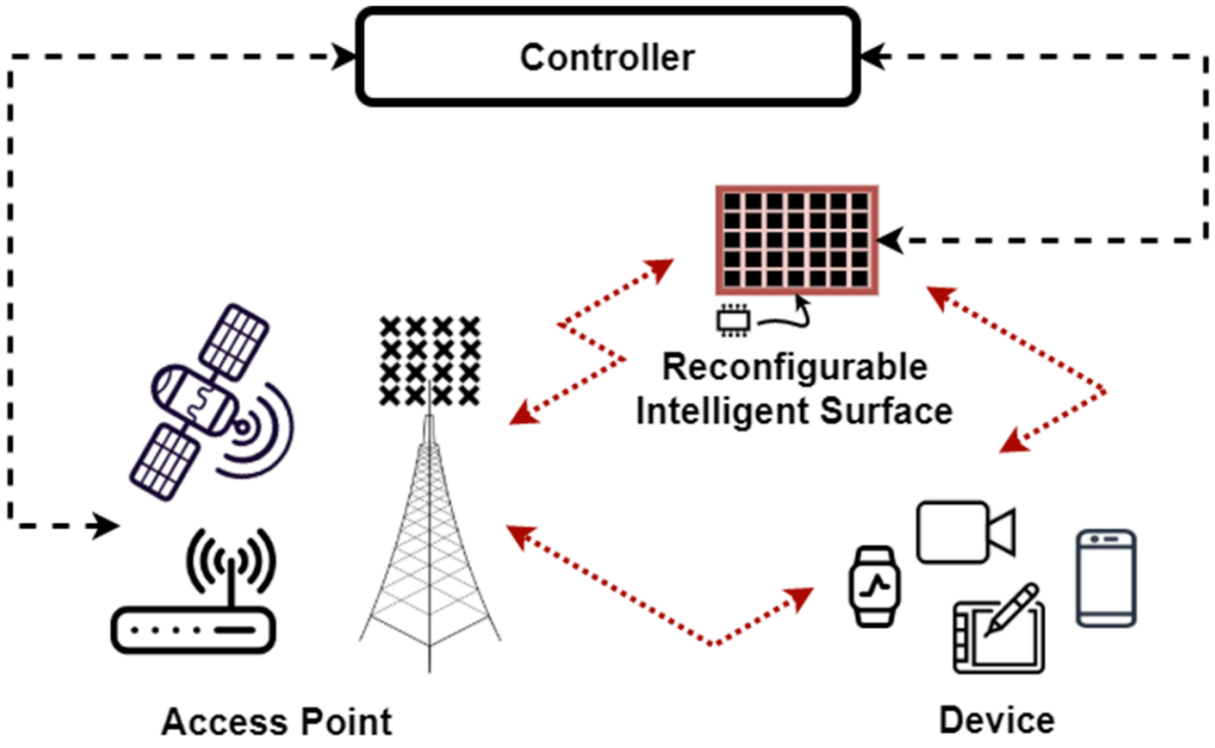

Figure 3.1: Illustrative diagram of RIS, a new type of network node where its response can be adapted to the status of the propagation environment through control signalling (Credits: ETSI ISG RIS)

3.3 ETSI ISG RIS

ETSI is a leading organization for the development of standards on information and communication technologies, fulfilling European and global market needs. ETSI has over 900 members from 64 countries over 5 continents. ETSI produces specifications, standards, reports and guides, enabling technologies in a multi-vendor, multi-network, multi-service environment. Standards are created in an open approach, thanks to the direct participation of members and contribution-driven consensus-based working procedures. The standardization work is carried out in different technical groups, which include ISG.

ISGs are the perfect tool for developing early standardization activities, resulting from fundamental and applied research projects, targeting for the publication of deliverables where technological aspects are streamlined for consideration by standards organizations. In September 2021, ETSI launched ISG-RIS, with the objective of reviewing and establishing global standardization activities for the IS technology, which focused on the following aspects:

- Definition of use cases, key performance indicators, and deployment and operational scenarios;
- Radio-frequency aspects, including surface models, channel characterization, radiation characterization, and radiation exposure limits;
- RIS-aided air-interface technologies, mechanics, and requirements;
- System and network level control signaling aspects;
- System and network architecture considerations;
- Baseline evaluation methodology and performance analysis (link-level and system-level);

- RIS microelectronics, enabling technologies, and proof-ofconcepts (prototyping);
- RIS verification and validation.

In the first phase from 2021 to 2023, the activities of ISG-IS were focused on three main work items (WIs), including:

- WI-1: Use cases, deployment scenarios and requirements – WI-1 focused on identifying relevant use cases for RIS, with the corresponding general key performance indicators, deployment scenarios, and operational requirements for each identified use case. This includes system/link performance, spectrum, co-existence, and security.
- WI-2: Technological challenges and impact on architecture and standards – WI-2 focused on technological challenges to deploy RIS as a new network entity, the internal architecture, framework and required interfaces for RIS and the potential recommendations and specifications to standardization groups for supporting RS as a network entity.
- WI-3: Communication models, channel models, and evaluation methodology – WI-3 focused on communication models striking a suitable trade-off between electromagnetic accuracy and simplicity for performance evaluation and optimization at different frequency bands; channel models (deterministic and statistical) that include pathloss and multipath propagation effects, as well as the impact of interference for application to different frequency bands; channel estimation, including reference scenarios, estimation methods, and system designs; and key performance indicators and the methodology for evaluating the performance of RIS for application to wireless communications, including the coexistence between different network operators, and for fairly comparing different transmission techniques, communication protocols, and network deployments.

The second phase (initial specifications) of ISG-IS kicked off in September 2023. The group is currently working on the following three WIs:

- WI-4: Implementation and practical considerations – The scope of WI-4 is to investigate relevant implementation and practical considerations for RIS in a wide range of frequency bands and deployment scenarios and provide possible solutions and prototyping results.
- WI-5: RIS-aided air-interface technologies and mechanics – The scope of WI-5 is to identify use cases, deployment scenarios, and transmission and reception schemes for diversity and multiplexing in RIS-aided channels.
- WI-6: Multi-functional IS – Modeling, optimization, and operation – The scope of WI-6 is to identify technological challenges and solutions for multi-functional RIS, incorporating transmission, reflection, sensing, computation, and other potential functions, as well as corresponding appropriate deployment scenarios and resource allocation schemes.

The activities of ISG-RIS during the second phase will be tailored to providing an initial specification framework for the technology. A major objective of ISG-RIS is to establish collaborations with other relevant ISGs, which are focused on emerging technologies that have strong ties with RIS. The most relevant and related ISGs are ISG-THz on THz communications and ISG-ISAC on integrated sensing and communications (ISAC). Specifically, ISG-THz concentrates on channel sounding and modeling for IS-aided channels and ISG-ISAC concentrates on how IS can be exploited for improving the performance of ISAC, as well as how ISAC can be exploited for improving the operation and deployment of RIS. In summary, standardization activities for RIS and its applications in THz communications and ISAC are under a vivid debate by standards organizations.

In what folliws, we summarize the use cases and scenarios identified by ISG-RIS during the last three years.

3.4 ISG-RIS Use Cases

RIS is envisaged as a new enabling candidate wireless technology for the control of the radio signals between a transmitter and a receiver in a dynamic and goal-oriented way, turning the wireless environment into a service. This

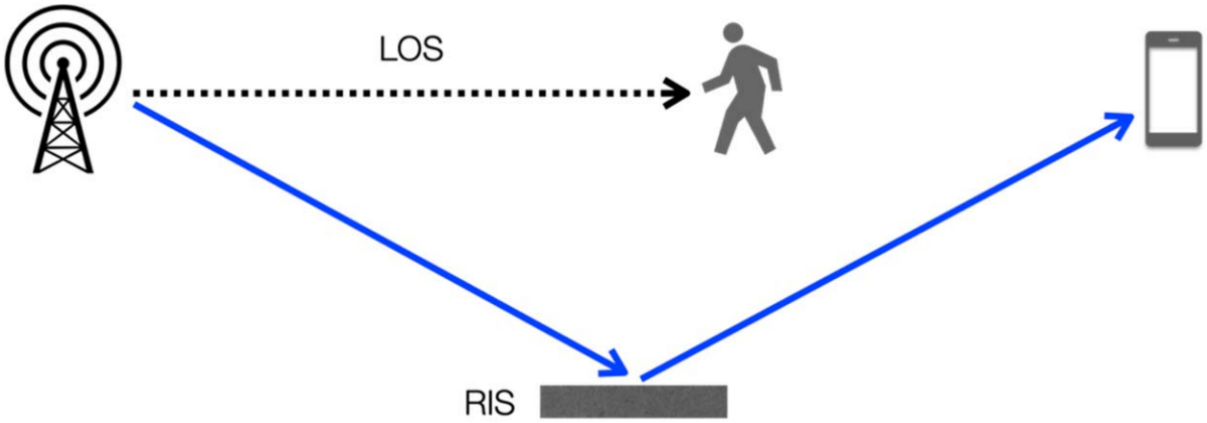

Figure 3.2: RIS as a solution to blockage (Credits: ETSI ISG RIS)

has motivated a host of potential new use cases targeting at: a) the enhancement of various system KPIs; and b) the support of new wireless technology applications and capabilities. These include enhancements to the capacity, coverage, positioning, security, and sustainability, as well as the support of further sensing, wireless power transfer, and ambient backscattering capabilities.

3.4.1 Coverage enhancement

Due to the influence of obstacles such as buildings and trees, the wireless signal coverage is uneven and the problem of weak coverage often occurs in the actual mobile communication system. Weak coverage areas may be small and discrete, however their adverse effects may be serious. Terminals in these areas may not be able to obtain guaranteed quality-of-service. Deploying more access points in the weak coverage area is a method of high cost and low efficiency. RIS provide a low-cost and easy-to-implement method. By deploying RIS in the appropriate location, line-of-sight propagation paths between the access point and the RIS as well as between RIS and the terminal can be established in the weak coverage area to achieve coverage enhancement. Simple reflecting RIS may be sufficient to provide robust communication links toward end terminals, but in more demanding scenarios, use cases involving more advanced RIS hardware architectures, like ones performing coherent/non-coherent modulation, baseband measurement collection, and consequently sensing, or acting as decodeand-forward relays may prove more effective despite their increased cost. RIS can enhance the cell coverage in many realistic scenarios listed as follows.

Figure 3.2 demonstrates the most common and intuitive application of RIS, i.e. serving as a solution to blockage issues, which applies to both outdoor and indoor scenarios. Figure 3.3 illustrates a quite common variant of the blockage problem, in which the BS deployed in one corridor needs to serve UEs in a perpendicular hallway. Due to the high penetration loss, such a link is not feasible without the assistance of RIS. In addition, to avoid blockages in a complicated environment, multiple RIS can be configured in a cascaded manner for coverage extension, as shown in Figure 3.4. Figure 3.5 shows an outdoor scenario, in which a BS on the roof of a building needs to serve a UE in street canyon. Given the ordinary antenna radiation pattern, the downtilt angle, and the building blockage, the quality of service provided to the UE can be expected to be poor. Using a huge RIS installed on the wall of the opposite building can effectively reflect the signal to the blind spot, thus enhancing the cell coverage. Figure 3.6 shows an example coverage enhancement application of RIS in an Outdoor To Indoor (O2I) scenario, in which BS can serve UE in underground garage with the help of RIS links, given the extraordinary blockage and O2I loss

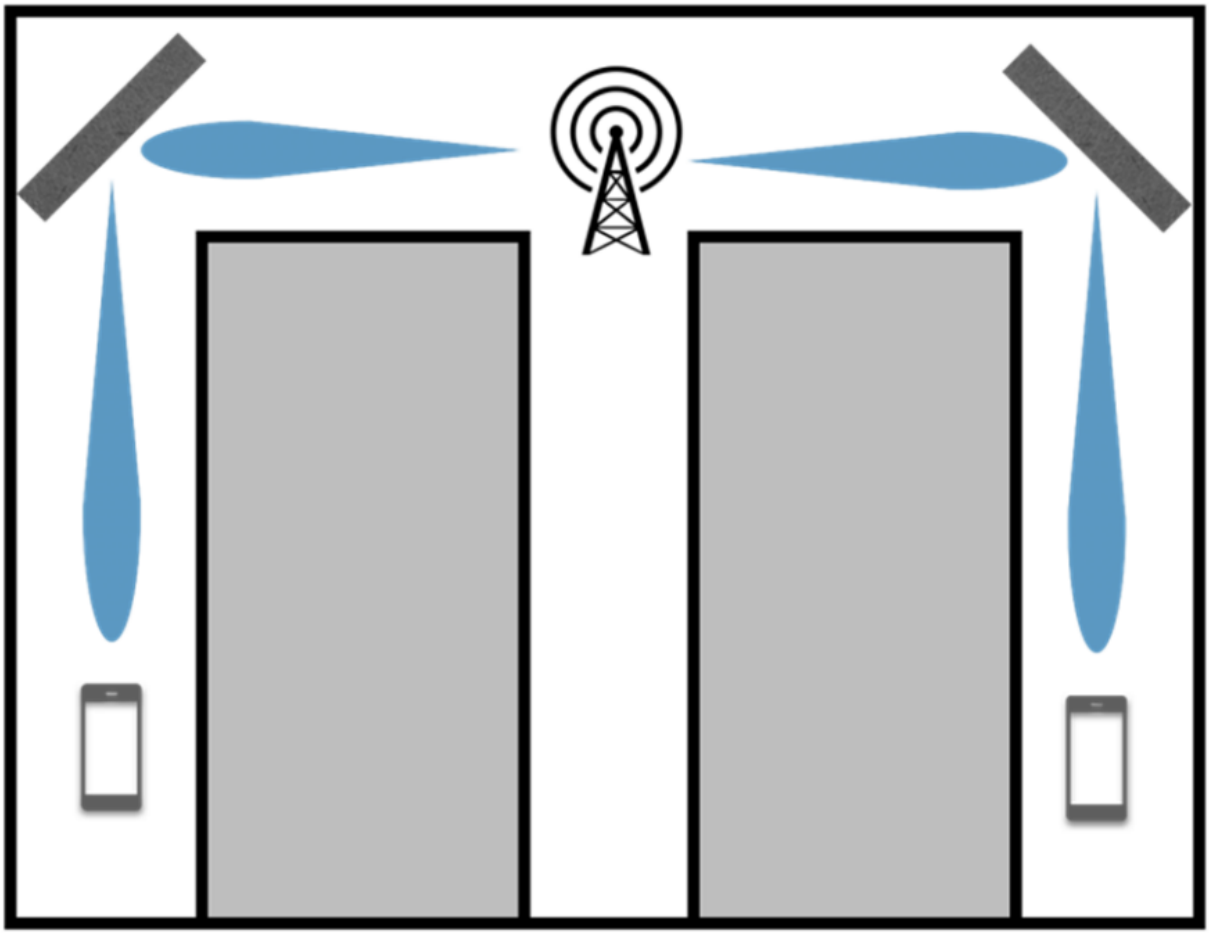

Figure 3.3: RIS redirects beams to form link between BS and UE in different hallways (Credits: ETSI ISG RIS)

3.4.2 Spectral efficiency

In wireless communication networks, channels between the transmitter antennas and the receiver antennas may have strong correlation, which limits the number of eigen channels for parallel data transmission. By deploying RIS, the channel correlation problem can be alleviated. With more eigen channels, the communication networks can obtain higher spatial multiplexing gains and spectral efficiency. In particular, the increased received signal power that enhances coverage also translates into increased spectral efficiency. However, there are several additional mechanisms by which a RIS may increase spectral efficiency. In various scenarios, for example at higher frequencies, the channel is often dominated by one or two paths. With the addition of a RIS, the available degrees of freedom in the channel increases, and the spatial multiplexing rank can be increased. Beyond improving the signal power and rank of the desired terminal, a RIS can also be used to suppress interference, e.g. co-channel and inter-cell interference. Just like a RIS is capable of signal boosting towards a certain area, a RIS may also be capable of signal nulling.

The general link topology of these use cases is illustrated in Figure 3.7. In addition, as a configurable component that affects the communication channel, RIS potentially provides a new degree of freedom for multiple access. An example of RIS multiple access is demonstrated in Figure 3.8, in which different BS/UE links can utilize different sub-arrays on a RIS panel. It has been argued that adding an RIS may have beneficial effects on the channel distribution and rate of fading, for example from a fast-fading Rayleigh distribution without RIS to a slower-fading

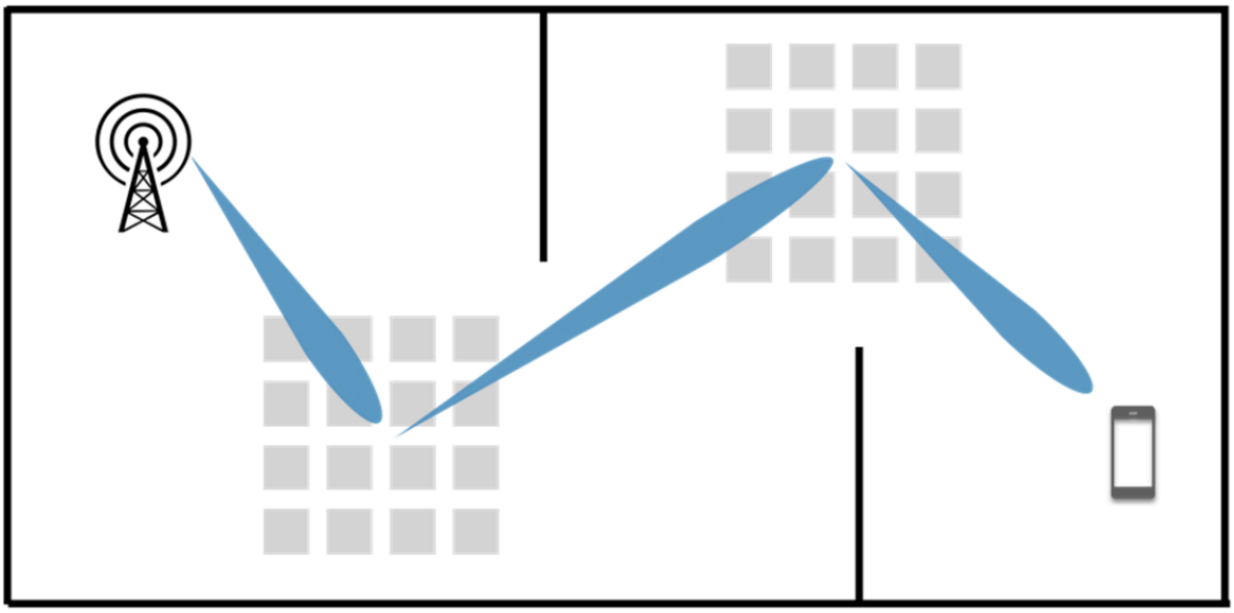

Figure 3.4: Cascading RIS links assist UEs to form links with BSs regardless of blockage (Credits: ETSI ISG RIS)

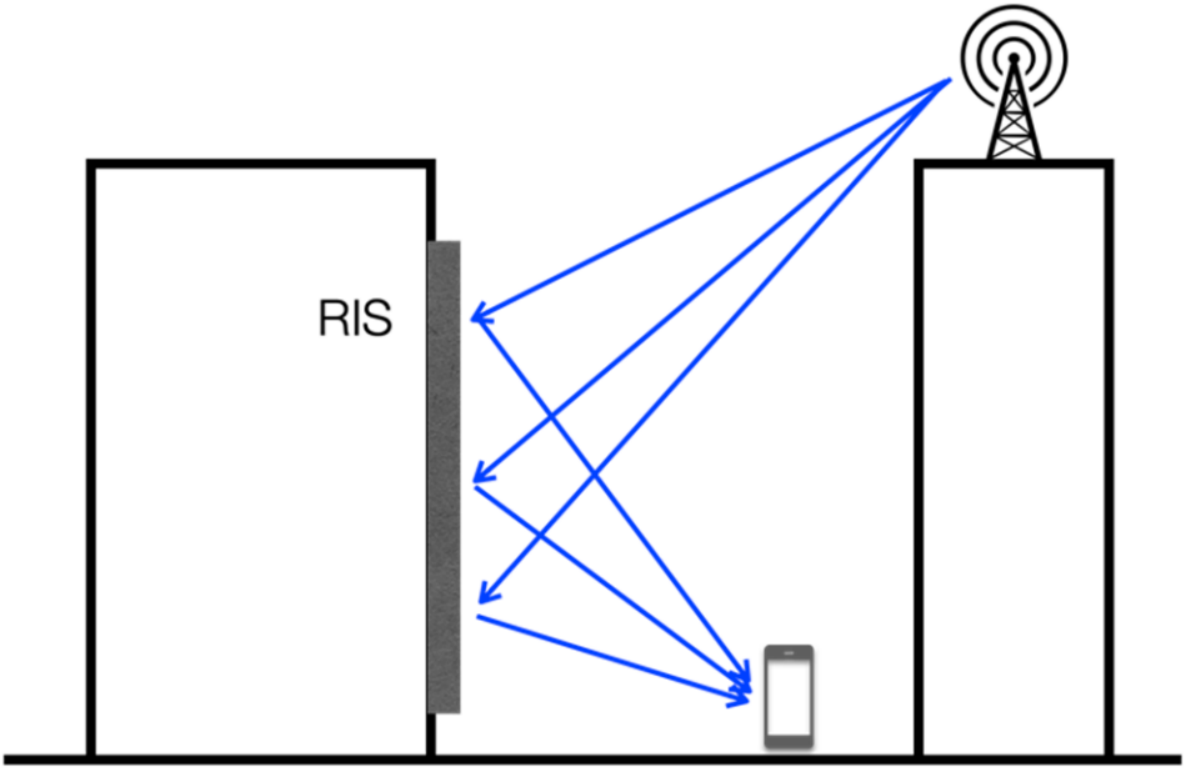

Figure 3.5: BS serves UE in street canyon using large RIS on building walls (Credits: ETSI ISG RIS)

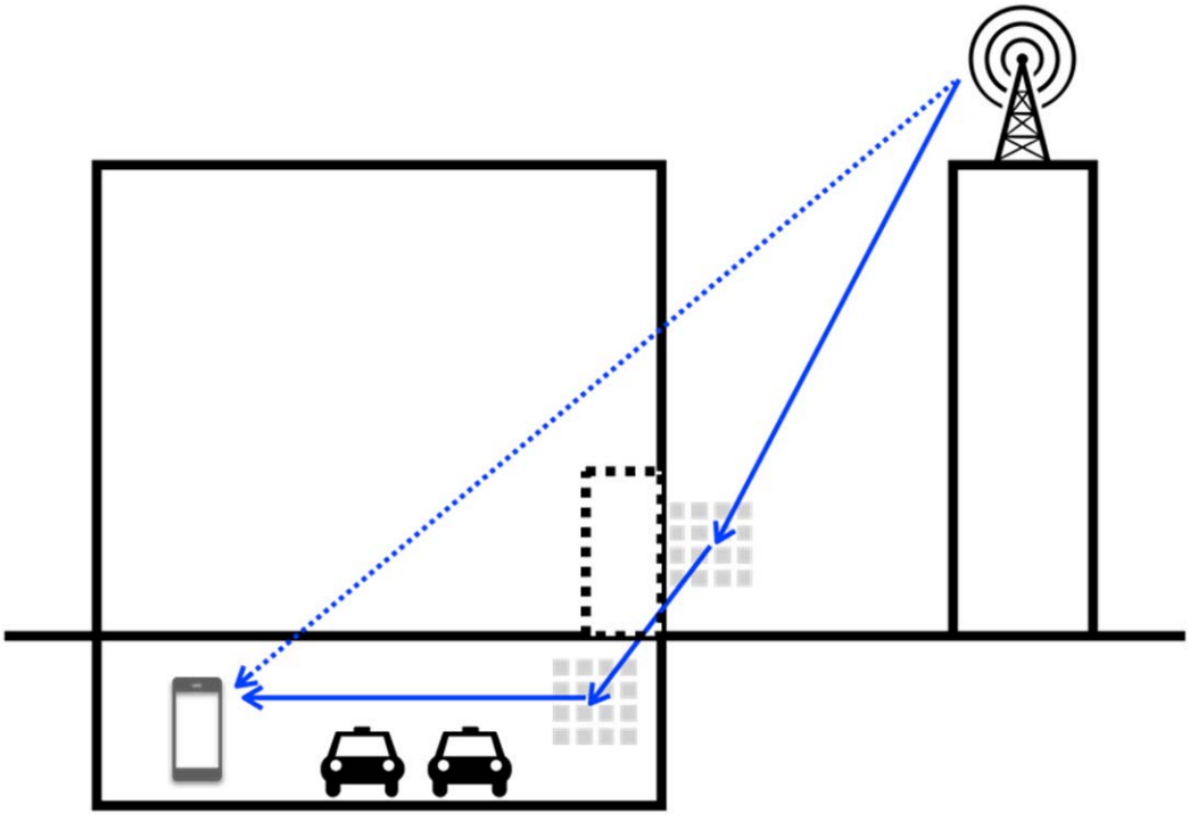

Figure 3.6: RIS application in an O2I scenario, in which BS serves UE in underground garage using RIS (Credits: ETSI ISG RIS)

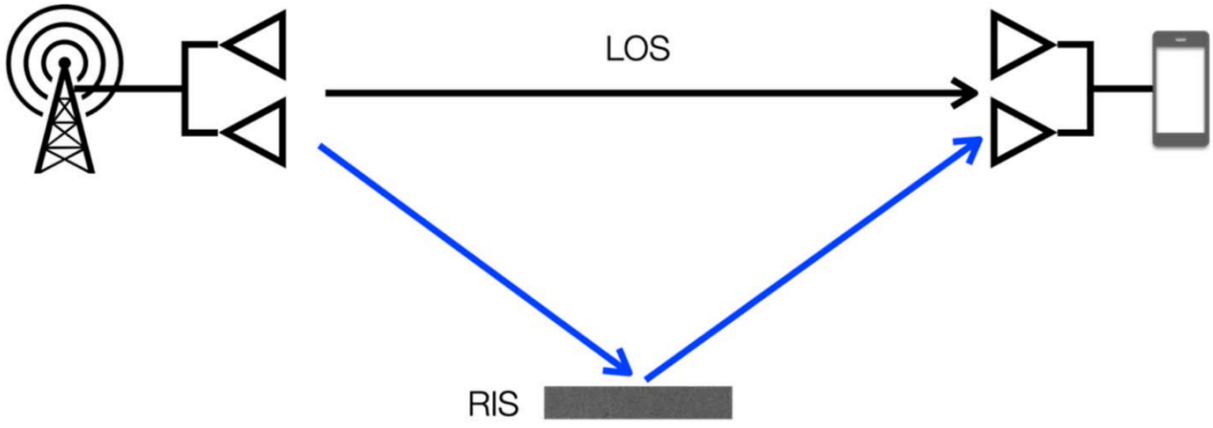

Figure 3.7: Utilizing RIS with MIMO: multiplexing and interference management (Credits: ETSI ISG RIS)

Rician distribution with RIS. Such effects may positively impact both spectral efficiency and reliability, for example through more efficient link adaptation.

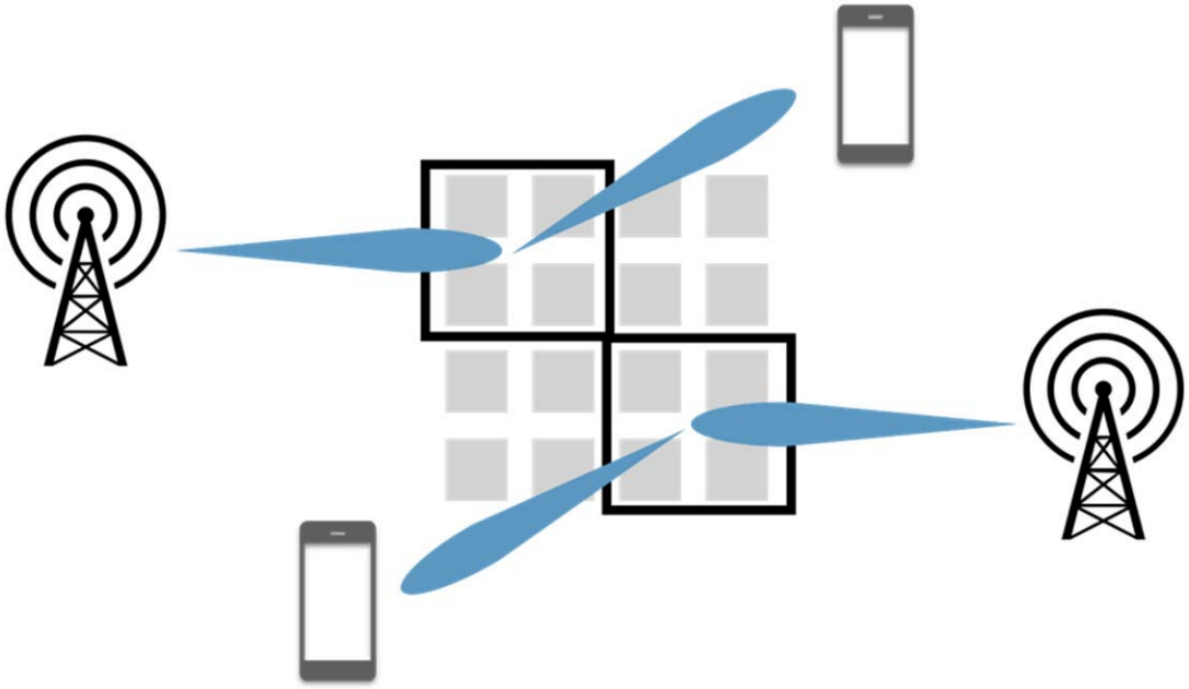

Figure 3.8: RIS multiple access (Credits: ETSI ISG RIS)

3.4.3 Beam management

In wireless communication systems such as NR, beam management is widely used to mitigate signal propagation losses during wireless transmission. Beam management is aimed at establishing and maintaining a set of beam pair links between the transmitter and the receiver, which can improve the system's spectral efficiency and provide a cost-effective solution with reliable coverage, especially in high frequency bands. The RIS beamforming can be realized by adjusting element's reflecting angle. RIS will manage different group of elements pointed to different user and the signal strength of it will be proportional to the number of elements. Compared with massive MIMO, less power is used by RIS to reach a same beamforming gain. Similar to MIMO, a multipleelements RIS can produce beams to focus the signal at specific users or towards certain directions. The reflective elements on RIS can send the same signal with equal wavelengths, therefore the targeted beam is provided with enhanced signal strength in a specific direction. Beam management is one of the most essential blocks for aiding communication, particularly in higher frequency range such as FR2 (24,25 GHz - 71 GHz). Typically, multiple beams are configured by network and from the configured set of beams, one or more beams are indicated to the UE for downlink and/or uplink. Due to dynamic variables in the environment, the path between the BS and the UE(s) may be blocked and this may lead to the issue of beam blockage, more so in FR2. For this reason, multiple TRPs can be deployed by network to provide an additional/alternative set of beams from another TRP. However, deploying multiple TRPs require network planning and increased cost for network deployment. RIS can provide an alternative solution or further complement multiple TRP based deployment. RIS elements can be configured to adjust the properties of the reflecting signal in terms of phase, amplitude, polarization, etc. With optimal configuration, highly direction beams can be reflected from RIS towards the intended target receiver. Essentially, with RIS deployment, additional/alternative beams can be configured and dynamically indicated. Moreover, this can be done in both cost and energy efficient manner.

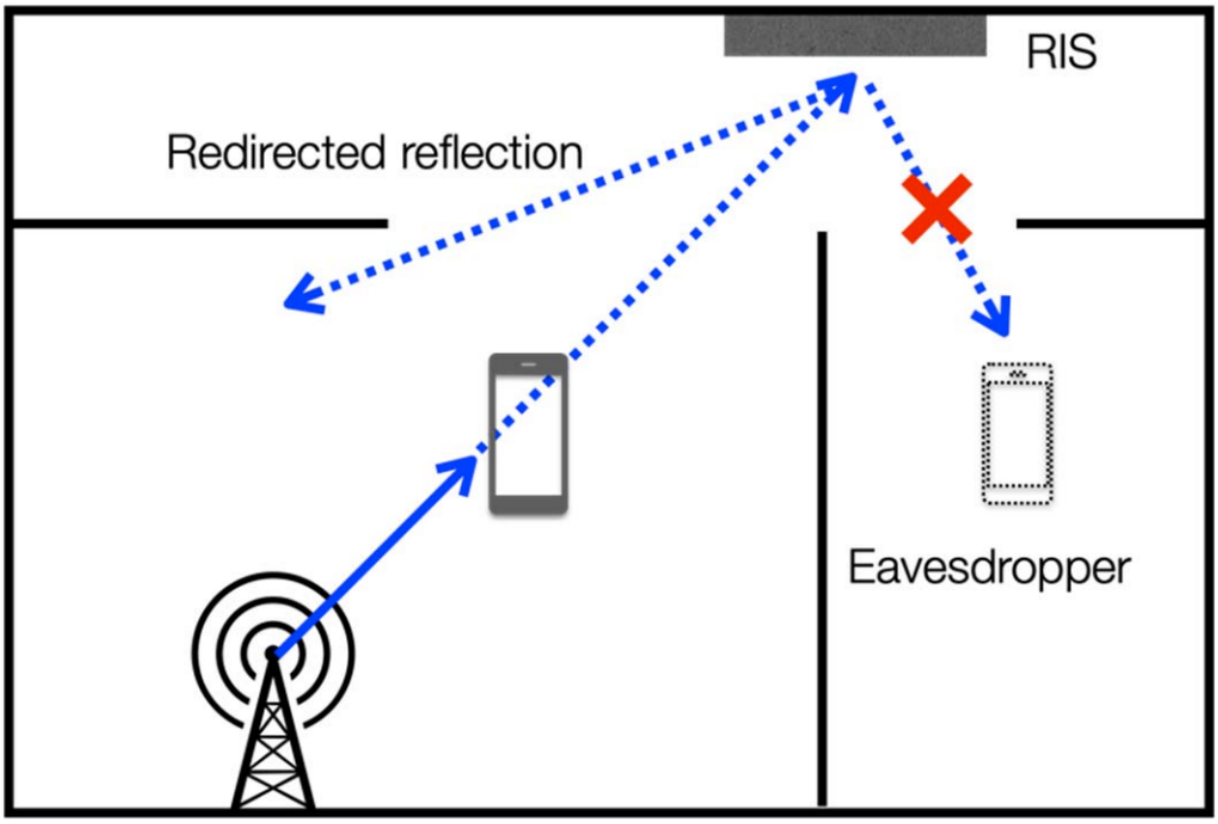

Figure 3.9: Utilizing RIS for secure communication (Credits: ETSI ISG RIS)

3.4.4 Physical layer security

The uncontrolled propagation of confidential signals caused by the uncertainty of wireless propagation channels is one of the reasons that affect the security of communication systems. Building an intelligent and controllable wireless propagation environment by deploying RIS can effectively avoid the leakage of confidential signals to eavesdroppers and improve the security of communication systems.

As is illustrated in an example scenario in Figure 3.9 without RIS, the data sent to a UE can be easily leaked to eavesdroppers via natural reflections by the wall, ceiling, etc. To solve this problem, RIS can redirect the reflections to a trusted region, which hence reduces the data leakage to potential eavesdroppers and enhances the communication security. RIS, as many other technologies with high potential for wireless applications, can also be deployed in malicious ways, that is, an eavesdropper may install a RIS to benefit from its capability to provide a strong wireless link towards a legitimate system, thus enabling the successful decoding of the legitimate transmitted data. In such cases, the adoption of only artificial noise transmissions by the legitimate system may be incapable of guaranteeing secrecy, necessitating also the consideration of a legitimate RIS.

3.4.5 Localization and sensing

Positioning service is already available in the traditional wireless communication systems. However, the accuracy is limited by the location, availability of LoS and number of BS. Compared with deploying BS, deploying RIS is more flexible and the cost is lower. With the assistance of RIS, the communication networks can obtain higher spatial resolution and positioning accuracy. The positioning accuracy of indoor scenario can also be improved by the deployment of RIS.

In the future 5G advanced and 6G wireless networks, many new applications strongly impose requirements on both the communication and sensing performance. Integrated Sensing And Communication (ISAC) systems are envisioned as a promising technology where the network has the capability to collect and extract information from the environments. Generally, sensing mainly depends on the Line of Sight (LoS) link between the transmitter and the target for the cellular based ISAC system. It is quite challenging to sense targets without LoS connections. And in the legacy system, only either Base Station (BS) or User Equipment (UE) can be considered as valid entity to conduct the sensing operation. Such services are only available in the localized region and additional set-up (including RFs) may be required. Moreover, the sensing performance (e.g. localization) of BS will be decreased with the increase of target distance from the receiver. By deploying RIS, a LoS link can be established to provide the sensing service for the NLoS areas and an extra LoS reflected link can be provided by the RIS to sense the target from a different angle, thus the sensing performance of the RIS-assisted networks can be significantly improved. Further, the different type and capabilities of assisted RIS, e.g. the fully-passive RIS and the semi-active RIS, can be considered according to the different scenario requirements of the RIS-assisted ISAC systems.

3.4.6 Energy efficiency

Wireless power transfer – Wireless power transfer has been proposed to enhance the use time of devices powered by batteries. The RIS can realize the power transfer between the BSs and users when the signals are blocked between the transmitter and energy harvesting users. With the assistance of RIS, the users can not only receive the communication signal, but also the harvested energy from the RIS, permitting a reduction of transmit power and improving the energy efficiency.
Energy harvesting – Current wireless networks have been designed primarily for communications purposes, in turn allowing other use cases such as communications-based positioning. Therefore, in existing wireless networks, even low-power devices such as Internet of Thing (IoT) devices, wireless sensors, and Machine to Machine (M2M) type devices still rely on an external power source, e.g. a battery, for communication. Since radio waves can carry both information and energy, RIS is a promising component in self-sustained wireless networks because RIS can enhance both information and energy transfer performance. For example, RIS may be partitioned and some of RIS elements or partitions could be utilized for collecting radio-frequency energy from the environment, while other RIS elements or partitions could be used for aiding communication. Deployment of the RIS could be simplified, one of the main reasons is that it does not rely on external power source(s) if energy harvesting for RIS is possible. In some cases, RIS may be integrated onto IoT devices to harvest the energy and directly power such devices. Signal energy may also be focused to other devices for enhanced energy harvesting at the devices.
Power saving –With the highly demand data rate requirements of future wireless networks, the energy consumption has been a great concern. Many energy-efficient solutions have been developed to ensure green and sustainable wireless networks. The network performance in terms of coverage and data rates can be significantly improved by deploying RIS, less BS transmit power and fewer BSs would be required in the RIS-assisted scenario to achieve a given coverage or data rate target. RIS-assisted deployments can be an attractive solution to enhance network performance, while reducing network energy consumption and improving network energy efficiency compared with legacy amplify-and-forward relay solutions. Similarly, deploying RIS can also improve the energy efficiency of users considering the uplink transmission assisted by the RIS. In other words, RIS can be considered as an energy efficiency enabler for the future wireless communication networks.

The available RIS hardware architectures can be classified into passive, hybrid, semi-active and active types according to their capabilities to manipulate the impinging signal. A passive RIS consists of passive or nearly passive components that might not require dedicated power supply, enabling connectivity for massive connections with extremely low power consumption and minimal complexity. An active and semi-active RIS, on the other hand, may embed radio-frequency circuits, signal processing units or power amplifiers.

The RIS power consumption depends mainly on the type and resolution of its individual reflective elements. Both passive and active RIS are designed to consume less power than the traditional solutions such as micro BSs or relays. Although the active RIS requires additional power dissipation to support its active load impedance, its basic operating mechanism remains the same as that of passive RIS, directly reflecting the incident signal and making the required adjustments at electromagnetic level.

Using RIS as a part of new solution for indoor and outdoor radio access networks will help to reduce the power

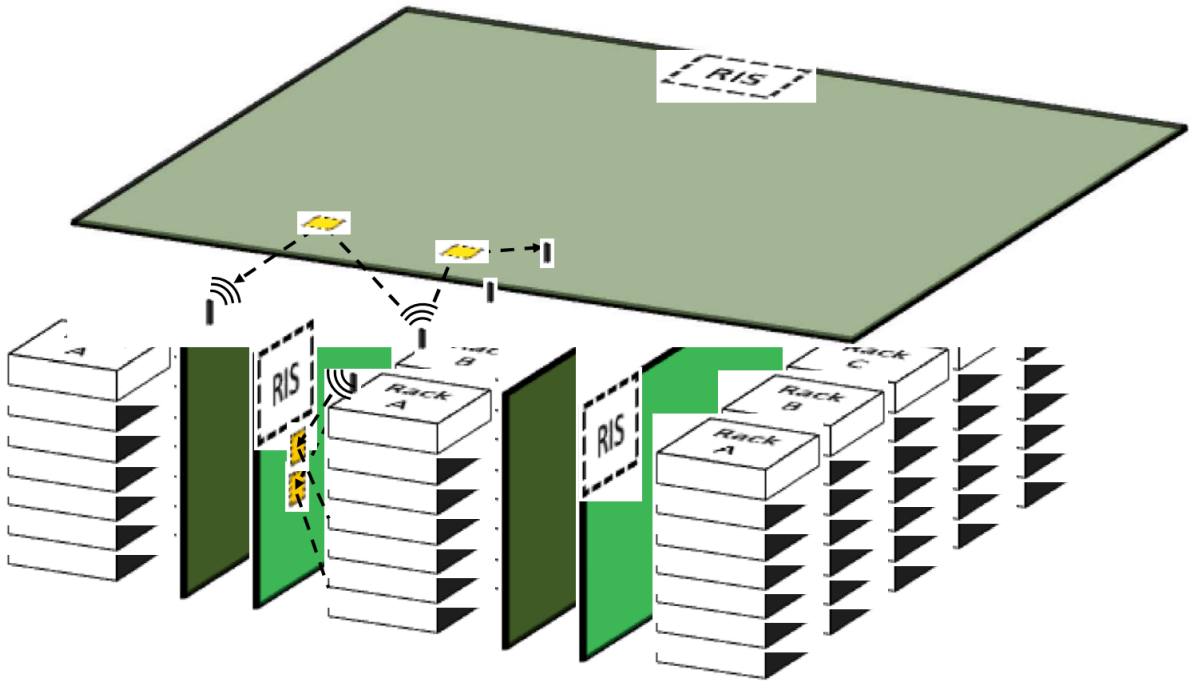

Figure 3.10: Programmable wireless data centers with RIS installed (Credits: ETSI ISG RIS)

consumption of the network. Specifically, to provide coverage to a given area, RIS-assisted networks require less BSs to be deployed.

EMF exposure minimization – Another perspective of the power consumption is the ElectroMagnetic (EM) exposure to human bodies. There are requirements for arbitrary low EM thresholds for certain services and/or in certain areas, as required by some customers or the regulatory bodies of some regions. Thus, one of the potential requirements for next-generation networks is to limit the level of transmission power to meet requirements for low EMF exposure, while guaranteeing the network performance.

Using RIS as network nodes can help limiting EMF exposure in two different ways. Using RIS can help to provide coverage and enhance transmission without significantly increasing the transmission power of the network and/or the user equipment, and thus, limiting the EM exposure level around the BS and/or close to the UE. Certain optimization can also be carried out jointly for BSs and RIS to meet strict EM constraints in special deployment scenarios.

3.4.7 Programmable Wireless Data Centers

Agile network management system in data centers can require advanced technological solutions, such as RIS, to alleviate the cabling cost and boil down the overall connection complexity. Each server placed in the data center is connected with a wireless connection component enabling communication via directive wireless propagation via the physical propagation elements of the RIS. RIS can be placed on the rear panel of the racks as well as walls and ceiling to dynamically and remotely control directive wireless communication links, e.g. TeraHertz or mmWave technologies, between different servers within a single rack i.e. intra-rack connection management, and between different racks, i.e. inter-rack connection management, as shown in Figure 3.10. Given the daunting complexity of setting-up and controlling such a system, machine-learning-based approaches can be deployed to automate the multiple processes required in a systematic manner. This RIS-based solution can enable a new level of automation in data-centers (re-)configuration as well as resilience to hardware failures and upgrades.

3.5 ISG-RIS Deployment Scenarios

Whilst there are clear benefits and capabilities offered by RIS, its deployment still remains on the conceptual level. RIS may require a very large number of unit-cells to achieve significant performance gains. This in turn renders the effective configuration of the RIS response in a dynamic fashion challenging. RIS may also require rapid channel sounding operations to estimate channels between the RIS, TRPs, and UEs. However equipping RIS with signal processing capabilities would increase the deployment cost due to hardware, but also reduces the attractiveness of RIS in terms of ease of deployment, as well as increasing the complexity of the algorithms and protocols needed for its seamless integration. It is therefore important to develop a clear understanding of where RIS may serve as an attractive deployment solution versus other technologies.

3.5.1 Operating environment

Indoor scenarios – For indoor scenarios, line-of-sight transmission cannot be guaranteed in some areas such as corridors, corners and stairs. In addition, shadow fading may be serious due to the influence of obstacles such as human bodies and furniture. Deploying RIS on the surface of walls or furniture can establish additional transmission links to improve coverage, increase received signal strength as well as SNR. Data rates can be improved for individual users and the overall system throughput can be improved as well. Indoor scenarios such as automated industrial factories may also benefit from the improvements in localization accuracy.
Outdoor scenarios – For outdoor scenarios, mobile terminals and UEs at the edge of the cell or in the shadow area may suffer serious propagation loss including path loss and shadow fading caused by obstacles such as buildings or trees. RIS can be deployed on the facade of the building or along with base stations to establish additional transmission links. In this way, the performance of these terminals can be significantly improved. In outdoor environment, mobility can become more significant than indoor scenarios, especially considering that UEs on high speed trains can travel at a speed of 350 km/h. In this case, dynamically reconfigurable phase shift matrices on RIS are needed for fast beam tracking.
Hybrid scenarios – Hybrid deployment scenarios for RIS involve both indoor and outdoor environment, or describe a mixed environment which is hard to be characterized by any single scenario. One example of hybrid scenario is the outdoor to indoor scenario. It is challenging for base stations deployed outdoors to serve indoor users due to the signal attenuation introduced by the walls or window glasses. The attenuation is more significant in FR2. One conventional solution is to deploy micro-BS inside the building, which is of high cost. In this scenario, RIS are placed on facades of buildings or are manufactured as transparent surfaces which can also be used as window glasses. The RIS placed on facades can reflect signals to indoor environment of another building. RIS used as window glasses, which are usually transparent, can focus the incident signals into certain areas in the room and achieve good coverage. The focus points of such transparent RIS can be pre-configured according to indoor environment or dynamically changed based on real-time demands.

3.5.2 RIS deployment

Static RIS – In a typical deployment, the RIS is mounted on a stationary structure, such as a building wall. In such a deployment, the radio channel between a stationary base station and the RIS is largely static. The radio channel between the RIS and a UE as well as between the base station and the UE may experience fast fading due to movements at the UE side.
Nomadic RIS – Nomadic deployment option assumes possibility for RIS to change its physical location or orientation in time. In some deployments, the RIS may be mounted on a non-stationary structure, such as a train or a vehicle. For nomadic deployment of RIS, multiple scenarios are considered depending on where the RIS is integrated including personal RIS, UE-integrated RIS, vehicle-integrated RIS.

In such a deployment, the radio channel between a stationary base station and the RIS as well as between the base station and the UE may experience fast fading due to a moving RIS and a moving UE. However, if the UE is moving with the non-stationary structure, for example if the UE is in the train, the radio channel between the RIS and UE may fade relatively slowly. On the other hand, if the UE is not moving with the non-stationary structure, the RIS to UE channel may fade rapidly as well.

Three cases have been idetified:

1. Personal RIS scenario – In the personal RIS scenario, RIS is owned by an end-user, and the user can change the location of RIS based on his own preferences without asking a permission from the network and without notifying the network. Typically, personal RIS is a physically small device that is located in indoor areas, for example, home or office spaces. The deployment option of multiple personal RIS within the same indoor area could also be considered.

2. UE-integrated RIS scenario – In another scenario, RIS could be integrated into a user device, e.g. a mobile device. In this case, mobility of the device implies the mobility of RIS, including the dynamic change of both position and orientation.

3. Vehicle-integrated RIS scenario – Another common scenario for RIS deployment is placement of RIS on mobile vehicles such as cars, trains, buses, etc. In this case, the mobility of the vehicle determines the mobility of the RIS. Depending on the vehicle type, size, and location of operation, one or multiple RIS can be integrated onto vehicle's windows, roof, etc. Such nomadic RIS deployments could be facilitated by network operators, enterprise owners (operating the vehicles) and end-users (for personal vehicles).

3.5.3 RIS control plane

The RIS control plane comprises of a large set of functions, which run to trigger RIS configurations at different time scales and to acquire instantaneous RIS states. Control plane functions can be defined according to the RIS management as per the categories: i) BS Centralized management; ii) BS Distributed management; iii) autonomous RIS; and iv) UE-controlled RIS.

The RIS control plane controls a set of RIS and is responsible for the channel quality improvement for the selected DL/UL/SL links in the dedicated area. The following functionalities can be supported by the RIS control plane: 1) Channel measurements between RIS and network nodes, between RIS and mobile devices; 2) Positioning measurements. 3) RIS control mode selection; 4) RIS configuration selection, providing the selected configuration to the RIS; 5) Gathering and conveying to the RIS controller the relevant status information of data and control planes (e.g. users data buffer states, traffic patterns, resource allocation decision, QoS information, etc.)

RIS control plane can allow the abstraction of logical functions from the underlying physical technology. In this architecture option, link layer may comprise of links implemented based on different physical/MAC technologies, operating on different bands (in-band, out-band), being wired or wireless. RIS control plane can implement a specific scheduling mechanism for signalling within the RIS control plane.

Centralized management – Centralized management of RIS at the network side can assign and update one or multiple base stations to provide the necessary configuration for RIS. Essentially, the control plane is located at a central node, where the measurements and/or feedback information is processed, and corresponding decisions are made to update RIS configuration. Up on determining the updated RIS configurations, the central node shares the information with the BS(s) and instructs them to provide the updated configuration to RIS. In case of centralized management, coordination among the participating BS(s) is not necessary.

Distributed management – Distributed management of RIS at the network side is handled locally by the participating BS where the RIS control plane is located. The BS communicating with the RIS is responsible for processing the measurements and/or feedback information and making the decisions to update RIS configuration. For the distributed management, multiple BSs may communicate with RIS and in such cases coordination among the participating BS(s) is necessary to avoid any conflict. In addition, multiple RIS can be managed by multiple distributed BSs, based on cooperative schemes, in order to achieve the optimization of the network's system metric, such as improving the achievable sum-rate performance.

Autonomous RIS – Autonomous RIS is capable of optimizing the gain of a reflected beam between a base station and a user equipment without requiring dedicated control-plane functions. Autonomous RIS can require power sensing capabilities, falling into the Hybrid RIS category, as per clause 4.2.3 of the present document. Autonomous RIS can acquire a power profile through a sequential activation of probing beams. In particular, an autonomous RIS can obtain the angular position of the base station and the user equipment by identifying power profile peaks in

the acquired power profile. The autonomous RIS can locally compute the optimal configuration and autonomously trigger it based on the angular positions.

UE-controlled RIS – In an indoor deployment scenario, RIS can be deployed as part of a personal network or local access network. The local access or personal network can be the one operating in unlicensed spectrum such as a WiFi network or the one operating in licensed spectrum such as a Customer Premises Network (CPN) 3GPP TR 22.858 or Personal Internet of Things Network (PIN) 3GPP TR 22.859. As CPN and PIN are identified as small-scale, personal networks within the coverage area of a public network, the personal network entities such as evolved Residential Gateway (eRG) for CPN and PIN element with management capability for PIN are responsible for network management and/or control aspects. For WiFi networks, the WiFi access point(s) that provide(s) the coverage is responsible for network management and control aspects. Moreover, it is expected that the UEs belong to these personal and local access networks may have either direct or indirect connections or both.

3.6 Conclusion

This chapter has summarized relevant use cases and deployment scenarios for RIS according to the recommendations from ETSI RIS, which will be considered as departing point for the research work conducted in the project.

Chapter 4 : Performance Metrics and Advanced PHY Layer solutions

4.1 Performance Metrics in Cell-Free Networks

The performance of modern radio access networks is essentially (at least in dense areas) limited by in-band interference, more specifically interference from users and/or base stations in close geographical proximity; this is due to the necessity to operate in a limited bandwidth, which imposes some degree of spatial reuse of the available radio spectrum. However, the impact of this interference on the network performance is affected by several factors:

Receiver-side processing and interference cancellation: If a receiver is able to decode and cancel interference rather than treat it as noise, the effective SINR for the remaining users is increased. In a large radio access network, we expect every signal to be decoded at some point in the network. Thus, in principle and considering an ideal centralized joint decoder, all interference could be canceled. In practice, there are limitations due to (i) the amount of information exchange required for the implementation of a fully joint decoder, and (ii) the latency it would create if applied to large geographical areas.

Transmitter-side coordination and waveforms: The impact of in-band interference can be partly mitigated through proper resource allocation and precoding, if the overhead (in terms of computing, signaling, and latency) associated with this coordination can be tolerated. On a deeper level, the choice of waveforms, coding rate, and the pilot allocation strategy will have an impact on the ability of the receiver to perform efficient multi-user interference cancellation with acceptable complexity.

The above discussion highlights the following important points:

- Information-theoretic models and metrics alone are not sufficient for the purpose of qualifying the performance of a large, multi-site network; algorithmic limitations (in particular, those associated to the complexity and latency of the distributed processing expected to take place in cell-free networks), should be taken into account.
- Transmitter-side coordination can have a major impact on performance, however it typically involves significant overhead; whether this overhead is acceptable in turn depends on the type of traffic (e.g. synchronization overhead may be negligible in eMBB applications but become a dominant factor when considering sporadic IoT-type traffic).

Thus, a sound performance evaluation framework should establish a trade-off between reliability and efficiency metrics (spectral efficiency, area spectral efficiency, energy efficiency...) and the resources in terms of computing and signaling overhead required to achieve them; it should take into account the targeted class of traffic.

4.1.1 Metrics of Interest

Typical metrics in use to evaluate the performance of wireless networks are typically a combination of a few relevant quantities:

- per-user and aggregate throughput,
- latency,
- reliability (packet error rate, end-to-end delivery time…),
- radiated power,
- consumed power (including overhead such as computing, cooling, power amplifier efficiency etc.),
- PAPR,
- bandwidth.

For single-cell scenarios, fundamental bounds from information theory can provide relevant benchmarks since the channel is sufficiently close to canonical models such as the broadcast (downlink) or multiple-access (uplink) channels. Furthermore, the performance of a given approach can often be characterized (sometimes approximately) analytically, and compared to the fundamental limits, allowing to draw universal (e.g. regardless of algorithmic choices) and fairly interpretable conclusions. For instance, the spectral efficiency or the packet error rate achieved by a given approach can be compared to the fundamental limits provided by the channel capacity region and the finite blocklength capacity, respectively.

Conversely, in a multi-cell scenario, the situation is more intricate since the cell density plays a major role in many performance trade-offs. Cell density can be modified through the inter-site distance, or through dynamically powering on or off some of the access points or carriers; it impacts both the signal and the interference part of the signal-to-interference ratio (SINR) analysis, and thus analyzing its effect on the overall system performance is non trivial, especially when taking into account the impact of propagation, antenna array design, signaling, spatial reuse of pilot and spectrum, algorithmic choices, etc. In multi-cell scenarios, it is generally more difficult to obtain analytical performance characterizations allowing to draw universal conclusions about the relative merits of the proposed approaches; in that case, one has to resort to numerical simulations.

In the cell-free context considered in NF-PERSEUS, some analytical performance characterization results have been derived [61] [59] under simplified assumptions regarding e.g. propagation, synchronization, etc. However, we expect that a significant amount of numerical evaluations will be required when considering non-trivial combinations of propagation, hardware, signaling, and algorithmic architectures.

Thus, we suggest to focus on a small number of prototypical systems and scenarios, for which the baseline approaches and the novel contributions developed in NF-PERSEUS will be evaluated using either analytical or numerical approaches.

4.2 Hardware-aware Precoding/Combining for Cell-free massive MIMO

4.2.1 Introduction and Motivation

Cell-free massive MIMO (CF-mMIMO) has emerged as a revolutionary wireless technology leveraging the most advantageous features of ultra-dense networks and cellular mMIMO technology while mitigating their associated drawbacks.

Unlike conventional cellular networks, where the coverage area is divided into disjoint cells served by individual base stations, CF-mMIMO systems rely on a large number of distributed access points (APs) connected to a central processing unit (CPU). This distributed architecture aims to provide seamless wireless coverage and capacity across the entire coverage area without cell boundaries. Very recently, a new scalable version of the CF-mMIMO was introduced in [14], which incorporates fully distributed processing.

Although CF-mMIMO shows great promise in improving wireless communication, its real-world implementation faces practical challenges [4]. One notable challenge is the densification aspect of CF-mMIMO, which can lead to

increased system efficiency but comes with the trade-off of higher energy consumption and hardware costs. Indeed, the impact of hardware quality on CF-mMIMO systems is particularly significant, especially when both APs and UEs are equipped with high-quality hardware components. However, the use of low-cost hardware may be appealing due to its affordability, despite the potential downside of decreased system efficiency. Therefore, it becomes crucial to strike a balance between hardware cost and system performance to optimize the overall effectiveness of CF-mMIMO deployments.

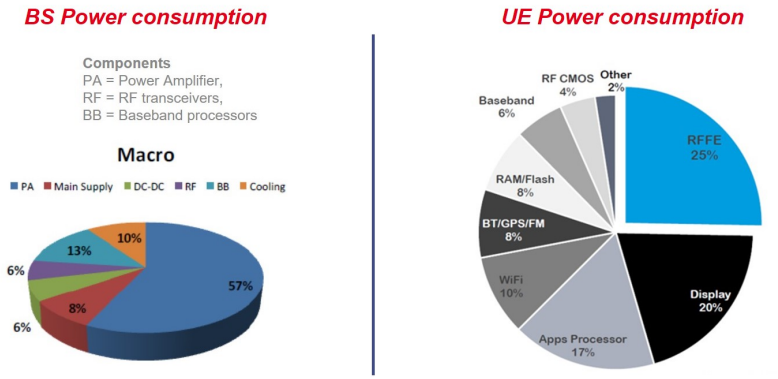

Figure 4.1: Power Consumption at BS and UE

As shown in Fig. 4.1, Power amplifiers (PAs) are among the most energy-consuming components in both base stations and UE in wireless communication systems. Within this framework, PA non-linearity (NL) stands out as a significant hardware impairment (HWI) within the analog transmission chain of communication systems. Specifically, the non-linear distortion (NLD) introduced by non-linear power amplifiers (NL-PAs) can degrade both channel estimation and data transmission.

4.2.2 Methodology, current achievements

In broadband multipath wireless channels, encountering significant delay spread results in frequency-selective fading, particularly in sub-6GHz bands. To effectively mitigate such channel imperfections, adopting orthogonal frequency-division multiplexing (OFDM) scheme proves to be the most effective approach. OFDM encodes digital symbols across multiple orthogonal subcarriers, thereby enabling robust transmission in frequency-selective fading channels.

Thus, we propose combining OFDM with the scalable version of CF-mMIMO. This combination represents a highly promising solution to address the escalating demands for higher data traffic and enhanced link readability. Following 5G-NR, based on TDD mode, the uplink (UL) and downlink (DL) transmissions share the same frequency band but are separated in time.

Our focus was on examining the effects of NL-PAs on both the UL and DL transmissions of CF-mMIMO-OFDM systems. Specifically, in the UL scenario, user equipments (UEs) are equipped with NL-PAs, necessitating the development of an iterative non-linear distortion (NLD) cancellation technique to mitigate the impact of NL-PAs on transmission performance. Existing studies in the literature have predominantly focused on examining the impact of HWIs at APs and/or UEs on the performance of CF-mMIMO systems, rather than addressing strategies to mitigate this effect. In our works, we proposed techniques that can be implemented in a distributed and scalable fashion, achieving benefits of CF-mMIMO-OFDM while taking into account the effects of hardware impairments caused by NL-PAs.

OFDM-BASED UL CF-MMIMO UNDER HWIs

The presence of NL-PA at UEs affects both channel estimation and UL transmission. Consequently, we introduced in [85,86] two NLD cancellation algorithms adequate for the scalable CF-mMIMO-OFDM systems. These algorithms

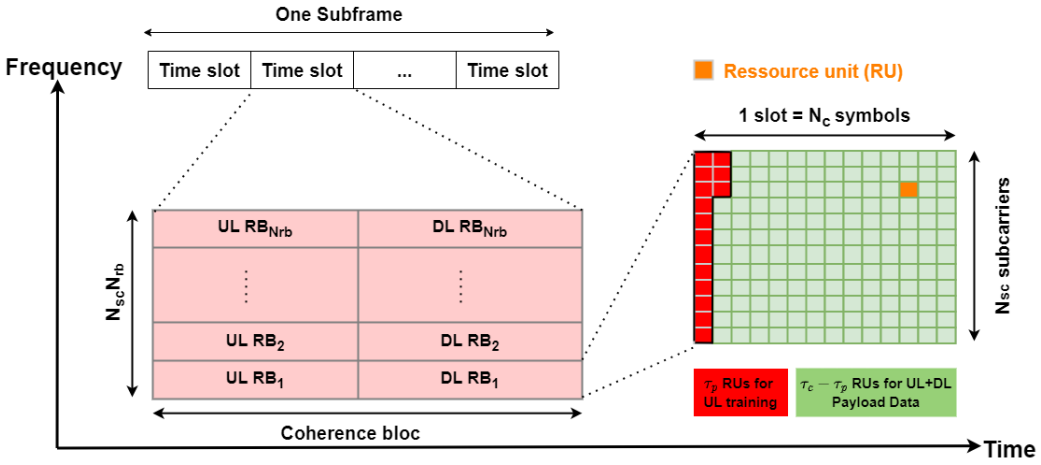

Figure 4.2: OFDM TDD frame structure.

are designed to enhance the accuracy of channel estimation and mitigate the NLD effects on the UL transmission phase. As shown in Fig. 4.3, NLD cancellation is performed locally at each AP in a distributed manner. Notably, this implementation has the potential to simplify the system architecture by eliminating the need for additional processing at both the UEs and the CPU.

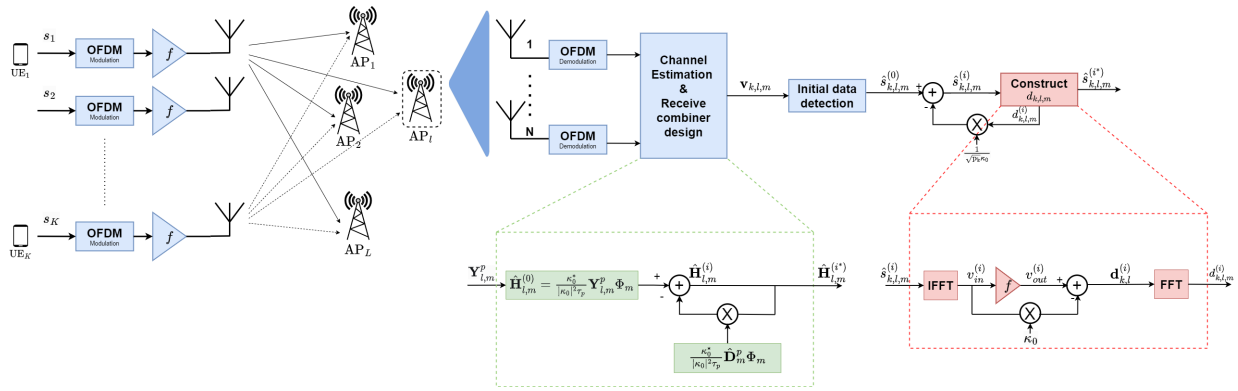

Figure 4.3: CF-mMIMO-OFDM system with NLD cancellation algorithms. The algorithms are implemented in a distributed manner, i.e, They are executed locally at each AP.

The proposed successive NLD cancellation techniques tries to mitigate the effects of using NL-PAs by estimating and subtracting the distortion signal from the received signals (pilot symbols and data symbols). The initial estimated distortion is generally inaccurate, and the iterative process is used to refine the remaining distortion. The iterative cancellation algorithm is mainly based on the following main steps : initial symbol estimation, distortion approximation and distortion removal.

1. Initial information estimation : This step involves the initial estimation of the symbols (pilot/data) that were originally transmitted by UEs. This estimate is used as a starting point for the distortion approximation and removal steps.

2. Distortion approximation : In this step, the initial symbol estimate is used to estimate the distortion between refined signal and the received one. We note that the NLD cancellation approach in channel estimation and data transmission differs based on the available information. In fact, in channel estimation, the presence of known

pilot symbols at APs provides a reference for approximating the distortion term, while in data transmission, the absence of this prior knowledge imposes a different distortion approximation method.

3. Distortion removal : After approximating the distortion, the goal of this step is to remove the estimated distortion from the symbol estimate.

Steps 3 to 5 are repeated iteratively.

The outcomes of the simulations have indicated that the proposed technique has a great promise in mitigating the significant impact of HWIs, improving the spectral efficiency (SE) and energy efficiency (EE) performance of the UL CF-mMIMO-OFDM systems.

OFDM-BASED DL CF-MMIMO UNDER HWIs

CF-mMIMO-OFDM systems exhibit a high peak-to-average power ratio (PAPR) during signal transmission. Hence, the commercial viability of CF-mMIMO-OFDM systems is only possible if APs are deployed using power-efficient and low-cost hardware. However, transmitting signals with high PAPR using such hardware leads to significant HWIs, primarily caused by NL-PAs. As shown in Fig. 4.4, we note that the distortion induced by the NL-PAs is directly proportional to the power allocated to the desired signal. Consequently, UEs with stronger channel gains, i.e., the most robust connections, are disproportionately affected by this distortion, while weaker users experience less impact. In classical massive MIMO systems, which typically involve co-located antenna arrays at the BS, a

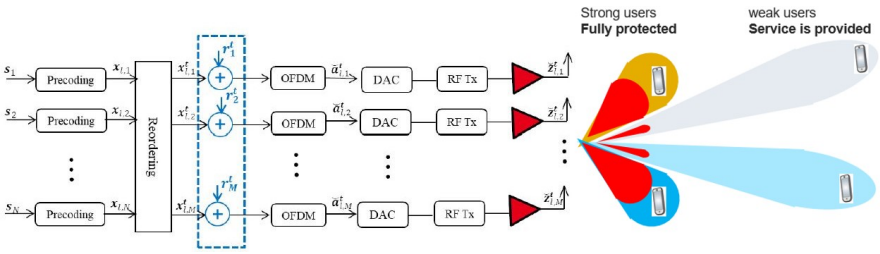

Figure 4.4: Beamforming without taking into account HWI.

significant number of degrees of freedom (DoFs) are available due to the large number of antennas compared to the number of served UEs. Several techniques have been proposed and investigated in the literature to exploit these DoFs for PAPR reduction, as documented in references [8, 139, 140].

These techniques are impractical in centralized CF-mMIMO-OFDM systems, where high-capacity front-haul connections are needed to enable data transfer between APs and a CPU. In response to the challenges posed by heavy front-hauling overhead in centralized CF-mMIMO-OFDM systems, we propose a novel PAPR reduction technique that operates locally at each AP. This technique eliminates the need for instantaneous information sharing, thereby reducing front-hauling overhead significantly.

The proposed solution revolves around anticipating and mitigating distortion in transmitted signals. Rather than subjecting signals to high PAPR that leads to severe, uncontrollable distortion from NL-PAs, our approach opts for transmitting low-PAPR signals [138].

The key idea of our proposed solution, as shown in Fig. 4.4, is that each AP: (i) computes the frequency-domain precoded signals $\{\mathbf{x}_m^t, \forall m\}$, which are the reordered versions of $\{\mathbf{x}_n, \forall n\}$ and (ii) optimizes frequency-domain signals $\{\mathbf{r}_m^t, \forall m\}$, referred to as peak-canceling signals (PCSs), that reduce the PAPR of the resulting OFDM modulated signals $\{\mathbf{a}_m^t, \forall m\}$. Frequency-domain PCSs are fine-tuned to ensure that distortion affecting the strongest UEs is minimal or even eliminated, while distortion affecting the weakest UEs remains within acceptable limits. In particular, distortions associated with PCSs are directed towards the weakest UEs in a flexible manner, allowing us to maintain service continuity for these UEs.

4.2.3 Future works

Joint PZF and Hardware aware precoding/combining

In the proposed techniques, we have evaluated and compared the performance of different combining/Precoding techniques at the APs. It is shown that partial zero-forcing (PZF) combining/precoding scheme outperforms other alternatives in terms of SE. The PZF scheme operates by categorizing UEs into strong and weak sets according to their path loss, with a predefined grouping threshold. Typically, as mentioned in prior studies [20, 144], this grouping threshold is set manually. However, by dynamically adjusting the grouping threshold based on the current environment and channel characteristics, the PZF scheme can effectively adapt to changes in the strength and distribution of UEs, thereby maximizing SE and overall system performance.

In the realm of CF-mMIMO-OFDM, addressing the dual challenge of minimizing PAPR and improving signal quality is crucial. In response to this challenge, we aim to introduce a joint distributed technique for PZF precoding and PAPR reduction. Since the grouping strategy is instrumental in controlling the distortions in the context of PAPR reduction, the grouping threshold should be adjusted based on the system requirements and the optimization goals. Hence, the idea here is dynamically adjust the grouping thresholds depending on the specific objective being considered: either PAPR reduction or PZF precoding. This dynamic adjustment ensures that the system optimally adapts to the requirements of each objective, enhancing performance accordingly.

In the same direction, for PZF combining, we aim to adopt an adaptive grouping strategy that adapts to changing channel conditions and maximizes the SE jointly with NLD cancellation. In other words, we choose the optimal grouping threshold ensuring a balance between inter-user interference and desired power enhancement.

Sequential precoding for cell-free with serial fronthaul

We consider the serial fronthaul topology in CF-mMIMO-OFDM systems where APs are connected in a chain-like fashion. This topology enables the transmission of HWI between APs in a successive manner. This means that the HWI data is communicated from one AP to the next in a sequential fashion along the fronthaul network.

We aim to introduce a sequential hardware-aware precoding scheme designed to uphold the constructive summation of contributions from each AP while mitigating the impact of hardware-induced distortion received by UEs on every subcarrier. This is achieved through the exchange of local channel state information and estimated distortion noise among successive APs.

4.3 Precoded Filter Bank waveforms

4.3.1 Introduction and Motivation

New wireless systems aim to cover a wide variety of application scenarios. Applications ranging from the connectivity of thousands of devices with low power consumption to high mobility scenarios with high transmission rates. In this context, a waveform that can optimize the use of the available spectrum is essential in addition to mitigating the various challenges present in the communication process in order to provide more stable and efficient communications. Orthogonal Time Frequency Space (OTFS) technology has emerged as one of the promising solutions to face such challenges and is an alternative to Orthogonal frequency-division multiplexing (OFDM). Its ability to provide ultra-high data rates, low latencies and, above all, robustness in high mobility scenarios, make OTFS an interesting alternative within the 5G ecosystem [49]. Operating in the delay-Doppler (DD) domain, the OTFS technique can be seen as a 2D Fourier transform introduced before the OFDM system. This makes OTFS convert time-varying channels into invariant channels in a DD domain, making it robust in high mobility scenarios. On the other hand, Filter Bank Multicarrier (FBMC) systems have received a lot of attention to guaranty good time-frequency localization and robustness to asynchronism. However, the complex orthogonality criterion is not satisfied since the filter bank itself generates self interference in the system. Various precoding techniques have been proposed in the literature in order to compensate for this interference and restore the complex orthogonality [27, 137]. In many cases, the basis is to spread the symbols across the entire time band or across all subcarriers for this purpose [94] [100].

4.3.2 Methodology, current achievements

In [69], the authors have introduce a filter-bank system with complex orthogonality as an alternative waveform to OTFS. By employing part of the OTFS scheme, specifically part of the Symplectic Finite Fourier Transform (ISSFT), the complex orthogonality of the system is recovered, resulting in a waveform that incorporates the main characteristics of OTFS systems and and the use of well-located filters. The robustness in high mobility scenarios and better spectral localization stands out. This new structure allows also the use of low complexity equalizers in the time frequency domain. Figure 4.5 illustrates the complete block diagram of the 2D-FFT filter bank system.

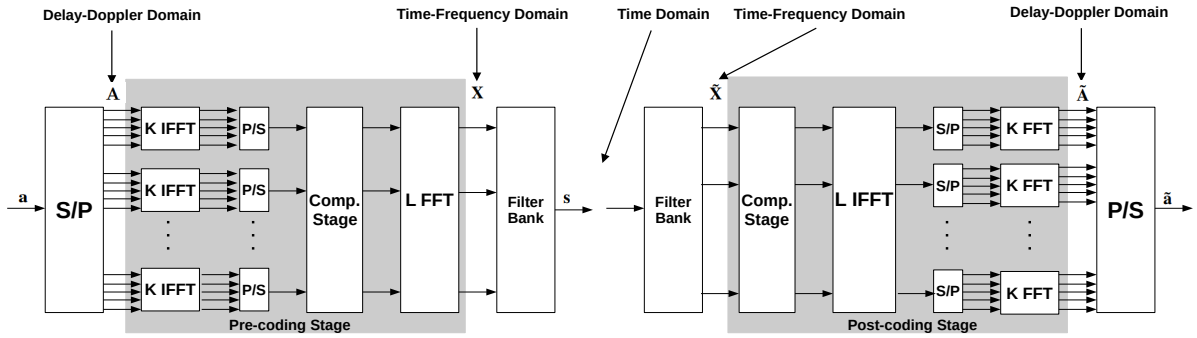

Figure 4.5: Block diagram of the 2D-FFT filter bank system

Simulation results have shown that the presented technique presents the same benefits as the OTFS technique such as low latency, robustness to high mobility scenarios and also the benefits of the FBMC technique such as good spectral localization. Furthermore, due to the filtering process, the system presents good error performance in high mobility scenarios using a simple equalizer in the frequency domain, a performance that cannot be obtained with OTFS modulation.

In [68] we have proposed a generalization of the so called 2D-FFT filter bank by making changes in the waveform structure to obtain advantages in the symbol detection process. We have shown that by relaxing the rate factor of the filter bank structure, the proposed scheme achieves a greater robustness in different application scenarios. We have also perform a detailed analysis of the impact of this generalization in terms of PAPR and error performance via the signal-noise-plus-interference ratio (SINR) and the signal-interference ratio (SIR).

4.3.3 Future works

In this workpackage, we will generally speaking propose and study waveforms for cellular and cell free MIMO systems taking into account the main KPI (complexity, out of band radiation, robustness to non linearities, MIMO compatibility, ...). We will also study channel estimation in the context of 2D-FFT filter bank scheme and evaluate the potential of those waveforms in the context of the integrated and sensing communication (ISAC) [134]. The optimization of the prototypes filters for filtered multicarrier communication will also be studied [40] [24]

4.4 Waveform transceiver design for improved robustness to impairments

4.4.1 Context and motivation

Since the introduction of the 4G/LTE, the data traffic increases significantly each year and new wireless applications and services are continuously emerging [105]. This requires extremely reliable connections, with an availability of 99.999%. The latency also becomes a crucial constraint for emerging applications such as tactile Internet or factory automation. Finally, efficiency in terms of resources utilization, such as energy and radio spectrum, is becoming more and more critical.

Aforementioned services, including enhanced Mobile Broadband (eMBB), Ultra-Reliable low Latency Communications (URLLC), Vehicle to everything (V2X), etc), must coexist in a unique wireless environment. This introduces

new challenges, requiring investigation on new techniques to fulfil network constraints, from the application layer to the physical layer. For the latter, the current Orthogonal Frequency-Division Multiplexing (OFDM) waveform used in 4G/5G may not be adapted to support all the resulting constraints [122]. In fact, OFDM represented an attractive solution thanks to its high robustness against multipath channel through the introduction of a Cyclic Prefix (CP), its orthogonality in both the time and frequency plane, its straightforward implementation with a Fast Fourier Transform (FFT), and the simple per-subcarrier equalizer. OFDM is also known to efficiently support multiple Multiple-Input Multiple-Ouput (MIMO) schemes [56] including massive MIMO.

However, the high Out-Of-Band Power Leakage (OOBPL) of OFDM compromises the coexistence of multiple services in the same band as foreseen in next generation systems. In addition, it requires strict synchronization with the base station in time and frequency for each user, which adds important signaling overhead. Consequently, the latency and the energy consumption are highly impacted. In fact, with the emergence of efficient resource allocation techniques for grant-free multiple-access, the support by the physical layer of relaxed synchronization becomes of paramount importance. The waveform plays the central role in this regard. In this context, candidate waveforms for beyond 5G will be investigated with a special focus on Filter Bank Multi-Carrier (FBMC)/Offset Quadrature Amplitude Modulation (OQAM) [104] [53] and transformed domain waveforms such as Orthogonal Time-Frequency Space (OTFS) [49].

However, filtered waveforms are considered several times more complex than state-of-the-art OFDM. Particularly concerning FBMC, the use of the OQAM scheme requires to duplicate the processing units (or to double the processing rate) when compared to OFDM. In addition, the filtering stage may introduce a non-negligible complexity increase. Therefore, it is of high interest to investigate novel algorithms and hardware optimizations in order to reduce the complexity and the energy consumption of these waveforms. While FBMC/OQAM offers several interesting advantages with respect to OFDM, it has few important issues that need to be addressed. For instance, the filtering operation introduces a ramp-up and ramp-down transitions at the beginning and the end of each transmitted frame. To avoid significant spectral efficiency loss, the frame duration must be increased. However, beyond 5G systems aim to use short frame sizes for several communication scenarios in order to reduce the latency. In addition, certain techniques designed for OFDM are not directly applicable to FBMC due to the OQAM scheme. Among these techniques, there are the pilot structure for channel estimation, the FFT-spread to reduce Peak-to-Average Power Ratio (PAPR), and the efficient support of MIMO schemes. Finding appropriate solutions to these technical issues is crucial if a filtered waveform is adopted for certain services in future communication systems.

4.4.2 Tackled challenges and study objectives

The scientific and technical objectives can be summarized as follows:

- Physical-layer support for service coexistence within one waveform symbol in future networks.
- Limited out-of-band power leakage.
- Improved support of grant-free multiple access through relaxed synchronization.
- Improved robustness to time/frequency offsets and Doppler effects.
- Increased multiple access efficiency/Improved User separation.

The tackled technical challenges are:

- Filter design for reduced latency, improved user separation/performance.
- Advanced receivers for efficient interference management, service co-existence or numerology.
- Improved support of grant-free multiple access through relaxed synchronization.
- Efficient massive MIMO support.
- Reduced complexity transceivers for integration.

Chapter 5 : Algorithms for Radio Resource Management

5.1 Introduction

The **NF-PERSEUS** project (PEPR-NF PC3) aims at achieving power and spectrum efficient massive access in scalable B5G sub-7GHz networks, based on distributed massive multi-antenna (MIMO) infrastructures. In this context, workpackage 4 (WP4) deals with radio resource management and aims at introducing novel multi-user access schemes and resource allocation algorithms dedicated to distributed antenna systems. The work in WP4 is organized into two main tasks: 1) the proposal of new resource allocation algorithms dedicated to distributed massive MIMO (mMIMO) and 2) the study of novel non-orthogonal and grant-free multi-user (MU) access techniques.

This chapter provides an overview of the progress of the studies undertaken in WP4 and their progress by the end of 2023. It is organized as follows: Section 5.2 deals with resource management and innovative detection algorithms for non-orthogonal multiple access (NOMA) techniques. The first topic addresses the challenges of imperfect knowledge of the transmission channel while the second studies new multi-user detection algorithms for wireless transmission systems based on a quantum architecture. Section 5.3 describes two studies undertaken on novel grant-free MU access techniques, with the use of artificial intelligence/machine learning (AI/ML) techniques for system optimization. At last, Section 5.4 focuses more globally on optimizing resource management in cell-free massive MIMO (CF-mMIMO) systems. The first theme jointly addresses network architecture, resource allocation orchestration and multi-antenna processing. Then, the problem of resource allocation and precoding in the challenging context of centralized CF-mMIMO-OFDM based on the dynamic cooperation clustering framework is dealt with. Finally, the third topic studies the trade-off between interference avoidance through antenna collaboration and interference cancellation through NOMA techniques. Section 5.5 concludes the chapter.

Given that most of the WP4 tasks started in September or October 2023, the related work is still in its early stages. Therefore, for each topic, the state of the art is presented, as well as the various directions of research planned for the future.

5.2 Resource management and detection algorithms for NOMA

5.2.1 Leveraging channel predictions for improved fairness and sum-rate capacity of NOMA

Context

NOMA provides a possible way to increase the system capacity by scheduling multiple users on the same channel. The multiplexing can be done in the power domain [62] or in the code domain [74]. In power-domain multiplexing, the transmitter divides its total transmit power between the users that are scheduled in the same time-slot and/or on the same frequency. While this reduces the rate of each user compared with what it would have obtained had it been scheduled individually without the other users, the overall sum capacity can be increased under certain circumstances [32]. In order to experience these benefits, more computations are required at the receiver since the receiver has to perform successive interference cancellation (SIC). Furthermore, as mentioned in [95], the

improvements thanks to NOMA rely on perfect knowledge of channel conditions by the base station (BS), which is not always the case in practice.

NOMA has been shown to be beneficial is several different settings: in uplink and downlink [126], in Nakagami fading channels [5], for MIMO [80, 141], for visible light communication technology without [129] and with [83] optical intelligent reflective surfaces.

One of the problems in applying NOMA resides in determining which cluster or pair of users to be multiplexed, and how much power to allocate to each one of them, in order to achieve a given objective, which may include fairness [77, 78]. In these latter works, pairing and power allocation are obtained solely on the basis of information about the channel conditions at the decision instants, which is assumed to be perfectly known. However, some work has been carried out on the problem of power allocation when only imperfect channel information is available [121]. It has also been recently shown that by using predicted future channel information of users, proportional fair allocation (or other similar concave fairness objectives) can be improved for vehicular users [87, 93]. In earlier works, power allocation was performed based on the knowledge of parameters describing current channel conditions. This gives good performance when the channel parameters form a stationary sequence. However, when channel parameters are correlated, having some information on the future channel conditions can be helpful in the decision making. For example, if the BS knows that some user will be going through an area of poor signal strength (gray area, tunnel, etc.) in the near future, it may be useful to allocate some additional rate before this adverse event in order to improve fairness. The information on the future channel conditions can become available from signal-to-noise ratio (SNR) maps that give average SNR conditions of a particular geographical region as a function of time. When combining SNR maps with the mobility patterns of the users, the BS can predict future channel conditions and leverage this information in its decisions.

Objectives

Given that the knowledge of future channel conditions has been shown to improve fairness in vehicular networks, the overarching aim of this task is to leverage this same knowledge to design user-pariring (or clustering) and power allocation algorithms for both downlink and uplink NOMA in order to improve user fairness and sum-rate over a given time-horizon. Towards this aim, we divide this task into two different subtasks:

- In the first one, we shall investigate optimal joint user-pairing (or clustering) and power allocation under imperfect channel conditions in a given time-slot and quantify the gains with respect to OMA. This improves over the existing works in which user-pairing is fixed or given. Since future information is not perfectly known, this can introduce some suboptimality in the decisions compared to when the perfect information is given. This subtask will help understand how adversely imperfect information can influence the benefits of NOMA.
- The second task will consider the optimization problem of user-pairing and power allocation over a give time horizon instead of a single time-slot as is done in most of existing works. This dynamic optimization problem will be based on SNR maps and future channel information of users. We shall aim to characterize how much future information can help in improving the ergodic capacity or fairness as compared to the setting in which only the current information is used.

In both subtasks, we shall aim to characterize analytically the benefits of NOMA with channel predictions (or future information) and shall design lightweight user-pairing and power allocations algorithms [87, 93] since these problems are generally complex and impractical to be solved adequately in real-time.

5.2.2 Quantum algorithms for NOMA detection/decoding

Introduction and motivation

In the context of the Internet of Things (IoT), the scientific community and operators are interested in the wireless transmission of short packets (mainly upstream), resulting from the sporadic transmission of several hundred thousand nodes. Current technologies, based on the allocation of resources prior to transmission, are no longer suitable. Indeed, their establishment cost (bandwidth, delays) is too large compared to the amount of data to transmit. Ideally, one would therefore completely remove these resource allocation mechanisms, particularly for ultra

reliable and low latency communications (URLLC) applications [106]. To this end, a NOMA system identifies each node by a unique coded sequence which allows distinguishing it with a high probability from other nodes [109]. This approach introduces interference (which can be treated with signal processing techniques), nevertheless it allows for detecting the subset of active nodes at each moment at the BS. However, in practice, identifying active nodes is very expensive in terms of computational resources. Indeed, it is necessary to test all possible combinations to identify the most likely one. The search being done through an unsorted database, the maximum reliability is obtained by exhaustive search, whose complexity grows at least linearly in the size of the set with classical algorithms. There are sub-optimal routines to reduce this complexity, but at the cost of a performance degradation (in terms of detection reliability).

The emergence of quantum technologies opens new perspectives. Indeed, the exhaustive quantum search algorithms allow speeding up the computation time by exploiting the superposition principle [47]. Such algorithms have already been considered for the detection of transmitted data in a multi-user wireless transmission system [16], [128]. In particular, in [48], the Grover algorithm has been applied for the identification of active nodes and revealed an advantage over classical approaches. Nevertheless, there are many avenues for improvement. Our goal is to propose new multi-user detection algorithms for wireless transmission systems, based on a quantum architecture.

Methodology, current achievements

We consider a network where each user is assigned a unique code c_i. The bitstring of active users $(b_i)_{1\leq i\leq N}$ is given by $b_i = 1$ (resp. $b_i = 0$) if the i-th user transmits its code (resp. remains silent). The users' signals are propagated over the same channel and are observed at the receiver side as a summation of all transmitted contributions. In addition, we consider a transmission model where **all emitted signals arrive simultaneously at the receiver with the same amplitude** (thanks to a feedback loop for example). **We model the channel as a perfect one** with gain $h = 1$, along with an additive white Gaussian noise (AWGN) denoted by n. Thus, the received signal can be written as follows:

$$y = \sum_{i=1}^{N} b_i c_i + n \tag{5.1}$$

Our goal is to find the bitstring (b_i) that minimizes the error between the measured signal $\hat{y}$ and the reconstruction made from our solution:

$$\hat{b} = \underset{b_1,\dots b_N}{\arg\min} \left\{ ||\hat{y} - \sum_{i=1}^{N} b_i c_i||^2 \right\} \tag{5.2}$$

In a previous work, the team has considered the use of Grover algorithm to perform the minimum search.

Future perspectives

However, there is still room for improvement as the Grover algorithm is designed to find solutions which verify a binary constraint (for example, belonging to a set, verifying an equality or inequality,...). Meanwhile, the minimum search does not fall in this category. Although our previous study has used Grover to converge iteratively toward the minimum, there is still room for a more efficient search.

To this aim, we want to address two main research directions. First, we want to better customize the Grover algorithm to the specific needs of the targeted application. This can be done for the NOMA active user detection problem, but also for the configuration of reconfigurable intelligent surfaces (RIS) in collaboration with some project partners. In addition, we plan to consider the use of analog quantum algorithms, which opens the way for new algorithms, more appealing for the minimum searching case.

5.3 Novel grant-free multi-user (MU) access techniques

5.3.1 AI/ML techniques for distributed resource allocation in uplink NOMA

Introduction and motivation

Due to their dense deployment, machine-type devices (MTDs) produce a large amount of data to be transmitted. Moreover, the mobile data traffic still follows an exponential increase with time. Widely-used beyond-5G applications are expected to enforce a set of technical constraints such as massive connectivity, low latency and high throughput [6] despite the spectrum crunch. Therefore, the investigation of new multiple access techniques becomes of paramount importance towards meeting the aforementioned requirements. Driven by the above considerations, NOMA has been proposed as a promising multiple access method for such networks.

With NOMA, several users can be served at different power levels while simultaneously reusing a given classical orthogonal multiple access resource block made of the same set of time, frequency and space or antenna parameters. Although most studies related to power-domain NOMA focus on the downlink setting, some work recently considered the application of NOMA in uplink scenarios [22, 145]. Other studies have also shown that NOMA helps achieve massive connectivity and low latency communications [125], making it a promising candidate for next generation communication networks [89].

To reduce the signaling overhead, uncoordinated spectrum access has received significant interest in recent literature [7, 75]. That said, few works have considered the uncoordinated spectrum access in an uplink NOMA system. In fact, most of the available literature body on NOMA considers fully coordinated systems. Only a few recent works considered semi-grant free communication systems [31] and fully uncoordinated ones [66].

The use of reinforcement learning and game theory for uncoordinated resource allocation has also recently received increasing attention. Several studies [1, 133, 147] have considered reinforcement learning, and especially the multi-armed bandits (MAB) framework, to enable users to organize their transmissions on the available channels [133]. In the MAB framework, a set of players compete to find the actions, also called arms, that maximize their expected gain or welfare [13]. Since the arm rewards are previously unknown to the players, there is a need to achieve a trade-off between exploring the arms to learn their associated rewards, and exploiting the optimal arms to maximize the achieved gain. Multiple algorithms have been proposed to solve problems modeled using the MAB framework [1]. These algorithms have been widely used to study, among others, the opportunistic spectrum access problem in cognitive radio systems [79], and the uncoordinated spectrum access problem [133].

In future communication networks, adding relays and RISs could be a solution to improve the quality of the links, hence achieving higher spectral efficiencies to alleviate network congestion. A trade-off can always be made between increasing the coverage area and the achieved throughput. In addition to that, they can be used to restore communication links in damaged networks [131, 132]. In order to ensure low-latency and high data rates in massive networks, full-duplex capabilities at the relay/RIS level can be leveraged.

Proposed methodology, tackled challenges and objectives

To support the aforementioned key challenges for future networks represented by the never-ending increase in mobile data traffic and massive connectivity, the proposed work targets grant-free multiple access where data is transmitted without prior handshake with the base station to reduce both communication latency and signaling overhead. However, signal collisions arise in the absence of central coordination. We propose to mitigate these collisions through reinforcement learning techniques. Moreover, we propose to associate grant-free multiple access to NOMA since it enables the support of multiple connected devices on the same resource. Finally, the introduction of relays and RISs is expected to improve the link quality and hence enable higher spectral efficiencies while improving the robustness of the network to fault and congestion.

The scientific and technical objectives can be summarized as follows:

- Largely improve spectral efficiency for future networks.
- Design of auto-configurable networks with agility and flexibility to improve robustness to failures and congestion.

- Improve end-to-end delay and adapt resource allocation strategy to the requirements of the different traffic types (latency, throughput, etc.).

The tackled technical challenges are:

- Efficient management of the problem of signal collisions due to the uncoordinated spectrum access, i.e. due to the lack of a central controller and the distributed nature of the access demands.
- Efficient association of NOMA, grant-free access and relaying/RISs.
- Simultaneous support of the different traffic types in the same system, while satisfying the requirements of their corresponding devices.
- Evaluation of the impact of resource allocation algorithms, NOMA, grant-free access and relaying on network performance indicators such as number of served users, spectral and power efficiencies.

5.3.2 Distributed massive access processing for NOMA

Introduction and motivation

Several important scenarios are considered in the context of cellular networks and the NF-PERSEUS project, including those involving devices with specific communication patterns. One such scenario is the massive machine-type communication (mMTC), where a large number of devices transmit sporadic, small packets on the uplink channel, as also described in section 5.3.1. In traditional cellular communication, each device is allocated orthogonal resources prior to data transmission in the uplink channel through a *grant* mechanism. However, this orthogonal allocation requires signaling traffic to be exchanged on the control channels, which can be larger than the amount of data being transmitted by the device, and hence, may lead to inefficient use of resources. Consequently, *grant-free methods* [107] that eliminate or reduce control traffic are suitable for addressing these scenarios.

Naturally, removing the coordination introduces non-orthogonality, which results in the superposition of signals from some or all of the devices. The efficient recovery of device transmissions requires specific methods that are inherently related to NOMA and random access. Indeed, NOMA schemes have been the subject of a specific study item in 3GPP for potential inclusion in Release 16 (5G), particularly for uplink transmissions, as reported in [135]. Several of these schemes rely on the SIC technique. When part of the superposed signal is successfully recovered, it can be reconstructed and then subtracted from the superposition, thereby reducing its interference with the other signals, which can then be (better) recovered.

Focusing exclusively on the SIC technique, a recent family of random access protocols, sometimes promoted as *"modern random access"*, has been popularized in the past decade. It is mostly derived from the seminal protocol Irregular Repetition Slotted ALOHA (IRSA) [84], and a whole family of protocols [12, 97] have been developed. It is based on the SIC applied at the packet level. However, most importantly, assuming transmissions in time slots, it introduces and is based on *inter-slot* SIC: packets are transmitted several times, and recovering one of the replicas allows the removal of the signal for all copies, including those of other slots.

This method shares similarities with some NOMA techniques but can also be applied to any packet transmission technique. It has often been studied using an abstract and idealized channel model, such as a collision channel without feedback [88], to which the assumption of perfect inter-slot SIC has been added. As such, it has been studied as a random access technique and has renewed research in this field. Using methods from "*modern coding theory*", specifically density evolution for low-density parity-check (LDPC) codes, the seminal study [84] demonstrated how to characterize the performance of the IRSA random access protocol, optimize its parameters, and achieve high-performance results through numerical optimization (e.g., 0.965 packets/slot). It has been proven to asymptotically achieve a throughput of 1 packet per slot for infinite frame lengths [91], which is the maximum achievable throughput for the idealized channel model.

Adapting these methods to the context of grant-free mMTC in the context of cellular networks is thus of prime interest, and the objective of the related tasks of the project.

Proposed methodology, tackled challenges and objectives

The literature has proposed numerous variations of the IRSA protocol, exploring different enhancements and employing less idealized, more realistic channel models. Some of these variations have even closed the gap with the NOMA literature, for instance, by considering channel estimation [114] and SIC failures [35] and applying both intra- and inter-slot SIC [3, 72, 115], etc.

Building upon this body of work, our study will focus on variants of modern random access by considering realistic physical-layer features, including the capture effect. Our main objectives are to enhance their performance and practicality in the context of cellular networks. Specifically, we aim to introduce advanced NOMA techniques, including the methods developed in this project. IRSA-based protocols can work with any modulation, including already existing transmission schemes, and they do not necessarily require NOMA features such as advanced multi-user detection. However, they can certainly benefit from NOMA methods that improve SIC.

It is worth noting that some results of the IRSA literature, namely those obtained through density evolution, are valid only asymptotically when the frame size grows toward infinity. Thus, the non-asymptotic performance can be significantly lower, and it is difficult to evaluate precisely. However, this decrease in performance may be alleviated by using any form of external knowledge, feedback, or partial synchronization. Optimizing IRSA with one or both types of considerations is challenging, and we will study the application of AI/ML techniques, which can be helpful in addressing these issues. For example, in [54], an entire interaction protocol was learned through reinforcement learning with proximal policy optimization (PPO) prior to IRSA transmission, and slot selection was also performed through the policy model.

In summary, we aim to study variations of IRSA in realistic settings, incorporate NOMA improvements, optimize through AI/ML techniques, consider forms of feedback, and finally, perform actual experimentation.

5.4 Resource management for cell-free systems

5.4.1 Radio resource orchestration for CF-MIMO systems

Introduction and motivation

The challenge of future telecommunication networks is threefold: unavoidable energy efficiency, high quality of service and dynamic network deployment [149]. The open-radio access network (O-RAN) architecture defined by the Open-RAN Alliance is part of the solution. In the O-RAN, the fronthaul connects a set of geographically dispersed radio units (RU) to a distant O-cloud. Each RU is in charge of lower PHY functions and the O-cloud is organized so as to enable resource sharing and virtualization of higher-layer functions. To further enhance the flexibility, the O-cloud is split into an O-central unit (O-CU) connected via the midhaul to several O-distributed units (O-DU). The O-DU are not necessary colocated, some of them are interconnected and they operate intermediate network layers (radio link control, medium access control, higher PHY). The constraints imposed on the midhaul as well as the fronthaul are to be considered for an holistic approach. [42] generalizes the O-RAN architecture and it points key elements to be considered with a view to optimizing. Another part of the solution to take up the threefold challenge is cell-free massive MIMO [92]. It consists in deploying a large number of multi-antenna RUs that serve fewer single-antenna user equipments (UE) for each time-frequency resource unit. Multi-antenna processing (MAP) combined with power control ensures multiple access. Improvements of the original scheme were necessary to ensure scalability at the expense of a limited degradation of the throughput (see e.g. [14]): they rely on dynamic user-centric cluster definition with locally-estimated chanel state information (CSI) and locally-processed MAP. Different issues raised by the combination of cell-free massive MIMO with O-RAN architecture are considered with some outline solutions in [102]. The radio channel capacity is obviously further increased thanks to MAP techniques. Nevertheless, this is not the only major concern for an operator. A second key parameter is the choice of the access network architecture due to its prevalence on the whole energy consumption. A third one is the resource allocation to keep the promise of a high quality of service to all its subscribers. Holistic approaches with global energy consumption are not straightforward. Even if it depends on the selected model, some useful guidelines might be identified [2]. A first attempt dealing with the combination of cell free massive MIMO and O-RAN architecture can be found in [149].

Proposed methodology, tackled challenges and objectives

This project aims at an holistic optimization of a scalable CF-mMIMO system within O-RAN framework. The heterogeneity of the service requests is considered in addition to usual assumptions. Achievement passes through multiple levers to be dealt with jointly: the network architecture, the resource allocation orchestration and the multi-antenna processing. It takes into account different criteria among which global energy consumption and service request satisfaction for all users.

In this project, we expect to address the following topics:

- the definition of fixed and dynamic parts of the network architecture (connections between O-DU, between O-DU and O-RU), with mixture of split 7.2 and split 8 as defined by the O-RAN Alliance,
- the proposition of relevant coordination schemes that orchestrate the cooperation inter O-DU through channel estimation (depth and nature of its distribution) and MAP,
- the dynamic UE allocation (UE association to a group of RUs and pilot sequence allocation) together with the dynamic cluster definition (user-centric, network-centric or hybrid),
- the optimization of multi-antenna processing (inter and intra clusters),
- the consideration of the service request heterogeneity in the system optimization together with the energy consumption.

5.4.2 Multi-user algorithms for spatial multiplexing

Introduction

As shown in studies such as [18, 37], mMIMO has proved its efficiency in boosting the throughput performance of 5G and beyond networks. However, its implementation in downlink raises many questions especially with regards to the optimal number of users to be spatially multiplexed on a common time-frequency resource through precoding. Some research works have shown that the recommended ratio of antennas to beams should be in the range of 2 to 8 [15, 38], while others have proposed to push this range to much larger values by leveraging two non-incompatible strategies:

- Devising efficient user-to-subband assignment techniques that are particularly suitable to the mMIMO context. Such techniques are based on various selection criteria for user clustering, such as the inter-user channel correlation, the channel condition number (CN), the achievable rate, etc.
- Incorporating NOMA techniques into mMIMO systems, which has shown to boost the number of users that can be served on a common subband, as reported in [33, 82, 150].

Additionally, it is important to note that the improvements of these strategies can only be reaped when they are coupled with adequate beamforming techniques, as shown in various studies [70, 110–112]. For instance, [70] proposes a simple clustering solution where highly channel-correlated users with maximum channel gain difference are selected to be assigned to a single subband. The above approach is generalized in [110] for multi-subband allocation with a variable number of clusters per subband and a moderate number of served users. In [112], a greedy assignment technique of users to subbands and beams is introduced in the context of a crowded system, based on a gradual relaxation of the correlation constraints. [111] proposes several resource allocation techniques that aim to effectively serve a large number of users over a limited number of subbands, by leveraging the transmission channel CN as an efficient criterion for subband loading. It was shown that the CN criterion, when used effectively, can greatly overcome the correlation criterion that is widely used in most previous works in the field. Additionally, it can yield system performance that is very close to that of the total throughput criterion, while having much lower complexity.

Challenges and proposed methodology

Despite the numerous advances recently realized in resource allocation for mMIMO, the application of these techniques to the CF-mMIMO context remains a challenge to be met. Indeed, most of the works previously developed in CF-mMIMO merely considered single-carrier transmission. In other words, subband allocation was rarely considered, except for the work in [67] that proposes a simplistic user-specific resource allocation method for the cell-free massive MIMO-OFDM (CF-mMIMO-OFDM) context. Additionally, precoding and user scheduling become particularly challenging in a centralized CF-mMIMO-OFDM that relies on dynamic cooperation clustering (DCC). In DCC, the network of access points (AP) is divided into partially overlapping subsets such that each UE is exclusively served by a set of APs that are pre-selected offline. The centralized DCC configuration comes as a trade-off, from the signaling load perspective, between the centralized 'All' scheme where all UEs are served by all APs with precoding vectors that span the network size, and the distributed DCC configuration. The latter, where precoding is performed on an AP-basis, necessitates the smallest amount of exchanged signaling information among all system configurations, but also presents the lowest spectral efficiency.

In this work, we will tackle the problem of joint user scheduling, subband allocation and precoding in the challenging centralized DCC framework. We will develop efficient allocation techniques that fulfill the scalability requirement of cell-free systems. These techniques will allow to accommodate a massive number of served users with a moderate number of activated APs, while ensuring heterogeneous QoS demands for UEs.

5.4.3 Hybrid NOMA/MIMO framework for interference avoidance or cancellation

Introduction and motivation

As the demand for high data rates and connected devices continues to rise, paradigm shifts are proposed for an efficient management of the available resources in wireless communication systems. Over the years, system architectures underwent an evolution from the unique central antenna system (CAS) per cell, to distributed antenna systems (DAS) or remote radio heads (RRH) and cloud radio access networks (C-RAN) [124] to bring the access nodes closer to the end users. This enables a better cell coverage and enhances the cell capacity by improving the link quality due to reduced path loss and additional spatial diversity favoring line-of-sight communication. Moreover, network densification increases the reuse per unit area of the available spectrum which significantly improves the network capacity while enabling massive access. However, network densification cannot be indefinitely exploited as one of the limits lies in the growing interference caused by the decreasing inter-site distance [29] which degrades the network performance. Hence, a system wide coordination is required to mitigate the resulting inter-cell interference.

With coordinated multipoint (CoMP), cooperating cells can share the CSI of users when scheduling is performed [34,98]. This sharing makes joint scheduling possible, hence avoiding interference. Different CoMP techniques have been proposed in [34], out of which the most elaborate CoMP technique, joint transmission (JT-CoMP) performs a joint precoding of the information signals, to enable a coherent reception. This requires enough backhaul capacity so that user information is available at every transmission point of the CoMP BSs, and tighter synchronization between JT cells is required. Despite its appeal, important challenges are yet to be tackled for full network wide RRH cooperation in terms of complexity and required fronthaul signaling.

An alternative to interference avoidance resides in NOMA techniques where additional users can be served at different power levels while simultaneously reusing a given classical orthogonal multiple access resource block made of the same set of time, frequency and space or antenna parameters [10, 30, 103]. NOMA finds its roots in the study of broadcast channels in information theory which consists of a single transmitter sending separate information to multiple receivers. In the early seventies, a proposed coding scheme applying superposition coding (SC) at the transmitter, coupled with SIC at the receiver, was shown to be optimal [11, 25], i.e. actually achieving system capacity.

Hence, as a solution to the network-wide complexity and scalability, we propose to leverage a tradeoff between interference avoidance through RRH collaboration and interference cancellation driven by NOMA techniques.

Proposed methodology, tackled challenges and objectives

As mentioned earlier, cooperation between RRHs comes at the cost of a proportionally considerable amount of fronthaul signaling and scheduling complexity with a difficulty to achieve the required scalability.

As a solution, we propose a two-step scalable approach to manage the resulting interference from the multiple RRH operation through the application of collaboration and cancellation. First, we want to define a building block for interference cancellation resorting to NOMA techniques applied to distributed antennas. Then, we propose to scale multiple instances of the resulting component into dense RRH and user deployment scenarios through selection/collaboration procedures. Hence, the approach is expected to be highly scalable by nature and is designed to mitigate fronthaul signaling while applying the best tradeoff between interference avoidance through RRH collaboration and interference cancellation through NOMA pairing.
The scientific and technical objectives can be summarized as follows:

- Improved network spectral efficiency through interference-limited user grouping and multiple RRH associations.
- Simultaneous support for uplink and downlink communication in the resulting dense network.
- Evaluation of end-to-end performance and obtained gains with respect to current state-of-the-art.

The tackled technical challenges are:

- Improved spectral efficiency for the 2-user/2-RRHs building block thanks to NOMA-inspired interference mitigation.
- Scaling of the 2-user/2-RRH building block to support larger connectivity through advanced RRH collaboration/selection and environment-aware user clustering techniques with minimum fronthaul overhead.

5.5 Conclusion

This chapter presents a summary of the various studies undertaken as part of WP4, dealing with resource management in CF-mMIMO networks. The work in WP4 focuses on innovative resource (time, frequency, antenna, transmit power) allocation algorithms, the proposal of novel non-orthogonal and grant-free multi-user access techniques and global energy-efficient orchestration for CF-mMIMO systems.

Given that most of the WP4 tasks started in September or October 2023, the related work is still in its early stages. Therefore, for each topic, the state of the art is presented, as well as the various planned directions of research for the future.

Chapter 6 : RIS Modeling: Preliminary Results

6.1 Introduction

A reconfigurable intelligent surface (RIS) is a planar structure that is engineered to dynamically control the electromagnetic waves. In wireless communications, RISs have recently emerged as a promising technology for realizing programmable and reconfigurable wireless propagation environments through nearly passive signal transformations. With the aid of RISs, a wireless environment becomes part of the network design parameters that are subject to optimization.

RIS-empowered smart radio environments are an emerging field of research in wireless communications with several open research issues to be tackled, in order to quantify the gains that can be expected in realistic wireless network deployments. The major open research challenges encompass how to efficiently perform channel estimation, how to enable the control of the RIS, where to best deploy RISs, how to efficiently integrate RISs in system-level and ray tracing simulators, etc. A major open research issue, in addition, consists of developing models for RISs that are electromagnetically consistent and sufficiently tractable for evaluating the performance and for optimizing RIS-assisted wireless networks from a signal-level and system-level perspective.

In this charpter we first overview electromagnetically consistent communication models for RISs and then we show preliminary results obtained based on a model based on multiport network theory.

6.2 Communication Models for RISs

We overview three communication models for RISs that have recently been proposed in the literature. The considered communication models are given as examples, in order to clarify the modeling assumptions and the conditions under which they can be applied.

6.2.1 Locally Periodic Discrete Model

A widely used model for RISs is based on a locally periodic design, in which periodic boundary conditions are applied at the unit cell level. In general, each RIS element is assumed to be comprised of several identical unit cells. To illustrate this communication model, which is widely utilized in wireless communications, we consider the analytical expression of the path loss.

The RIS is modeled as illustrated in Fig. 6.1. For ease of description, we assume that (i) each RIS element is constituted by a single unit cell, (ii) all the unit cells have the same size and shape, and (iii) the inter-distance between adjacent unit cells is the same. Therefore, the RIS is modeled as a periodic arrangement of identical unit cells. The scattering response of each unit cell is configured thanks to a tuning circuit and a biasing line. We assume that there exist M unit cells in each row and N unit cell in each column of the surface. Therefore, the total number of reconfigurable unit cells is MN. The surface area of each unit cell is $d_x d_y$, with d_x and d_x being the horizontal and vertical sizes of each unit cell, respectively.

The RISs considered in this chapter are assumed to operate as a reflecting surface and, therefore, each unit cell is characterized by a complex reflection coefficient, which is defined as the ratio between the reflected electric field and the incident electric field. We denote the reflection coefficient of the (m, n)th unit cell as $\Gamma_{m,n}$. In particular, the example of considered RIS comprises unit cells that can apply two phase shifts (binary cells) depending on the

Table 6.1: Examples of reflection and transmission coefficients for RISs with discrete-valued phase shifts (two-state and four-state control).

Reference	Reflection Coefficient	Transmission Coefficient
$f = 27$ GHz	$\lvert\Gamma_1\rvert = 0.9, \quad \angle\Gamma_1 = 165^\circ$ $\lvert\Gamma_2\rvert = 0.7, \quad \angle\Gamma_2 = 0^\circ$	–
$f = 33$ GHz	$\lvert\Gamma_1\rvert = 0.8, \quad \angle\Gamma_1 = 150^\circ$ $\lvert\Gamma_2\rvert = 0.8, \quad \angle\Gamma_2 = 0^\circ$	–
$f = 3.6$ GHz	$\lvert\Gamma_1\rvert = 0.46, \quad \angle\Gamma_1 = 20^\circ$ $\lvert\Gamma_2\rvert = 0.55, \quad \angle\Gamma_2 = 215^\circ$	$\lvert T_1\rvert = 0.58, \quad \angle T_1 = 300^\circ$ $\lvert T_2\rvert = 0.81, \quad \angle T_2 = 123^\circ$
$f = 2.3$ GHz	$\lvert\Gamma_1\rvert = -1.2\,\mathrm{dB}, \quad \angle\Gamma_1 = -205.5^\circ$ $\lvert\Gamma_2\rvert = -1.2\,\mathrm{dB}, \quad \angle\Gamma_2 = -383.2^\circ$ $\lvert\Gamma_3\rvert = -0.8\,\mathrm{dB}, \quad \angle\Gamma_3 = -290.2^\circ$ $\lvert\Gamma_4\rvert = -0.7\,\mathrm{dB}, \quad \angle\Gamma_4 = -110.3^\circ$	–

Table 6.2: Example of reflection coefficient for an RIS with continuous-valued phase shifts

Voltage	Reflection coefficient amplitude ($\lvert\Gamma\rvert$)	Reflection coefficient phase ($\angle\Gamma$)
0 V	-1.517 dB	32.798°
0.25 V	-1.807 dB	40.854°
0.5 V	-3.156 dB	46.807°
0.75 V	-5.59 dB	53.543°
1 V	-9.576 dB	70.32°
1.25 V	-20.563 dB	-167.158°
1.5 V	-6.615 dB	-73.171°
1.75 V	-3.029 dB	-49.627°
2 V	-1.959 dB	-35.908°
2.5 V	-0.874 dB	-23.263°
3 V	-0.749 dB	-16.087°
3.5 V	-0.469 dB	-12.663°
4 V	-0.528 dB	-9.925°
5 V	-0.439 dB	-6.906°

configuration of the tuning circuit. For illustrative purposes, the values of the reflection coefficients are reported in Table 6.1. In Table 6.1 and Table 6.2, for completeness, we report two other examples of RISs that are modeled based on the same principle. One of the examples reported in Table 6.1 considers an RIS that can simultaneously reflect and refract the incident electromagnetic waves. For this reason, it is characterized by a reflection coefficient and by a transmission coefficient, $T_{m,n}$, which is defined as the ratio between the refracted electric field and the incident electric field. The unit cells of the RIS in can be configured in two different states that are characterized by the pairs (Γ_1, T_1) and (Γ_2, T_2). The other example reported in Table 6.1 operates as a reflecting surface but its unit cells can be configured in four different states. The RIS in Table 6.2 is modeled as a periodic array of unit cells. In addition, it operates only in reflection mode and is characterized by the reflection coefficient $\Gamma_{m,n}$. However, the reflection coefficient of each unit cell can be varied continuously as a function of a control voltage. Therefore, the phase shift applied by each unit cell can be tuned more finely. In the five examples of RISs reported in Table 6.1 and Table 6.2, we note that the amplitude and the phase of the reflection (and transmission) coefficient are not independent of each other. Also, the amplitude of the reflection coefficient is not unitary and it is not independent of the phase shift. In general, in addition, the reflection and transmission coefficients reported in Table 6.1 and Table 6.2 depend on the angle of incidence of the electromagnetic wave. The examples reported in the two tables are referred to the canonical case of normal incidence.

Assuming that the set of possible reflection coefficients (the RIS codebook), as a function of the tuning circuit,

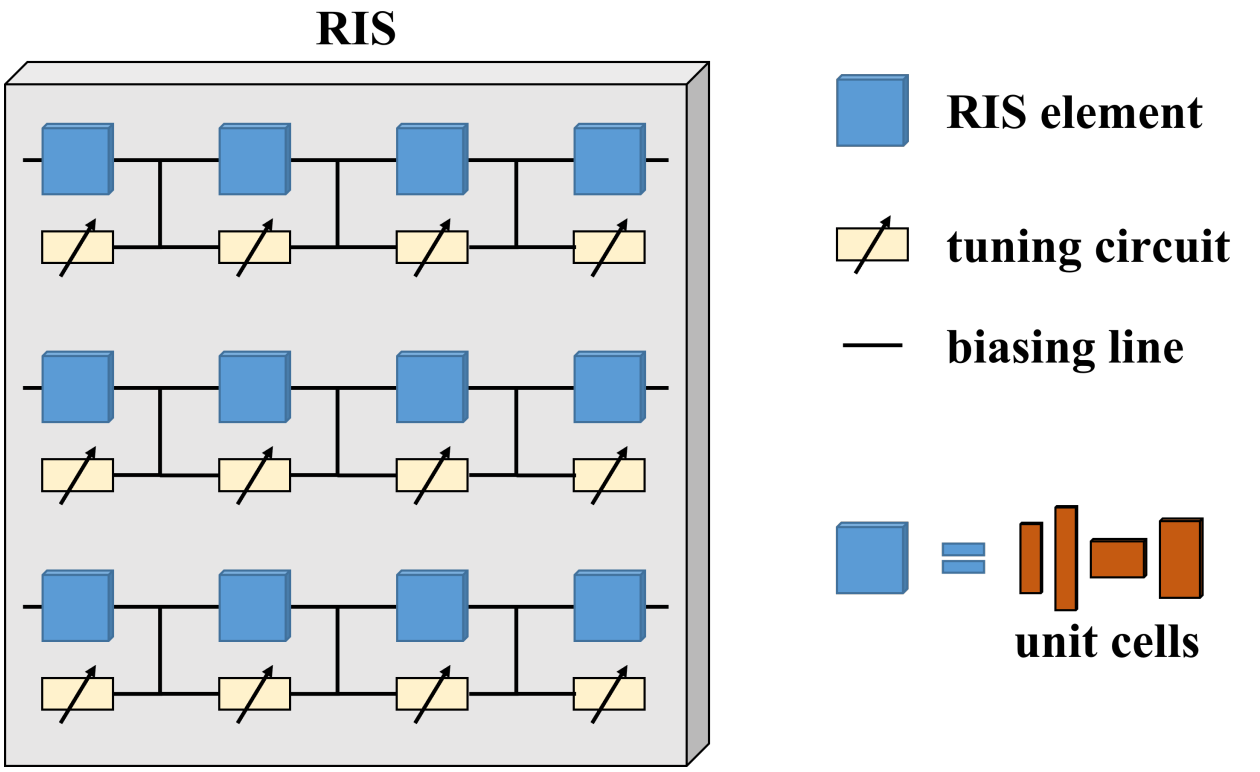

Figure 6.1: Conceptual architecture of a reconfigurable intelligent surface.

of a single unit cell of the RIS is given, we are interested in an analytical model for computing the power observed at a given location of an RIS-assisted communication link. The RIS is assumed to be centered at the origin and to lie in the xy plane (i.e., $z = 0$). The received power can be formulated as follows:

$$\frac{P^{(\mathrm{Rx})}}{P^{(\mathrm{Tx})}} = \frac{G^{(\mathrm{Tx})}G^{(\mathrm{Rx})}}{16\pi^2(d_x d_y)^2} * \left| \sum_{m=1}^{M}\sum_{n=1}^{N} \frac{\sqrt{F_{m,n}}\Gamma_{m,n}}{r_{m,n}^{(\mathrm{Tx})} r_{m,n}^{(\mathrm{Rx})}} e^{-j\frac{2\pi}{\lambda}\left(r_{m,n}^{(\mathrm{Tx})}+r_{m,n}^{(\mathrm{Rx})}\right)} \right|^2 \tag{6.1}$$

where

$$F_{m,n} = \left(\frac{\left(d_0^{(\mathrm{Tx})}\right)^2 + \left(r_{m,n}^{(\mathrm{Tx})}\right)^2 - (d_{m,n})^2}{2d_0^{(\mathrm{Tx})} r_{m,n}^{(\mathrm{Tx})}} \right)^{-1+G^{(\mathrm{Tx})}/2} * \left(\frac{z^{(\mathrm{Tx})}}{r_{m,n}^{(\mathrm{Tx})}} \right) \left(\frac{z^{(\mathrm{Rx})}}{r_{m,n}^{(\mathrm{Rx})}} \right) * \left(\frac{\left(d_0^{(\mathrm{Rx})}\right)^2 + \left(r_{m,n}^{(\mathrm{Rx})}\right)^2 - (d_{m,n})^2}{2d_0^{(\mathrm{Rx})} r_{m,n}^{(\mathrm{Rx})}} \right)^{-1+G^{(\mathrm{Rx})}/2} \tag{6.2}$$

and the following notation is used:

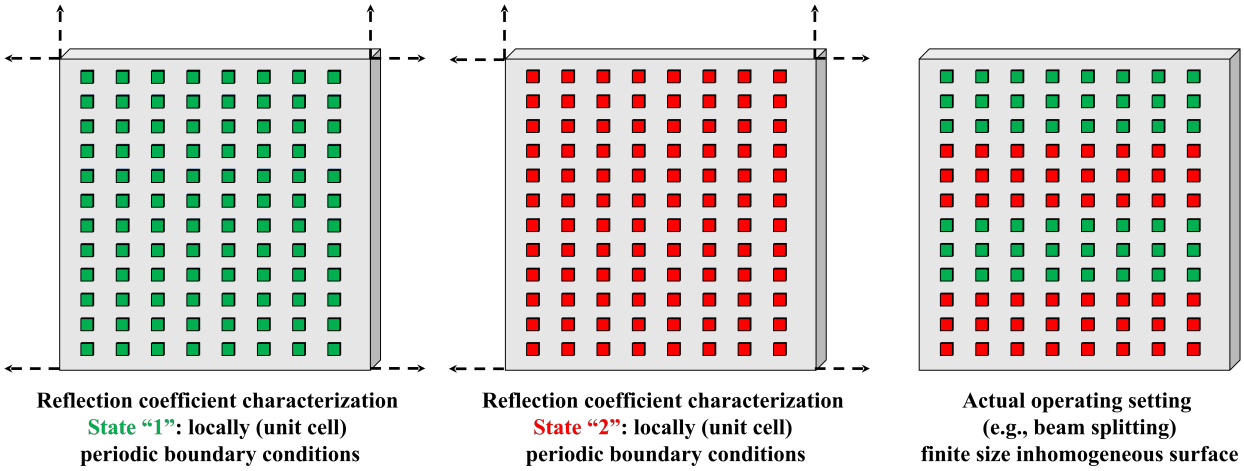

Figure 6.2: Illustration of the concept of (locally) periodic boundary conditions.

- $P^{(\mathrm{Tx})}$ and $P^{(\mathrm{Rx})}$ are the transmitted and received powers, respectively;
- $G^{(\mathrm{Tx})}$ and $G^{(\mathrm{Rx})}$ are the antenna gains of the transmitter and receiver, respectively;
- λ is the wavelength of the electromagnetic wave and $j = \sqrt{-1}$ is the imaginary unit;
- $r_{m,n}^{(\mathrm{Tx})}$ is the distance between the transmitter and the center point of the (m, n)th unit cell, and $r_{m,n}^{(\mathrm{Rx})}$ is the distance between the center point of the (m, n)th unit cell and the receiver;
- $d_{m,n}$ is the distance between the center point of the (m, n)th unit cell and the center point of the RIS (i.e., the origin);
- $d_0^{(\mathrm{Tx})}$ is the distance between the transmitter and the center point of the RIS, and $d_0^{(\mathrm{Rx})}$ is the distance between the center point of the RIS and the receiver;
- $z^{(\mathrm{Tx})}$ and $z^{(\mathrm{Rx})}$ are the Cartesian coordinates of the transmitter and receiver on the z-axis, respectively.

By using (6.1), it is possible to formulate the received power for any locations of the transmitter and receiver as a function of the location of the RIS and of the configuration of the unit cells. Therefore, the optimal configuration of the MN unit cells of the RIS can be identified in order to, e.g., maximize the received power depending on the location of the receiver. More precisely, let $\mathbf{\Gamma}$ denote the $M \times N$ matrix of reflection coefficients $\Gamma_{m,n}$ and let $\Gamma_{m,n} \in \{\Gamma_1, \Gamma_2, \ldots, \Gamma_\Sigma\}$ be the Σ possible reflection coefficients of each unit cell of the RIS. In Tables 6.1 and 6.2, we have $\Sigma = 2$ or $\Sigma = 4$ and $\Sigma = 14$. With this notation, a typical problem formulation reads as follows:

$$\max_{\mathbf{\Gamma}} P^{(\mathrm{Rx})}(\mathbf{\Gamma}) \tag{6.3}$$

$$\text{s.t.} \quad \Gamma_{m,n} \in \{\Gamma_1, \Gamma_2, \ldots, \Gamma_\Sigma\} \quad \forall m, n \tag{6.3a}$$

As mentioned, the set of Σ states in (6.3), i.e., the RIS codebook, is determined by characterizing the electromagnetic response of the constituent unit cell of the RIS by employing a local design. In order to understand the applicability and accuracy of the received power model in (6.1), based on the solution of the optimization problem in (6.3), it is instructive to analyze in detail the meaning of local design at the unit cell level and the concept of periodic boundary conditions mentioned in Section II. To this end, we consider, as an example, a binary unit cell that can take only two states, i.e., $\Sigma = 2$ and $\Gamma_{m,n} \in \{\Gamma_1, \Gamma_2\}$.

The reflection coefficients Γ_1 and Γ_2 are obtained by utilizing the procedure sketched in Fig. 6.2. The reflection coefficient Γ_1 is estimated by considering an infinite-size RIS whose unit cells are all identical and the tuning circuits

are set to the same configuration. Therefore, the RIS is effectively turned into an infinite and spatially homogeneous sheet with no phase variation along the entire surface. In this configuration, the reflection coefficient is well defined as the ratio between the reflected electric field and the incident electric field. Since the surface is spatially homogeneous and of infinite extent, only specular reflection is allowed. The obtained structure is usually analyzed with the aid of full-wave electromagnetic simulators, which model the infinite size of the surface and the periodic repetition of the elementary unit cell by applying the so-called periodic boundary conditions. Thanks to this procedure, the reradiation characteristics of the unit cell in the first possible state are characterized by taking into account that it is immersed into a neighbourhood of identical unit cells. This implies that the mutual coupling and the interactions among all the identical unit cells in the homogeneous sheet are inherently taken into account when characterizing Γ_1. The same procedure is repeated for estimating Γ_2, with the only difference being that the tuning circuits are set to the configuration that results in the reflection coefficient Γ_2.

Having characterized the reflection coefficients Γ_1 and Γ_2, if necessary as a function of the angle of incidence of the electromagnetic wave, the communication model in (6.1) stipulates that we may configure the state (either Γ_1 and Γ_2 in the example of Fig. 6.2) of each unit cell independently of the others and regardless of the states of the neighboring cells. An example is given in the right-hand side illustration of Fig. 6.2, in which the unit cells are configured to realize beam splitting. However, caution needs to be paid when (6.1) is utilized and the reflection coefficients Γ_1 or Γ_2 are obtained by applying locally periodic boundary conditions at the unit cell level. The reflection coefficients Γ_1 and Γ_2 are, in fact, determined by assuming that a unit cell configured in a given state is immersed in an infinite homogeneous repetition of identical unit cells. When the RIS is configured to operate in practice, as sketched in the right-hand side illustration of Fig. 6.2, each unit cell is, however, immersed in a spatially inhomogeneous array whose neighboring unit cells can be all different from each other. This implies that the spatial symmetry imposed by the periodic boundary conditions does not hold anymore and the interactions (mutual coupling) among nearby unit cells are taken into account only in an approximate manner. In addition, the RIS is not of infinite extent but has a finite size. This implies that the notion of reflection coefficient is only an approximation and it holds only under the limit of physical optics. For these reasons, the unit cells are not typically optimized individually and independently of each other, but they are optimized in groups, so as to ensure that the periodic boundary conditions utilized when characterizing each unit cell individually are approximately fulfilled during the normal operation of the RIS as well. The right-hand side illustration of Fig. 6.2 is a typical example in which the unit cells are split in groups, each containing 24 unit cells, and the groups are optimized such that the states (Γ_1 or Γ_2) of all the unit cells in a group are the same. The minimum required size of the group of unit cells for ensuring that (6.1) is accurate enough for wireless applications is usually characterized with the aid of full-wave simulations.

6.2.2 Multiport Network Model

The communication model for RISs introduced in the previous sub-section is widely employed in wireless communications and several optimization frameworks, under some simplifying assumptions. The local design at the unit cell level is a widely used method for characterizing the reflection and transmission characteristics of an RIS. However, the mutual coupling among the unit cells is only approximately taken into account, since the possible reflection coefficients of each unit cell (i.e., the RIS codebook) are typically characterized by applying periodic boundary conditions at the unit cell level. The accuracy of the model in (6.1) can be improved by, e.g., not characterizing the reradiation properties of each unit cell individually but by analyzing, with full-wave simulations, the reradiation of groups of unit cells as a function of all the possible combinations of their states. In this case, periodic boundary conditions may be applied at the granularity of a group of unit cells in lieu of a single unit cell. The optimization accuracy of the model usually increases at the expenses of the modeling and optimization complexity.

A different communication model that account for the electromagntical mutual coupling by design is based on multiport network theory. The model resembles a conventional single transmitter-receiver pair MIMO communication link in the presence of an RIS. The transmitter and the receiver are equipped with M_0 and $L_0 \leq M_0$ antenna elements, respectively. The antenna elements are assumed to be thin wire dipoles of perfectly conducting material. The model can be generalized for application to radiating elements different from thin wire dipoles, which are considered in [9] for analytical tractability. Each thin wire dipole at the transmitter is driven by a voltage generator that models the transmit feed line, and each thin wire dipole at the receiver is connected to a load impedance that mimics the receive electric circuit. For simplicity, we assume that the number of symbols (streams) sent by the

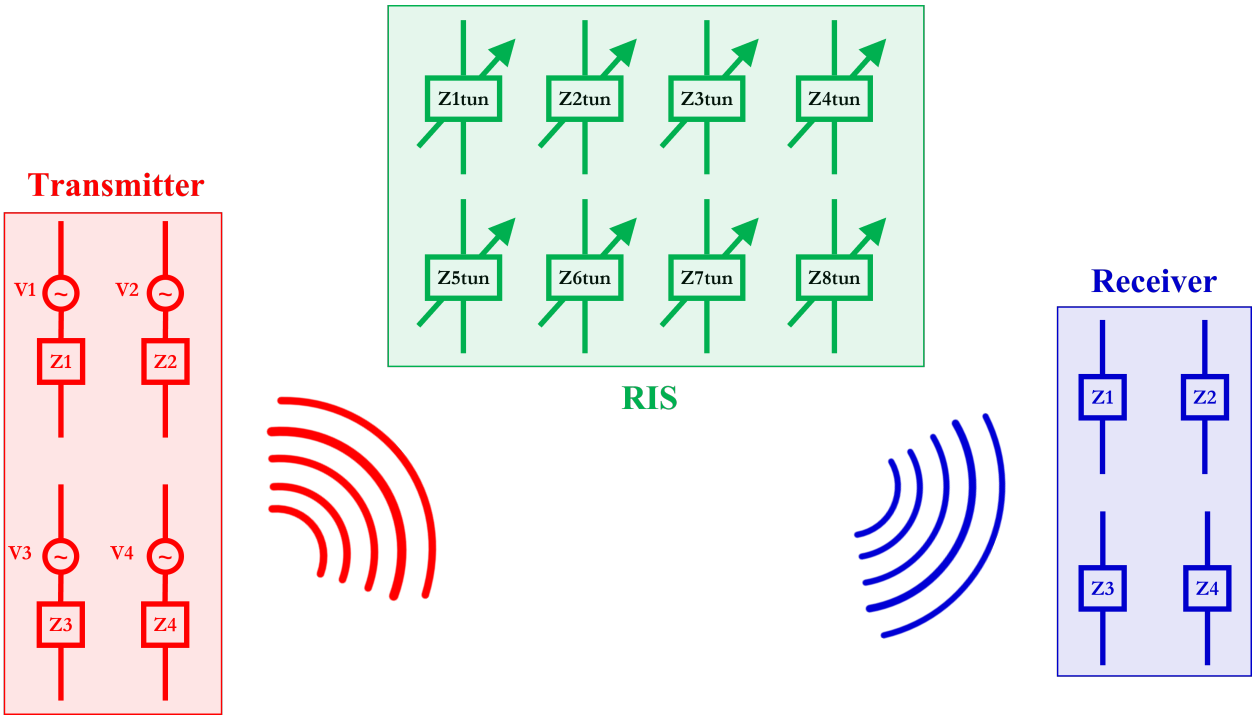

Figure 6.3: Communication model of a reconfigurable intelligent surface based on mutually coupled impedances.

transmitter is equal to the number of receive antennas. The transmission between the transmitter and the receiver is assisted by an RIS, which comprises P nearly passive thin wire dipoles that are independently configurable (by an external controller) through tunable impedances. Compared with the illustration of the RIS in Fig. 6.1, a thin wire dipole in Fig. 6.3 can be viewed as an approximation for a unit cell. The model can be generalized to different physical structures for the unit cells, e.g., patch antennas.

Based on the system model in Fig. 6.3, the RIS-assisted channel is optimized by appropriately setting the tunable impedances connected to the thin wire dipoles. More specifically, we are interedted in computing an $L_0 \times M_0$ end-to-end channel matrix that formulates the voltage measured at the ports of the receive antennas as a function of the voltage generators connected to the ports of the transmit antennas, i.e., $\mathbf{v}_{\mathrm{Rx}} = \mathbf{H}\mathbf{v}_{\mathrm{Tx}}$, where $\mathbf{v}_{\mathrm{Tx}}$ is the $M_0 \times 1$ vector that collects the driving voltages at the transmitter, $\mathbf{v}_{\mathrm{Rx}}$ is the $L_0 \times 1$ vector that collects the voltages measured at the ports of the antennas at the receiver, and $\mathbf{H}$ is the $L_0 \times M_0$ channel matrix that accounts for the radiating elements (the thin wire dipoles) and the propagation of the electromagnetic waves. Specifically, $\mathbf{H}$ can be formulated as follows:

$$\mathbf{H} = \left(\mathbf{I}_{L_0} + \mathbf{\Psi}_{r,r}\mathbf{Z}_r^{-1} - \mathbf{\Psi}_{r,t}(\mathbf{\Psi}_{t,t} + \mathbf{Z}_t)^{-1}\mathbf{\Psi}_{t,r}\mathbf{Z}_r^{-1}\right)^{-1}\mathbf{\Psi}_{r,t}(\mathbf{\Psi}_{t,t} + \mathbf{Z}_t)^{-1} \tag{6.4}$$

where $\mathbf{I}_{L_0}$ is the $L_0 \times L_0$ identity matrix, and $\mathbf{Z}_t$ and $\mathbf{Z}_r$ are the $M_0 \times M_0$ and $L_0 \times L_0$ diagonal matrices that comprise the internal impedances of the transmit generators and the load impedances of the receive antennas, respectively. Furthermore, the following shorthand notation is introduced:

$$\mathbf{\Psi}_{t,t} = \mathbf{Z}_{t,t} - \mathbf{Z}_{t,s}(\mathbf{Z}_{s,s} + \mathbf{Z}_{\mathrm{tun}})^{-1}\mathbf{Z}_{s,t} \tag{6.5}$$

$$\mathbf{\Psi}_{t,r} = \mathbf{Z}_{t,r} - \mathbf{Z}_{t,s}(\mathbf{Z}_{s,s} + \mathbf{Z}_{\mathrm{tun}})^{-1}\mathbf{Z}_{s,r} \tag{6.6}$$

$$\mathbf{\Psi}_{r,t} = \mathbf{Z}_{r,t} - \mathbf{Z}_{r,s}(\mathbf{Z}_{s,s} + \mathbf{Z}_{\mathrm{tun}})^{-1}\mathbf{Z}_{s,t} \tag{6.7}$$

$$\mathbf{\Psi}_{r,r} = \mathbf{Z}_{r,r} - \mathbf{Z}_{r,s}(\mathbf{Z}_{s,s} + \mathbf{Z}_{\mathrm{tun}})^{-1}\mathbf{Z}_{s,r} \tag{6.8}$$

where $\mathbf{Z}_{x,y}$, for $x, y \in \{t, s, r\}$ with t, s, and r identifying the transmitter, the RIS, and the receiver, respectively, is

the matrix of mutual (or self if $x = y$) impedances between the thin dipoles of y and those of x, which characterizes the signal propagation and the mutual coupling between x and y, and $\mathbf{Z}_{\text{tun}}^{(k)}$ is the $P \times P$ diagonal matrix of tunable impedances of the RIS. The matrices $\mathbf{Z}_{x,y}$ for $x, y \in \{t, s, r\}$ account for the microscopic structure of the RIS and the locations of the transmitter, RIS, and receiver. They can be either computed with the aid of full-wave simulators or can be computed analytically by relying on some approximations. For example, the induced electromagnetic field method can be utilized for computing the mutual and self impedances, as well as a sinusoidal approximation for the current distribution on the thin wire dipoles. Given the RIS microstructure and the system topology, the impedances in $\mathbf{Z}_{x,y}$ for $x, y \in \{t, s, r\}$ need to be computed only once, and are not usually considered optimization variables in the context of wireless communication systems of networks.

On the other hand, the matrix $\mathbf{Z}_{\text{tun}}$, which allows the reconfigurability of the RIS, is the matrix to be optimized for steering the electromagnetic wave that is emitted by the transmitter and impinges upon the RIS towards the location of the receiver. Let us consider, for example, that the transmitter and the receiver are equipped with a single antenna, i.e., $M_0 = L_0 = 1$, and that the objective is to maximize the power at the location of the receiver. Then, the matrix $\mathbf{H}$ is a scalar, i.e., $v_{\text{Rx}} = H v_{\text{Tx}}$, and the optimization problem as a function of $\mathbf{Z}_{\text{tun}}$ can be formulated as follows:

$$\max_{\mathbf{Z}_{\text{tun}}} |H(\mathbf{Z}_{\text{tun}})| \tag{6.9}$$

$$\text{s.t.} \quad Z_{\text{tun},p} \in \{\mathcal{Z}_1, \mathcal{Z}_2, \ldots, \mathcal{Z}_\Xi\} \quad \forall p = 1, 2, \ldots, P \tag{6.9a}$$

where $Z_{\text{tun},p}$ is the pth element of $\mathbf{Z}_{\text{tun}}$ and $\{\text{Z}_1, \text{Z}_2, \ldots, \text{Z}_\Xi\}$ is the set of Ξ possible discrete values of the tuning impedances that can be implemented.

The matrices defined in (6.5)-(6.8) have a physical meaning and interpretation as well. For example, $\mathbf{\Psi}_{r,t}$ represents the transfer matrix (the channel) between the transmitter and the receiver, which accounts for the direct link ($\mathbf{Z}_{r,t}$) and the RIS-reradiated link $\mathbf{Z}_{r,s}(\mathbf{Z}_{s,s} + \mathbf{Z}_{\text{tun}})^{-1}\mathbf{Z}_{s,t}$. This latter term is the product of three factors: $\mathbf{Z}_{s,t}$ represents the transfer function from the transmitter to the RIS; $\mathbf{Z}_{r,s}$ represents the transfer function from the RIS to the receiver; and $(\mathbf{Z}_{s,s} + \mathbf{Z}_{\text{tun}})^{-1}$ models the reradiation from the RIS. The matrix $\mathbf{Z}_{s,s}$ is, in general, a full matrix and reduces to an almost diagonal matrix, i.e., the amplitudes of the elements in the main diagonal are much larger than the off-diagonal elements, diagonal matrix, if the mutual coupling between any pair of thin wire dipoles is negligible.

The channel matrix in (6.4) can be simplified in several scenarios of practical relevance. If, for example, the transmitter, the receiver, and the RIS are in the far-field of each other, (6.4) can be simplified without ignoring the mutual coupling among the thin dipoles of each RIS. The self impedances $\mathbf{Z}_{x,x}$ are, in fact, independent of the transmission distances of the transmitter-receiver, transmitter-RIS, and RIS-receiver links, and they depend only on the inter-distances between the thin wire dipoles that comprise the transmitter, the RIS, and the receiver. In the far-field region, therefore, the following simplifications can be applied:

$$\mathbf{\Psi}_{t,t} \approx \mathbf{Z}_{t,t} \tag{6.10}$$

$$\mathbf{\Psi}_{r,r} \approx \mathbf{Z}_{r,r} \tag{6.11}$$

$$\mathbf{\Psi}_{r,r}\mathbf{Z}_r^{-1} - \mathbf{\Psi}_{r,t}(\mathbf{\Psi}_{t,t} + \mathbf{Z}_t)^{-1}\mathbf{\Psi}_{t,r}\mathbf{Z}_r^{-1} \approx \mathbf{\Psi}_{r,r}\mathbf{Z}_r^{-1} \tag{6.12}$$

In the far-field region, therefore, $\mathbf{H}$ in (6.4) can be approximated as follows:

$$\begin{aligned}\mathbf{H}_{r,t} \approx{}& \left(\mathbf{I}_{L_0} + \mathbf{Z}_{r,r}\mathbf{Z}_r^{-1}\right)^{-1}\mathbf{Z}_{r,t}(\mathbf{Z}_{t,t} + \mathbf{Z}_t)^{-1} \\ &- \left(\mathbf{I}_{L_0} + \mathbf{Z}_{r,r}\mathbf{Z}_r^{-1}\right)^{-1} \\ &\quad * \mathbf{Z}_{r,s}(\mathbf{Z}_{s,s} + \mathbf{Z}_{\text{tun}})^{-1}\mathbf{Z}_{s,t} \\ &\quad * (\mathbf{Z}_{t,t} + \mathbf{Z}_t)^{-1}\end{aligned} \tag{6.13}$$

In (6.13), it is not difficult to recognize that the first addend on the right-hand side corresponds to the direct link between the transmitter and the receiver, and that the second addend on the right-hand side corresponds to the RIS-reradiated link that accounts for the internal impedances of the voltage generator at the transmitter, the load at the receiver, the transfer matrices $\mathbf{Z}_{s,t}$ and $\mathbf{Z}_{r,s}$ that characterize the propagation of the electromagnetic wave from

the transmitter to the RIS and from the RIS to the receiver, respectively, and the term $(\mathbf{Z}_{s,s} + \mathbf{Z}_{\text{tun}})^{-1}$ that accounts for the mutual coupling and the tuning circuits of the RIS.

The communication model in (6.4), and especially the simplified version in (6.13), are relatively simple to use in wireless communication systems and networks due to the resemblance of $\mathbf{H}$ with a typical MIMO channel model. It is necessary to understand, however, the assumptions and the conditions under which (6.4) can be applied. Besides the computation of the matrix $\mathbf{Z}_{s,s}$ that, if done analytically, usually requires some approximations, the main assumption made to obtain $\mathbf{H}$ in (6.4) is that the tiny antenna elements are assumed to be minimum scattering antennas. In simple terms, this assumption implies that a radiating element (a thin wire dipole in Fig. 6.3) does not radiate if it is open circuited, and, therefore, it is like if it is not present (it is "invisible") in the network. Concretely, this implies that the pth thin wire dipole that constitutes the RIS in Fig. 6.3 does not reradiate in the presence of an electromagnetic wave if $Z_{\text{tun},p} \to \infty$ and, therefore, it can be removed from the system model. This is, of course, an approximation, since the presence of the thin wire dipole always perturbs the electromagnetic field. This assumption is usually acceptable for scattering elements that are much smaller than the wavelength, as the elements of an RIS are usually assumed to be. Nevertheless, caution needs to be paid when applying the communication model in (6.4) for ensuring that the approximation of minimum scattering antennas is fulfilled.

6.2.3 Inhomogeneous Sheets of Surface Impedan

In this sub-section, we consider models for RISs that abstract their microscopic structure and are focused on the specific wave transformations that the metasurface, as a whole, is intended to realize. More precisely, a metamaterial-based RIS whose unit cells have sizes and inter-distances much smaller than the wavelength is homogenizable and can be modeled as a continuous surface sheet through appropriate surface functions. This modeling approach is not dissimilar from the characterization of bulk (three-dimensional) metamaterials, which are usually represented through effective permittivity and permeability functions that determine the wave phenomena based on Maxwell's equations. The only difference is that a metasurface is better modeled by effective surface parameters, which manifest themselves in electromagnetic problems that are formulated as effective boundary conditions. These boundary conditions can be expressed in terms of surface polarizabilities, surface susceptibilities, or surface impedances (or admittances). In this chapter, we focus our attention on modeling an RIS through surface impedances.

The adopted modeling approach is, specifically, referred to as macroscopic. Classical wave phenomena in materials or metamaterials are determined by the collective effects of a very large number of atoms that interact with the incident electromagnetic waves. The electromagnetic fields around individual atoms can be described by microscopic Maxwell's equations. If the sizes of the atoms that constitute the material and the distances between them are much smaller than the wavelength, the electromagnetic fields and the sources in the material can be spatially averaged, thus effectively transforming microscopic Maxwell's equations into macroscopic Maxwell's equations. For a metasurface-based RIS, the same principle applies: If the RIS is electrically large and is made of sub-wavelength reconfigurable scattering elements (unit cells) whose inter-distances are much smaller than the wavelength, it is homogenizable and can be modeled through continuous surface averaged (macroscopic) surface impedances. More specifically, two conditions need to be fulfilled to make an RIS homogenizable [41, Section 2.1]: (i) the first homogenization condition requires that the incident field varies little over one spatial period (the largest inter-distance among the unit cells) of the RIS, i.e., $\max\{d_x, d_y\} \ll \lambda$; and (ii) the second homogenization condition requires that the evanescent field scattered by the RIS is negligible at the observation point, i.e., $|z| > \max\{d_x, d_y\}$ for the RIS in Fig. 6.4, where λ is the wavelength of the electromagnetic wave, and d_x and d_y are the horizontal and vertical sizes of its unit cells (assuming that the unit cells are identical in size). The second condition is typically fulfilled in the far-field of the RIS microstructure.

Under these assumptions, an RIS can be modeled as an inhomogeneous sheet of polarizable particles (the unit cells) that is characterized by an electric surface impedance and a magnetic surface admittance, which, for general wave transformations, are dyadic tensors. These two dyadic tensors constitute the macroscopic homogenized model of the RIS. The average total electric and magnetic fields that illuminate the RIS induce electric and magnetic currents that introduce a discontinuity between the electromagnetic fields on the two sides of the RIS (below and above the surface), which provides the means for manipulating the wavefront of the incident electromagnetic waves. Once the homogenized and continuous electric surface impedance and magnetic surface admittance are obtained based on the desired wave transformations, the microscopic structure and physical implementation of the RIS

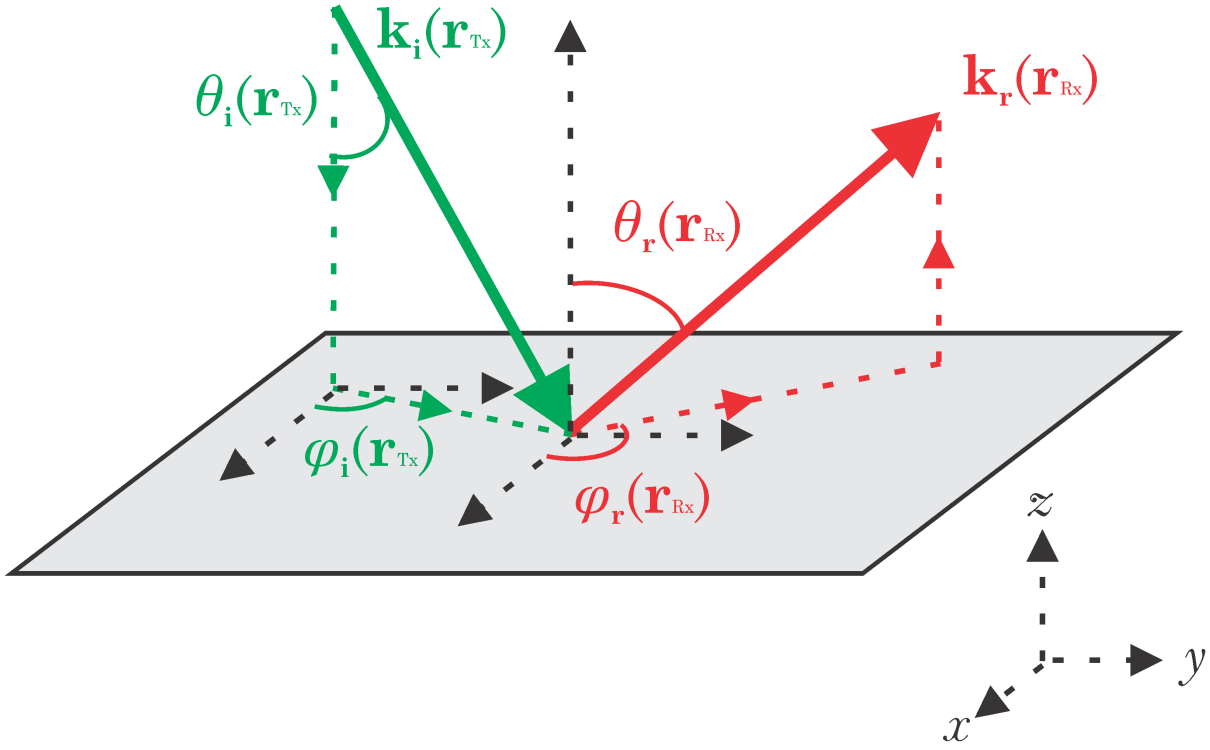

Figure 6.4: System model: An RIS as an inhomogeneous sheet (inhomogeneous boundary if the RIS is impenetrable) of surface impedance

in terms of unit cells can then be obtained. Generally speaking, once the macroscopic surface impedance and admittance are determined, appropriate geometric arrangements of sub-wavelength unit cells and the associated tuning circuits that exhibit the corresponding electric and magnetic response are characterized by, typically, using full-wave electromagnetic simulations.

Based on this modeling approach, an RIS is characterized by a set of algebraic equations that results in boundary conditions for the electromagnetic fields at the two sides of the surface. This set of equations is referred to as generalized sheet transition conditions. Under the assumption that only the tangential components of the electric and magnetic polarization densities are induced in the metasurface and that the RIS lies in the xy-plane (i.e., $z = 0$) as illustrated in Fig. 6.4, the generalized sheet transition conditions can be formulated as follows:

$$\begin{aligned}\mathbf{E}_{\mathrm{tot}}^{t}\left(x,y,z=0^{+}\right)+\mathbf{E}_{\mathrm{tot}}^{t}\left(x,y,z=0^{-}\right)&\\ =2\overline{\overline{\mathbf{Z}}}_{se}\left(x,y\right)\left(\hat{\mathbf{z}}\times\mathbf{H}_{\mathrm{tot}}\left(x,y,z=0^{+}\right)\right)&\\ -2\overline{\overline{\mathbf{Z}}}_{se}\left(x,y\right)\left(\hat{\mathbf{z}}\times\mathbf{H}_{\mathrm{tot}}\left(x,y,z=0^{-}\right)\right)&\end{aligned} \tag{6.14}$$

$$\begin{aligned}\mathbf{H}_{\mathrm{tot}}^{t}\left(x,y,z=0^{+}\right)+\mathbf{H}_{\mathrm{tot}}^{t}\left(x,y,z=0^{-}\right)\\ =-2\overline{\overline{\mathbf{Y}}}_{sm}\left(x,y\right)\left(\hat{\mathbf{z}}\times\mathbf{E}_{\mathrm{tot}}\left(x,y,z=0^{+}\right)\right)\\ +2\overline{\overline{\mathbf{Y}}}_{sm}\left(x,y\right)\left(\hat{\mathbf{z}}\times\mathbf{E}_{\mathrm{tot}}\left(x,y,z=0^{-}\right)\right)\end{aligned} \tag{6.15}$$

where $\overline{\overline{\mathbf{Z}}}_{se}\left(x,y\right)$ and $\overline{\overline{\mathbf{Y}}}_{sm}\left(x,y\right)$ are the electric surface impedance and the magnetic surface admittance dyadic tensors that constitute the homogenized macroscopic model of the RIS. In addition, the following definitions for the electric and magnetic fields in (6.14) and (6.15) hold:

$$\begin{aligned}\mathbf{F}_{\mathrm{tot}}\left(x,y,z=0^{+}\right)=\mathbf{F}_{\mathrm{inc}}\left(x,y,z=0^{+}\right)\\ +\mathbf{F}_{\mathrm{ref}}\left(x,y,z=0^{+}\right)\end{aligned} \tag{6.16}$$

$$\mathbf{F}_{\mathrm{tot}}\left(x,y,z=0^{-}\right)=\mathbf{F}_{\mathrm{tra}}\left(x,y,z=0^{-}\right) \tag{6.17}$$

$$\mathbf{F}_{\mathrm{tot}}^{t}\left(x,y,z=0^{\pm}\right)=\left(\hat{\mathbf{z}}\times\mathbf{F}_{\mathrm{tot}}\left(x,y,z=0^{\pm}\right)\right)\times\hat{\mathbf{z}} \tag{6.18}$$

where $\hat{\mathbf{z}}$ is the unit norm vector that is normal to the RIS as illustrated in Fig. 6.4, and $\mathbf{F}_{\mathrm{inc}}\left(x,y,z=0^{+}\right)$, $\mathbf{F}_{\mathrm{ref}}\left(x,y,z=0^{+}\right)$ and $\mathbf{F}_{\mathrm{tra}}\left(x,y,z=0^{-}\right)$ with $\mathbf{F}=\{\mathbf{E},\mathbf{H}\}$ are the incident, reflected, and transmitted (refracted) electric and magnetic fields evaluated on the two sides of the RIS, respectively.

The equations in (6.14) and (6.15) completely characterize the RIS in terms of wave transformations and can be utilized for the analysis and synthesis of an RIS. As far as the analysis is concerned, it is usually assumed that $\overline{\overline{\mathbf{Z}}}_{se}\left(x,y\right)$ and $\overline{\overline{\mathbf{Y}}}_{sm}\left(x,y\right)$ are known, and one is interested in solving (6.14) and (6.15) for obtaining the surface electric and magnetic fields in the close vicinity of the RIS, but at distances at which the homogenized model can be applied (as detailed in further text). As far as the synthesis is concerned, it is usually assumed that either the surface electric and magnetic fields in the close vicinity of the RIS are explicitly known or that an objective function that depend on them is known, and one is interested in identifying the corresponding functions $\overline{\overline{\mathbf{Z}}}_{se}\left(x,y\right)$ and $\overline{\overline{\mathbf{Y}}}_{sm}\left(x,y\right)$ that provide the desired electromagnetic fields or that maximize the objective function of interest. These techniques are referred to as direct and inverse source problems, respectively.

One of the main advantages of modeling an RIS through inhomogeneous sheets of impedance and admittance dyadic tensors lies in the possibility of incorporating them into Maxwell's equations by leveraging the equivalence principle and the radiation integrals, which allow us to express the electric and magnetic fields anywhere in the volume of interest directly as a function of $\overline{\overline{\mathbf{Z}}}_{se}\left(x,y\right)$ and $\overline{\overline{\mathbf{Y}}}_{sm}\left(x,y\right)$. The main assumption for using this approach consists of resorting to the physical optics approximation. Even though some approximations are usually needed to obtain the reradiated electromagnetic field, the resulting analytical framework is electromagnetically consistent and accounts for the physical implementation of the RIS. Another main advantage of the model for RISs based on inhomogeneous sheets of impedance and admittance dyadic tensors is that the mutual coupling among all the constitutive elements of the RIS (the unit cells) is inherently taken into account, since the model inherently abstracts the physical implementation of the RIS. The subsequent discretization of the RIS in unit cells based on the functions $\overline{\overline{\mathbf{Z}}}_{se}\left(x,y\right)$ and $\overline{\overline{\mathbf{Y}}}_{sm}\left(x,y\right)$ implicitly accounts for the local interactions and for the mutual coupling among the unit cell themselves.

When modeling an RIS as an inhomogeneous sheet of impedance and admittance dyadic tensors, caution needs to be paid, however, to some implicit assumptions that are made. One of these assumptions is that the RIS is modeled as a device with zero thickness. In practice, however, an RIS has a finite thickness and is made of discrete and finite-size unit cells. In order for the homogenized (continuous) version of the RIS, which is utilized at the design stage, to accurately represent the reradiation properties of the manufactured metasurface, it is necessary that the thickness of the RIS and the cross section of the unit cells are much smaller than the wavelength of the electromagnetic waves. If these conditions are met, the components of the surface fields that are related to the discretization of the RIS in unit cells can be ignored, provided that the observation point is not too close to the surface of the RIS. As a rule of thumb, the observation point should be at least at a distance $|z|>t/2+\max\{d_x,d_y\}$, where t is the thickness of the RIS and d_x and d_y are the horizontal and vertical sizes of its unit cells (assuming

that the unit cells are identical in size). In practice, this condition does not pose any constraints in the context of wireless communication systems and networks, since we are not usually interested in observation points that are so close to the RIS.

Due to these positive features, representing an RIS as an inhomogeneous sheet of surface impedance constitutes a suitable abstraction model for understanding the achievable performance limits of RISs in wireless networks and for their optimization as a function of different design criteria. In the next section, we utilize this modeling approach and elaborate how it can be leveraged for obtaining electromagnetically consistent analytical frameworks for RISs that are suitable for performance evaluation and for wireless networks optimization. In the next section, more specifically, we focus our attention on an RIS that operates in reflection mode and that is impenetrable, i.e., the electric and magnetic fields at $z = 0^-$ are equal to zero in (6.17). In this case, the RIS is an inhomogeneous boundary of surface impedance.

6.3 Multiport Network Theory – Preliminary Results

6.4 System and Channel Model

Let us consider an RIS-aided communication channel that consists of a transmitter with N_T antennas, a receiver with N_R antennas, and an N_S-port loaded scatterer that models the RIS. The RIS-aided communication link between the transmitter and the receiver can be represented by a linear network with $N = N_T + N_S + N_R$ ports. The N-port network can be characterized by a scattering matrix $\mathbf{S}$ that relates the vector $\mathbf{a}$ of the incident power waves on the ports with the vector $\mathbf{b}$ of reflected power waves from the ports. In mathematical terms, we have $\mathbf{b} = \mathbf{S}\mathbf{a}$.

The $\mathbf{S}$ matrix can be decomposed as

$$\begin{bmatrix} \mathbf{b}_T \\ \mathbf{b}_S \\ \mathbf{b}_R \end{bmatrix} = \begin{bmatrix} \mathbf{S}_{TT} & \mathbf{S}_{TS} & \mathbf{S}_{TR} \\ \mathbf{S}_{ST} & \mathbf{S}_{SS} & \mathbf{S}_{SR} \\ \mathbf{S}_{RT} & \mathbf{S}_{RS} & \mathbf{S}_{RR} \end{bmatrix} \begin{bmatrix} \mathbf{a}_T \\ \mathbf{a}_S \\ \mathbf{a}_R \end{bmatrix} \tag{6.19}$$

where $\mathbf{a}_x$ and $\mathbf{b}_x$ for $x \in [T, S, R]$ are the incident and reflected power wave vectors at the transmitter (T), RIS (S) and receiver (R) ports, respectively. Accordingly, $\mathbf{S}_{xy}$ for $x, y \in [T, S, R]$ are the scattering sub-matrices that relate the vectors $\mathbf{b}_x$ of the reflected power waves with the vector $\mathbf{a}_y$ of the incident power waves.

In a general configuration, the N_T ports of the transmitter are connected to voltage generators that are characterized by a set of power waves $\mathbf{a}_g = \{a_{g,1}, \ldots, a_{g,N_T}\}$ and a set of internal impedances $\mathbf{Z}_g = \{Z_{g,1}, \ldots, Z_{g,N_T}\}$. Also, the N_R and N_S ports of the receiver and the RIS are connected to the sets of loads $\mathbf{Z}_R = \{Z_{R,1}, \ldots, Z_{R,N_R}\}$ and $\mathbf{Z}_S = \{Z_{S,1}, \ldots, Z_{S,N_S}\}$, respectively. Therefore, the sub-vectors in (6.19) are related to the loads by the following expressions:

$$\mathbf{a}_T = \mathbf{a}_g + \mathbf{\Gamma}_T \mathbf{b}_T;\ \mathbf{a}_S = \mathbf{\Gamma}_S \mathbf{b}_S;\ \mathbf{a}_R = \mathbf{\Gamma}_R \mathbf{b}_R \tag{6.20}$$

Specifically, $\mathbf{\Gamma}_x$ for $x \in [T, S, R]$ is a diagonal matrix with entries $\Gamma_{x,i} = (Z_{x,i} - Z_{0,i})/(Z_{x,i} + Z_{0,i})$, where $Z_{0,i}$ is the reference impedance at the i-th port. Usually, $Z_{0,i} = Z_0 = 50\,\Omega$. To ensure that the ports of the transmitter and receiver are matched for zero reflection, we consider $\mathbf{\Gamma}_T = \mathbf{\Gamma}_R = 0$. Under these conditions, from (6.20) and (6.19) it is possible to derive the end-to-end channel matrix that relates the incident power wave vector $\mathbf{a}_T = \mathbf{a}_g$ and the output power wave vector $\mathbf{b}_R$, i.e., $\mathbf{b}_R = \hat{\mathbf{H}}_{e2e}\mathbf{a}_T$, as

$$\hat{\mathbf{H}}_{e2e} = \mathbf{S}_{RT} + \mathbf{S}_{RS}\mathbf{\Gamma}_S(\mathbf{U} - \mathbf{S}_{SS}\mathbf{\Gamma}_S)^{-1}\mathbf{S}_{ST} \tag{6.21}$$

where $\mathbf{U}$ denotes the identity matrix. By adjusting the matrix $\mathbf{\Gamma}_S$ of reflection coefficients of the RIS, the received power can be optimized.

An end-to-end communication channel model based on the impedance parameters can be utilized as well. Since the scattering and impedance matrices are related by the expression $\mathbf{S} = (\mathbf{Z} - Z_0\mathbf{U})(\mathbf{Z} + Z_0\mathbf{U})^{-1}$, the two channel models are equivalent. However, we show next that the representation in terms of scattering parameters may be more convenient when optimizing the end-to-end channel response as a function of the load impedances of the RIS. First, we discuss some interesting features of the representation in terms of scattering and impendance parameters for RIS-aided channels based on multiport network theory.

6.5 Scattering vs. Impedance Representations

The end-to-end channel matrix in (6.21) consists of the sum of two terms, where only the second depends on the loads connected to the ports of the RIS through the diagonal matrix of reflection coefficients $\mathbf{\Gamma}_S$. It is worth noting that the first term $\mathbf{S}_{RT}$ depends on the direct transmitter-receiver link and the transmitter-RIS-receiver link when the ports of the RIS are connected to matched loads, which results in $\mathbf{\Gamma}_S = 0$. Due to the physical presence of the RIS, this latter contribution is always present even if the direct transmitter-receiver link is blocked by the presence of physical obstacles, and it includes the structural scattering of the RIS. This is different from the representation in terms of impedance parameters, in which the structural scattering of the RIS is decoupled from the direct link and is embodied into the transmitter-RIS-receiver link. Therefore, the representations in terms of scattering and impedance parameters are equivalent, but the terms (and their physical meaning) in the two equations are not one-to-one related.

To better understand this subtle difference, let us consider the SISO setting, and let us assume that the ports of the RIS are all terminated to the reference impedance Z_0 (perfect port matching). Specifically, we obtain the following (always assuming that the ports of the transmitter and receiver are matched for zero reflection):

$$\hat{\mathbf{H}}_{e2e}(Z_0) = \mathcal{Y}_0 \left[Z_{RT} - \mathbf{Z}_{RS}(\mathbf{Z}_{SS} + Z_0\mathbf{U})^{-1}\mathbf{Z}_{ST} \right] \tag{6.22}$$

where $\mathbf{Z}_{SS}$ is the matrix of self and mutual impendances of the RIS.

If the ports of the RIS are terminated to Z_0, we have, as mentioned, $\mathbf{\Gamma}_S = \mathbf{0}$. Thus, the second addend in (6.21) is zero, and, by comparing (6.21) with (6.22), we obtain $S_{RT} = \hat{\mathbf{H}}_{e2e}(Z_0)$. It is apparent that S_{RT} depends on the RIS in contrast to Z_{RT} in (6.22).

To get further engineering insights, let us analyze the case study with no mutual coupling between the RIS elements. Also, let us assume $\mathbf{Z}_{SS} = Z_0\mathbf{U}$ in (6.22) but the ports of the RIS are terminated to generic impedances. From $\mathbf{S} = (\mathbf{Z} - Z_0\mathbf{U})(\mathbf{Z} + Z_0\mathbf{U})^{-1}$, therefore, we obtain $\mathbf{S}_{SS} = \mathbf{0}$. Then, (6.21) reduces to $\hat{\mathbf{H}}_{e2e} = \mathbf{S}_{RT} + \mathbf{S}_{RS}\mathbf{\Gamma}_S\mathbf{S}_{ST}$. In this case, we retrieve the transfer function that is usually utilized in wireless communications, with $\mathbf{\Gamma}_S$ denoting the diagonal matrix of reflection coefficients.

Let us analyze again the case study with no mutual coupling and $\mathbf{Z}_{SS} = Z_0\mathbf{U}$, but the ports of the RIS are terminated to Z_0. In this case, $\mathbf{\Gamma}_S = \mathbf{0}$ in (6.21). If $Z_{RT} = 0$, from (6.22) we obtain

$$S_{RT} = \hat{\mathbf{H}}_{e2e}(Z_0) = -\frac{\mathcal{Y}_0}{2Z_0}\mathbf{Z}_{RS}\mathbf{Z}_{ST} \tag{6.23}$$

Therefore, we see that, even if the direct transmitter-receiver link is blocked by physical objects and the reflection coefficient of the RIS is equal to zero, the received signal is not equal to zero, since $S_{RT} \neq 0$. This terms is equivalent to a specular reflection from the RIS and includes the so-called structural scattering, which occurs when all the ports of the RIS are terminated to Z_0. In communication papers, this term is usually ignored: In fact, if the direct transmit-receiver link is blocked and the reflection coefficient is zero, it is assumed that the received signal is zero as well. It is worth noting that in the model in (6.21) based on the scattering parameters, the structural scattering is contained in $S_{RT} \neq 0$. In the model in (6.22) based on the impedance parameters, on the other hand, the structural scattering is not contained in Z_{RT}, but in the RIS-dependent term.

Finally, let us consider (6.21) and let us assume that $\mathbf{S}_{SS}$ is a diagonal matrix for simplicity. Even if the reflection coefficients in $\mathbf{\Gamma}_S$ are assumed to have a unit modulus, we evince that the presence of the RIS has an impact on the amplitude and phase of the incident signal. Also, the impact of the phase and the amplitude cannot be decoupled. This is due to the term $\mathbf{\Gamma}_S(\mathbf{U} - \mathbf{S}_{SS}\mathbf{\Gamma}_S)^{-1}$. If the elements of $\mathbf{\Gamma}_S$ have a unit modulus, the RIS operates only on the phase of the incident signal if and only if $\mathbf{S}_{SS} = \mathbf{0}$. If $\mathbf{S}_{SS}$ is not a diagonal matrix, the relationship between the amplitude and the phase is, in general, even more pronounced.

6.6 RIS Optimization

The RIS optimization problem is formulated for the SISO case, i.e., $N_T = N_R = 1$. In this case, (6.21) can be written as

$$b_R = \left[S_{RT} + \mathbf{S}_{RS}\mathbf{\Gamma}_S(\mathbf{U} - \mathbf{S}_{SS}\mathbf{\Gamma}_S)^{-1}\mathbf{S}_{ST} \right] a_T \tag{6.24}$$

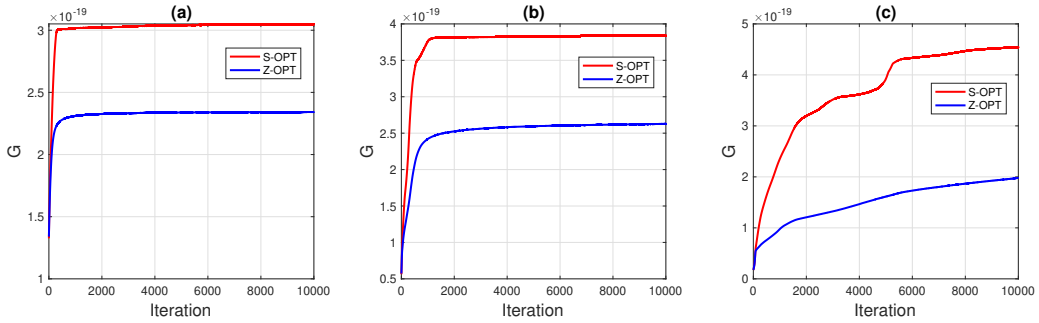

Figure 6.5: Convergence vs. iterations: (a) $d_y = \lambda/4$; (b) $d_y = \lambda/8$; (c) $d_y = \lambda/16$

In this setting, we consider the optimization problem

$$\max_{\mathbf{\Gamma}} \left| S_{RT} + \mathbf{S}_{RS}\mathbf{\Gamma}(\mathbf{U} - \mathbf{S}_{SS}\mathbf{\Gamma})^{-1}\mathbf{S}_{ST} \right|^2 \quad \text{s.t.} \quad |\Gamma_k| = 1 \text{ for } k = 1, \ldots, N_S \tag{6.25}$$

where $\mathbf{\Gamma} = \mathbf{\Gamma}_S$ and $\Gamma_k = \Gamma_{k,k}$ to simplify the notation.

The main challenge in solving (6.25) is that the objective function depends on the inverse of a matrix, which in turn depends on $\mathbf{\Gamma}$ that is the optimization variable. This makes the problem strongly non-convex. To circumvent this problem, we use an iterative algorithm that provably allows us to increase the objective function at each iteration and hence to find a local optimum for the problem at hand.

To elaborate, we denote by X_k the k-th tunable reactance of the RIS and by $\Sigma_k = \frac{jX_k - 1}{jX_k + 1} = e^{j\phi_k}$. Also, we assume that the parasitic resistances of the tunable impedances of the RIS are much smaller than $Z_0 = 50\,\Omega$.

The algorithm works iteratively and adjusts ϕ_k at each iteration, by introducing small perturbations with respect to the previous iteration, i.e., $\phi_k^{(m+1)} = \phi_k^{(m)} + \delta_k^{(m)}$. Under these assumptions, the matrix inversion can be linearized by using the Neumann series approximation, and the problem in (6.25) can be solved. Specifically, with the aid of some mathematical manipulations, one can show that the optimum $\delta_k^{(m)}$ at the m-th iteration is

$$\delta_k^{(m)} = \begin{cases} \Delta_m & \text{if } \left| A^{(m)} + C_k^{(m)}\Delta_m \right| \geq \left| A^{(m)} - C_k^{(m)}\Delta_m \right| \\ -\Delta_m & \text{otherwise} \end{cases} \tag{6.26}$$

where $\Delta_m \ll 1$ is the step-size, $\mathbf{\Gamma}^{(m)}$ is the vector of reflection coefficients at the m-th iteration, $A^{(m)} = S_{RT} + \mathbf{S}_{RS}\mathbf{Q}_m^{-1}\mathbf{S}_{ST}$, $\mathbf{Q}_m = \left(\mathbf{\Gamma}^{(m)}\right)^{-1} - \mathbf{S}_{SS}$, $C_k^{(m)} = b_{1,k}^{(m)} b_{2,k}^{(m)}$, where $b_{1,k}^{(m)}$, $b_{2,k}^{(m)}$ are the entries of $\mathbf{b}_1^{(m)} = \mathbf{S}_{RS}\mathbf{P}_m$ and $\mathbf{b}_2^{(m)} = \mathbf{Q}_m^{-1}\mathbf{S}_{ST}$, with $\mathbf{P}_m = j\mathbf{Q}_m^{-1}\left(\mathbf{\Gamma}^{(m)}\right)^{-2} e^{j\boldsymbol{\Phi}^{(m)}}$, where $e^{j\boldsymbol{\Phi}^{(m)}}$ is a diagonal matrix whose entries are $e^{j\phi_k^{(m)}}$.

6.7 Numerical Results

The RIS is centered at the position $(0, 0, 2)$ m, and the transmitter is located at the position $(4, 0, 3)$ m. The receiver is located at the position $(0, 7, 4, 1)$ m, i.e., it is located at an angle of nearly 80 degrees with respect to the direction of specular reflection. The transmitting and receiving antennas, as well as the scatterers of the RIS are identical perfectly conducting z-directed dipoles with radius $\lambda/500$ and length $L = 0.46\lambda$. The RIS dipoles are arranged as a uniform planar array, and the spacing of the elements is $d_y = \lambda/Q$ with $Q = 4, 8, 16$ in the y direction and $d_z = 3/4\lambda$ in the z direction. The RIS has approximately the shape of a square with an area $4\lambda^2$.

In Fig. 6.5, we illustrate the convergence properties of the proposed algorithm, which is denoted by S-OPT, and compare it against the benchmark scheme proposed based on the impedance parameters, which operates on the impedance parameters and is denoted by Z-OPT. The comparison is given in terms of the squared norm of the end-to-end transfer function in Sec. 6.4, which is denoted by G. Ae assume that the direct link is negligible due to the presence of obstacles between the transmitter and receiver.

It is observed that S-OPT outperforms Z-OPT. This is attributed to the fact that small perturbations of the step size of S-OPT result in larger variations of the S-parameters, hence increasing the convergence speed of the algorithm.

6.8 Conclusion

In this chapter, we have first overviewed the most utilized communication models for RIS. Then, we have focused on the multiport network model, and have compared the scattering and impedance representations for an RIS-aided channel. Also, we have developed an algorithm for optimizing the RIS configuration in the presence of electromagnetic mutual coupling based on the scattering parameters, which is shown to outperform existing algorithms based on optimizing the impedance parameters.

Chapter 7 : Radio-Frequency Front-End Modules, Reconfigurable antennas and RIS: preliminary results

7.1 Introduction

The content of this chapter relates to Radio-Frequency Front-End Modules, Reconfigurable antennas and RIS aspects of the project and constitutes WP2. This WP2 is thus composed of three parts which will be detailed in the next three paragraphs.
The WP as a whole comprises nine tasks:

- Task C2-1 : Design and manufacturing of Hybrid PA architecture
- Task C2-2 : Design and manufacturing of highly efficient miniature antennas
- Task C2-3 : Design of multifunction and reconfigurable antennas using in particular agile metamaterials (base station or gateway)
- Task C2-4 : High performance frontend transceivers for 5G MIMO applications
- Task C2-5 : Design, Realization and testing of reconfigurable antenna with biosourced technologies
- Task C2-6 : Reconfigurable antenna and advanced RF architectures
- Task C2-7 : RIS-assisted multiuser massive MIMO systems
- Task C2-8 : Holographic cell free massive MIMO
- Task C2-9 : MU-MIMO with low PAPR transmission

Only a few tasks have begun (C2-5). The others are planned later in the project, or have been delayed due to recruitment difficulties linked in particular to the authorities' response time regarding the validation of candidates.

The following paragraphs describe the context and objectives of each field of research gathering the different tasks listed above as identified in the WP2 working plan. The progress of the work and any next steps are also exposed.

7.2 Design of innovative power amplifier architectures

The shift to scalable and highly integrated distributed mMIMO solutions raises new research questions. One important research challenges is to increase the energy efficiency and linearity of the Power Amplifier (PA) over a wide bandwidth and a large output power back-off range.

7.2.1 Design and Manufacturing of Hybrid PA architectures

The transmitter and more specifically the PA usually dominates the energy consumption of wireless systems. The PA is a critical component that must be co-designed with the system architecture and digital signal processing functions, like Digital Pre-distortion, to minimize the overall energy consumption while respecting system requirements.

Objective
This work aims to develop next generation of energy efficient and scalable PA solutions for future distributed mMIMO systems. In this task, we will address key PA architecture and design challenges with emphasis on integration, power consumption reduction, linearity improvement and bandwidth extension. Exploration of load and supply modulation techniques together with GaN and silicon co-design/co-integration appears as key to address these needs. To fully utilize the potential of these technologies, we will investigate innovative Hybrid PA architectures and integration schemes.

Status
During the first period of the project, CEA has been working on compiling the state of the art of Load Modulated Power Amplifier architectures, focusing more specifically on Load-Modulated Balanced Amplifiers.

Next steps
In the next steps, new PA architectures and design will be investigated.

7.2.2 High performance front-end transceivers for 5G MIMO applications

Inherent nonlinearities in PAs introduce distortion, compromising signal quality and limiting system performance. To address this challenge, digital predistortion (DPD) has emerged as a powerful technique that compensates for PA nonlinearities, restoring signal integrity. Conventionally, DPD has been applied as a post-processing step, relying on post-measurement data to characterize PA nonlinearities and design the predistortion system. This approach, however, suffers from several limitations. First, it is necessary to manufacture the PA and measure its performance before DPD can be applied. This is a time-consuming and expensive process, especially for high-power PAs. Second, this post-manufacturing approach also means that the PA performance is fixed, which reduces the flexibility of the system and does not proactively address potential nonlinearities at the design stage. Third, the DPD system is usually designed as a standalone black-box model which does not take into account the PA architecture and its core features. Codesign involves integrating DPD into the PA design process, optimizing both the amplifier architecture and the predistortion system in a synergistic manner. Despite these advantages, codesign also presents challenges. One key challenge lies in the need to perform linearization as early as possible, typically at the electrical simulation level. This requires accurate nonlinear models of the PA and the DPD system, which can be time-consuming and computationally expensive to achieve.

Objective
The main target contribution of this task is to develop an efficient codesign methodology and framework for PA and DPD system, which can be applied at the electrical simulation level taking advantage of the latest advances in RF simulators. A secondary target contribution is to develop a new DPD model that is optimised to address the specificities of the PA architecture investigated in the other task of the work package.

Status
This task has not started yet. The task is being prepared: teams of WP2.1 are now coordinating to synchronize work schedules. (Delayed compared to project proposal (technical annex) but initial dates required refinements.)

Next steps
Job description will be published in April, targeting a recruitment of a 18-month fixed-term contract, R&D Engineer

or PostDoc for September 2024.

7.2.3 MU-MIMO with low PAPR transmission & Power Amplifier model for massive MIMO antenna

Status
This task has not started yet. A post-doc position (duration 18 months) is awaiting recruitment.

Next steps
Study the impact of its characteristics on the performance of a transmitter system for a 5G application using CF-mMIMO technology.

Major steps (dates to be set soon):

- State of the art on Digital Power Amplifier (DPA). Objective is to highlight the specific operating features of this type of power amplifier. Possibly a demonstrator.
- Modeling of the amplifier based on simulations (potentially a realized circuit).
- Integration of the model into a transmitter system
- (Depending on progress) Improvement of system linearity.

7.3 Design of advanced antenna structures

7.3.1 Context and motivation

Massive MIMO (mMIMO), one of the key technologies of the future mobile communication system, offers a large degree of beamforming capacity in order to improve spectral efficiency, network capacity, coverage, and feasible data rates. Massive MIMO uses multi-antenna elements to support multiple users simultaneously. The essential parameters of mMIMO antennas can be considered as frequency bands, gain, isolation, envelope correlation, radiation pattern, polarization, and beamwidth. One possible way to increase throughput and data transfer rates in current and future generations of mobile and wireless devices is to extend the bandwidth, as a higher bandwidth provides a higher data rate.
Reducing the mutual coupling effects between antenna elements in large-scale arrays with limited space will offer high isolation and low correlations for the system without limiting the system's performance. Using beamforming methods could boost the gain and efficiency of a mMIMO system. To enhance the overall system performance and capacity, beamforming can be defined as a signal processing approach that is utilized with multiple antenna arrays on the receiver side and/or transmitter side for sending or detecting multiple signals from multiple desired terminals at once.
So, the main challenges imposed by mMIMO technology are integration and deployment of new compact radiating structures in order to produce directional radiation with beamforming (or multi-beam) where the antenna spacing generates negligible coupling effects between antennas and thus facilitates the system design and reduce power consumption.
In summary, Cell-free mMIMO communication scenarios required multi-broadband aerials with multiple focusing radiation properties both at the base station and also at the user terminal level. The use of compact directional unit sources in dense antenna arrays for analog, digital or hybrid beam forming is a major area of innovation to optimize the communication performance of these systems.
To address these challenges, several innovative approaches based on the concept of superdirective antennas, metasurfaces antennas will be explored in mMIMO context. Moreover, the environmental footprint of mMIMO will be minimized by using the bio sourced approach.

7.3.2 Challenges and proposed methodology

During the course of the study, it is planned to foster collaborations with the partners involved in WP2 in terms of antenna design using conventional substrates (IETR, CEA Leti, and RFM² team at Télécom) and bio sourced substrates (DHREAMS team at CROMA).
The antennas thus defined will be built and measured to confirm the performance obtained. A life cycle analysis will be also realized to define a figure of merit (FoM) taking into account the performance and environmental impact. Depending on the degree of maturity of the proposed solution, this antenna could also be used for testing (WP5).

Superdirective antennas :

One of the most challenging problems in antenna design is that of superdirective array, where it attracted for years the interest of antenna engineers both from the theoretical and practical parts. Superdirective antenna array offers new opportunities for wireless applications in terms of spectral efficiency, reduced environmental impact and use modes. It is an attractive technique in overcoming the omnidirectional radiation pattern of small antennas; by forming an array of closely spaced elements ($d < 0.25\lambda$) an extraordinary directivity can be achieved namely "superdirective".

These highly coupled miniature element antenna topologies allow the radiation to be shaped more pronouncedly than their equivalent geometric surface assumed excited uniformly in phase and amplitude. This concept is particularly interesting for shaping the radiation of compact antennas, as observed by Uzkov in 1946 [43], who noted increased directivity of end-fire isotropic source arrays as the spacing between the elements decreases to zero. Long limited to theoretical developments, superdirectivity has been demonstrated experimentally in recent studies [50] [71] [23] [51] making it possible to reconsider the well-known sensitivity problems of practical realization. However, these studies have highlighted limitations such as limited radiation efficiency and/or reduced bandwidth. Complementary research works have been initiated to solve these problems, notably with specific optimization approaches [63] [119] [117] [108]. New superdirective antenna developments are necessary to match the requirement of cell-free telecommunication antennas, and most particularly to miniaturize, to improve efficiency, to reconfigure the radiation and to widen the operating frequency band.

Compact reconfigurable multi-access super directive antenna
The development of compact radiating sources with directional radiation over different frequency bands is consequently studied at CEA Leti by drawing inspiration from the concepts of superdirective antennas. CEA Leti's work initially focuses on understanding loss phenomena in compact super-directive antenna structures with the aim of optimizing radiation efficiency and obtaining supergain antennas. Using spherical wave expansion where a loss model has been introduced, radiation optimized designs are tested and analyzed. Ways to improve the gain of super directive antennas are finally considered. Also, the electronic reconfiguration of radiation is the object of study aimed at controlling the pattern shape or the polarization of the transmitted electromagnetic field. On the other hand, superdirective antenna bandwidth widening is studied for use in low cellular frequency bands where miniaturization of radiating sources is critical. Particular arrangements of broadband sources are studied with the tool based on spherical wave expansion in order to understand the limitations and propose improvements.
The following developments will consist in studying the integration of these concepts, partly on a typical user terminal and partly on a compact base station. At the user terminal level, research will be focused on multi-beam formation capability in low band and in the new FR3 low bands. For the base station, research activities aim to develop a compact reconfigurable multi-access super directive antenna solution to serve mixed digital-analog architectures suitable for MIMO processing.

Status
This task has not started yet.

Design of compact array made of superdirective antennas
The deployment of MIMO technology is based on the multiple-antenna array. However, when the MIMO antenna elements are closely placed to each other, the mutual coupling between them leads to impedance mismatch, reduces the radiation efficiency, and even affects the channel capacity. Thus, extensive efforts have been devoted to the

coupling reduction between antenna elements, and a series of solutions have been put forward. The objective of the work proposed by the IETR is to design a compact mMIMO system utilizing superdirective antenna arrays. Our focus lies on reducing the coupling between the array elements and between arrays themselves and also deploying the multi-objective optimization algorithm based on network characteristic modes that were previously developed in our laboratory [118] in order to achieve maximum directivity with the minimization of the input reflection coefficient in a large bandwidth. We propose to incorporate coupling in the optimization process. Moreover, we will integrate the reconfiguration function into the superdirective antenna arrays for beamforming. Although of the remarkable potential gain improvement introduced by the superdirective antenna arrays, there are several challenges that obstruct its practical realization, one of them is the superdirective beamforming vector that can affect the antenna array performance and the calculation of this vector is known as a very challenging problem. To empirically validate the theoretical and numerical results, we will fabricate various prototypes based on different technologies and assess them using the technical platforms provided by IETR. The specifications for this antenna will also be defined once the scenarios selected in WP1 have been studied.

Status
This work will be carried out as part of a PhD program. The candidate has been recruited since January 1st.

Next steps
The specifications for this antenna will also be defined once the scenarios selected in WP1 have been studied.

Metasurface antenna structure :

The objective of the work proposed by the RFM² team at Télécom Paris is to develop an access point antenna, associated with two metasurfaces, low profile, multi-band, with the possibility of having a steerable beam in one of the bands. Metasurfaces have proved useful for improving antenna performance, combined with traditional antennas, these metasurfaces can improve radiation properties. There are several types of metasurfaces with exotic properties that are impossible to obtain with conventional materials. However, metamaterials often exhibit their novel properties within a limited frequency range. This narrow frequency band characteristic is a real problem, as many practical applications are broadband and/or multiband. It is therefore necessary to design tunable metamaterials that can be reconfigured in frequency. With appropriate control, the metamaterial can be tuned to achieve the desired property at the working frequency. Tunable metamaterials can also be used for adaptive antennas to control their radiation pattern as a function of the environment, for example.
This work will be carried out as part of a PhD. The candidate has been identified and his recruitment is awaiting validation (since December 1). As soon as the candidate has started, a state of the art will be proposed. The specifications of this antenna will also be defined once the scenarios selected in WP1 have been studied.
The problem is as follows: in Rafael G. L. Melo's PhD [44], we demonstrated that it was possible to place two metasurfaces on either side of a broadband (bow-tie) antenna to obtain a low profile multiband directional antenna compatible with European 4G/5G and Wi-Fi 2.4/5/6E standards and operating in the following bands: 2.40-2.70 GHz, 3.40-3.80 GHz, 5.17-5.83 GHz, and 5.93-6.45 GHz.

The first metasurface exploits both the perfect electrical conductor (PEC) and perfect magnetic conductor (PMC) characteristics of a dual-band artificial magnetic conductor (AMC). The second metasurface, known as the Huygens metasurface, enables the beam to be de-pointed in one of the operating frequency bands. By controlling the polarization voltages on four varactor columns in the reconfigurable, multi-band Huygens metasurface, the beam can be dynamically steered to ±51°, continuously, over a frequency range within the European 5G frequency range (3.50 to 3.65 GHz) [45].
The aim of this thesis is to further develop this concept along several axes:

- Evolve the Huygens metasurface into a planar structure
- Add control elements to the artificial magnetic conductor to increase the antenna's number of degrees of freedom
- Develop a compact feeding system integrated into the antenna

Status
This task has not started yet.

Multi-feed pattern reconfigurable antenna using bio-sourced substrate :

Most of the antenna structures for 5G make use of conventional substrates that are generally considered as e-waste at the end of the life cycle. The primary goal of the work conducted at CROMA lab is then to reduce e-wastes by proposing a state-of-the-art comparable structure using bio-sourced substrates. However, these kinds of substrates are generally lossy with a low power handling. In this context, the objective is to design a multi-feed pattern reconfigurable antenna. The multiple feeds allow for the energy to be combined directly on the radiating structure, avoiding lossy power combination units generally required between a single feed antenna and the outputs of power amplifiers. This structure also offers more degrees of freedom to reconfigure and allows the integration of distributed amplifier network to enhance energy efficiency. Furthermore, to further reduce the losses, the multi-feed structure should potentially be configured to refrain from the implementation of lossy matching networks. The pattern reconfigurability, on the other hand, offers an increased space coverage thereby compensating the narrow main lobe due to high gain. The power to be delivered to the structure is considered to be between 20-30 dBm and the frequency range between 6-7 GHz.

This work will be carried out as part of a PhD student that has been identified. It has planned to go as follows:

- Characterize bio-sourced substrates to identify those with the best properties.
- Design and characterize conventional antennas using the selected bio-sourced substrate(s) to control error sources and master the fabrication process.
- Design a multi-feed antenna on the bio-sourced substrate(s) and evaluate power handling capability
- Design a reconfigurable multi-feed antenna on the bio-sourced substrate(s)
- Design the distributed amplifier active antenna on the bio-sourced substrate.
- Define the Figure of Merit (FoM) taking into account both antenna efficiency and environmental impact

Status
Rim Berro started her PhD on 01 December 2023. She is now working on the review of different biosourced substrates to select the potential substrates taking into account the RF (permittivity, loss) and mechanical (power handling capability, surface roughness, strength,...) properties. In parallel, she has started to design the first antenna based on air-filled technological platform to reduce the effect of the substrate at the expense of a larger footprint.

Next steps
The next steps are to fabricate and measure this antenna for the first demonstration and to study different transmission lines and antenna topologies.

7.4 Design of RIS

7.4.1 Context and motivation

Regarding the required key performance indicators (KPI's) which are planned for 6G wireless systems, the most challenging ones are the energy and spectrum efficiency targets, expected to be respectively at less 10 times and 5 times better for 6G than those of 5G. In these conditions, it is admitted that these KPI's won't be achieved by the 5G physical layer. This is particularly clear in the case of the spectrum efficiency since a prohibitive large number of antennas along with active radio frequency (RF) chains are needed for massive MIMO to achieve high spectrum efficiency and this results in high energy consumption and high hardware costs. The dense deployment of small

base stations is also a possible solution but this entails high maintenance costs, network energy consumption and hardware cost due to high-speed backhaul links. Furthermore, such network architecture is very demanding in terms of sophisticated signal processing algorithms for interference management. The use of RIS (reconfigurable Intelligent Surfaces) or IRS (Intelligent Reflecting Surfaces) combined with a cell free network architecture is maybe a promising response for the deployment of 6G wireless communication systems. The RIS has the amazing property to reconfigure the wireless propagation environment into a transmission medium with good transmission properties. Up to now, the wireless propagation medium was considered as a randomly time varying entity that disturbs the transmitted signals due to uncontrolled reflections, refractions and unexpected interference. Despite the use of powerful signal processing tools such as channel coding, channel precoding and channel equalization, the image of the wireless propagation medium as a disruptive environment is still present. Moreover, one has to recognize that signal processing techniques have reached a certain level of saturation and technical breakthroughs to improve data rate and performance reliability are unlikely to appear soon. It is logical in these conditions to think of the wireless propagation medium as a new additional variable to optimize. The main desirable characteristic of RIS/IRS is that they are composed of quasi passive low-cost reflecting elements. Each reflecting element can impose an independent phase shift/amplitude on the impinging electromagnetic signals in a fully customized way. The phase shifts imposed on the incident electromagnetic signals can be adjusted in real-time in reaction to the rapid variations in the wireless propagation environment. The principle consists in tuning the phase shifts of the RIS/IRS in order to combine constructively (or destructively in the case of interfering signals) the signals reradiated from the RIS/IRS with the signals from other paths. Unlike conventional relaying techniques, an RIS/IRS contains no active device such as power amplifier and thus it entails much reduced power consumption and reduced cost. Furthermore, due to its quasi passive nature, an RIS/IRS can be easily integrated in the surrounding environment including building facades, ceilings, street lamps and so on.

7.4.2 Challenges and proposed methodology

Of course, due to its appealing features, a lot of research work has been already published around RIS/IRS and their potential use for 6G. A very complete study about the benefits of the use of RIS/IRS in the context of massive 5G communications can be found in [148] with a very complete state of art concerning the signal processing techniques used with RIS/IRS. Then, a very important work in [148] describes the impact of practical hardware impairments on the performance of an RIS communication system. The work in [64] proved that it was possible in an indoor realistic propagation environment to obtain a 26 dB power gain for a RIS/IRS prototype with 1100 controllable elements, operating around 5.8 GHz band. The problem of joint carrier frequency offset (CFO) and channel estimation for RIS-aided orthogonal frequency division multiplexing (OFDM) systems has been studied in [65], [81] taking into account the presence of synchronization errors. In addition to these works one can add contributions in operation principles [46], transmission design and applications [28], electromagnetic modeling [116] and channel estimation [96].

Concerning the proposed work by XLIM, we would like to deal with the problem of huge number of channels to be estimated. Since the complexity is prohibitively important, the machine learning techniques will be probably considered. Quantifying the improvement due to the use of RIS/IRS in the context of a cell-free massive MIMO transmission system is the main task we are getting involved in WP2, where the imprecision of channel estimations could introduce significant degradation in rate.

Concerning the work proposed by L2S/ETIS, the research activities on RIS have been already conducted. During the first reporting period of the project, we have conducted extensive research on RIS-aided systems with focus on modeling and optimization, with special interest in utilizing models that are so-called electromagnetically consistent. The research activity has resulted in the publication of 9 research papers [90], [39], [123], [120], [101], [146], [99], [52], [127]. Among them, we describe in what follows [90] and [52], with the latter being a joint work between L2S and ETIS Lab. In [90], we focus on electromagnetically consistent models for RISs inheriting from a recently proposed model based on mutually coupled loaded wire dipoles. While existing related research focuses on free-space wireless channels thereby ignoring interactions between RIS and scattering objects present in the propagation environment, we introduce an RIS-aided channel model that is applicable to more realistic scenarios, where the scattering objects are modeled as loaded wire dipoles. By adjusting the parameters of the wire dipoles, the properties of general natural and engineered material objects can be modeled. Based on this model, we introduce

a provably convergent and efficient iterative algorithm that jointly optimizes the RIS and transmitter configurations to maximize the system sum-rate. Extensive numerical results show the net performance improvement provided by the proposed method compared with existing optimization algorithms. In [39], we consider an RIS-assisted multiple-input multiple-output (MIMO) system in the presence of scattering objects. The MIMO transmitter and receiver, the RIS, and the scattering objects are modeled as mutually coupled thin wires connected to load impedances. We introduce a novel numerical algorithm for optimizing the tunable loads connected to the RIS, which does not utilize the Neumann series approximation. The algorithm is provably convergent, has polynomial complexity with the number of RIS elements, and outperforms the most relevant benchmark algorithms while requiring fewer iterations and converging in a shorter time.

Status
A PhD student has been selected to work at XLIM on these aspects and is still waiting for the final administrative process to converge. A post-doc candidate will also be sought to work at L2S/ETIS and address the above working plan. Up to now, state of the art analysis and ongoing studies linked to the project in the different teams are being pursued to be able to rapidly produce new results as soon as the PhD and post-doc arrive.

7.5 Conclusion

This chapter summarizes the various planned and undertaken tasks of the WP2 (RF FEM, Reconfigurable antennas and RIS). The project is made up of three major tasks, each addressing a key element of the transmission chains of 5G and future 6G systems. The status of each major task is variable, given that most of the task are planned later in the project or have being delayed due to recruitment issues. However, some subtasks have successfully started.

This report introduces some strategic elements of the development of innovative power amplifier architectures (WP2.1), focusing on Hybrid PA architectures, digital predistortion and crest factor analysis for energy efficiency and scalability.

The report also provides an introduction to advanced antenna structures (WP2.2) along with a detailed classification and analysis of various antenna types and innovative substrates. The main performance enhancement techniques have been reviewed focusing on parameters like bandwidth, gain, and efficiency.

Additionally, the key role of RIS (WP2.3) in the development of 6G technologies has been introduced, along with the main challenges and research directions. The focus on efficient channel estimation methods for the composite RIS/IRS channel, and the development of optimal pilot symbol sequences and weight tap computations for phase shifters, are critical steps towards reaching the full potential of RIS/IRS.

The integration of all these technologies is critical for the evolution of mMIMO systems, offering promising solutions for the demands of future wireless communication systems.

Chapter 8 : Conclusion

The emergence of 6G wireless technology promises significant improvements in data rates and traffic capacities, along with a notable reduction in data connection latency compared to its predecessors. However, these advancements primarily benefit UEs near cell centers, leading to persistent challenges at cell peripheries, such as inter-cell interference and handover issues. To address these limitations, the transition to a cell-free paradigm, particularly through the use of cell-free massive multiple input multiple output (CF-mMIMO), is studied in this project.
In CF-mMIMO, a multitude of access points (APs) is strategically distributed across the deployment area, cooperating to optimize service for UEs by leveraging massive macro-diversity gain. This dense deployment reduces the average distance between UEs and serving APs, combating issues like shadow fading through spatial diversity. However, several challenges and open issues are associated with CF-mMIMO.
One critical aspect is channel estimation and pilot assignment in the uplink, where pilot contamination poses challenges despite the use of TDD. Proper pilot assignment techniques are essential, especially in scenarios with a massive number of UEs and APs, impacting the scalability of CF-mMIMO systems.
AP selection is another consideration, with Dynamic Cooperation Clustering (DCC) being a preferred framework over the impractical 'ALL' scenario where the whole set of APs cooperate to serve each UE. Moreover, adapting AP clustering schemes to high-mobility scenarios, such as V2I communications, is crucial and will be studied in this project.
The choice between centralized and distributed beamforming in CF-mMIMO introduces trade-offs. While centralized operations achieve higher SE, they pose scalability challenges. In contrast, distributed operations offer advantages in reduced fronthaul signaling but may sacrifice SE due to limited interference suppression capabilities.
Power allocation/control, particularly in low-latency contexts, requires careful design, and heuristic allocation techniques will be proposed to address heavy computational requirements of optimal solutions. Optimization of energy efficiency and battery life is also of great importance, necessitating further investigations.
As the density of APs grows, backhaul provisioning becomes a critical concern. Innovative strategies inspired by C-RAN methods will be developed in this project to minimize backhaul requirements, while considering challenges such as spectrum availability and high data rate delivery over wireless links.
The integration of reconfigurable intelligent surfaces (RIS) in cell-free networks offers a potential solution to enhance efficiency while minimizing hardware costs. RIS complements CF-mMIMO by reflecting incoming signals in a controllable manner. However, challenges in joint optimization of transmit beamforming vectors and RIS parameters, channel estimation, and optimal deployment positions must be addressed and constitute an important focus of this work.
In conclusion, while CF-mMIMO holds promise for overcoming the limitations of traditional cellular networks, addressing challenges related to channel estimation, AP selection, deployment scenarios, power allocation, backhaul provisioning, and integration of RIS is essential for realizing its full potential in future wireless communication systems. This projects aims at proposing innovative solutions that shall address this ensemble of challenges in order to reap the maximum profit from the cell-free context.

Bibliography

[1] Mohamed Ali Adjif, Oussama Habachi, and Jean-Pierre Cances. Joint channel selection and power control for noma: A multi-armed bandit approach. In *2019 IEEE Wireless Communications and Networking Conference Workshop (WCNCW)*, pages 1–6, 2019.

[2] Tania Alhajj, Nicolas Huin, Karine Amis, and Xavier Lagrange. Radio resource allocation in low- to medium-load regimes for energy minimization with C-RAN. In *Proceedings of the 26th International Symposium on Wireless Personal Multimedia Communications (WPMC)*. IEEE, November 2023.

[3] Ehsan E. Khaleghi; Cedric Adjih; Amira Alloum and Paul Mühlethaler. Near-far Effect on Coded Slotted ALOHA. *2017-IEEE 28th Annual International Symposium on Personal, Indoor, and Mobile Radio Communications (PIMRC)*, pages 1–7, October 2017.

[4] Muntadher Alsabah, Marwah Abdulrazzaq Naser, Basheera M. Mahmmod, Sadiq H. Abdulhussain, Mohammad R. Eissa, Ahmed Al-Baidhani, Nor K. Noordin, Sadiq M. Sait, Khaled A. Al-Utaibi, and Fazirul Hashim. 6G wireless communications networks: A comprehensive survey. *IEEE Access*, 9:148191–148243, 2021.

[5] Tasneem Assaf, Arafat Al-Dweik, Mohamed El Moursi, and Hatem Zeineldin. Exact ber performance analysis for downlink noma systems over nakagami- m fading channels. *IEEE Access*, 7:134539–134555, 2019.

[6] Eren Balevi, Faeik T. Al Rabee, and Richard D. Gitlin. Aloha-noma for massive machine-to-machine iot communication. In *2018 IEEE International Conference on Communications (ICC)*, pages 1–5, 2018.

[7] Meghana Bande and Venugopal V. Veeravalli. Adversarial multi-user bandits for uncoordinated spectrum access. In *ICASSP 2019 - 2019 IEEE International Conference on Acoustics, Speech and Signal Processing (ICASSP)*, pages 4514–4518, 2019.

[8] Hengyao Bao, Jun Fang, Qian Wan, Zhi Chen, and Tao Jiang. An ADMM approach for PAPR reduction for large-scale MIMO-OFDM systems. *IEEE Transactions on Vehicular Technology*, 67(8):7407–7418, 2018.

[9] A. Benalla and K.C. Gupta. Multiport network model and transmission characteristics of two-port rectangular microstrip patch antennas. *IEEE Transactions on Antennas and Propagation*, 36(10):1337–1342, 1988.

[10] Anass Benjebbour, Yuya Saito, Yoshihisa Kishiyama, Anxin Li, Atsushi Harada, and Takehiro Nakamura. Concept and practical considerations of non-orthogonal multiple access (noma) for future radio access. In *2013 International Symposium on Intelligent Signal Processing and Communication Systems*, pages 770–774, 2013.

[11] Patrick Bergmans. A simple converse for broadcast channels with additive white gaussian noise (corresp.). *IEEE Transactions on Information Theory*, 20(2):279–280, 1974.

[12] Matteo Berioli, Giuseppe Cocco, Gianluigi Liva, Andrea Munari, et al. Modern random access protocols. *Foundations and Trends® in Networking*, 10(4):317–446, 2016.

[13] Ilai Bistritz and Amir Leshem. Distributed multi-player bandits - a game of thrones approach. In S. Bengio, H. Wallach, H. Larochelle, K. Grauman, N. Cesa-Bianchi, and R. Garnett, editors, *Advances in Neural Information Processing Systems*, volume 31. Curran Associates, Inc., 2018.

[14] Emil Björnson and Luca Sanguinetti. Scalable cell-free massive MIMO systems. *IEEE Transactions on Communications*, 68(7):4247–4261, 2020.

[15] Emil Björnson, Erik G. Larsson, and Mérouane Debbah. Massive MIMO for maximal spectral efficiency: How many users and pilots should be allocated? *IEEE Transactions on Wireless Communications*, 15(2):1293–1308, 2016.

[16] Panagiotis Botsinis, Dimitrios Alanis, Zunaira Babar, Hung Viet Nguyen, Daryus Chandra, Soon Xin Ng, and Lajos Hanzo. Quantum Search Algorithms for Wireless Communications. *IEEE Communications Surveys & Tutorials*, 21(2):1209–1242, 2019.

[17] Sucharita Chakraborty, Özlem Tuğfe Demir, Emil Björnson, and Pontus Giselsson. Efficient downlink power allocation algorithms for cell-free massive MIMO systems. *IEEE Open Journal of the Communications Society*, 2:168–186, 2020.

[18] Robin Chataut and Robert Akl. Massive MIMO systems for 5G and beyond networks—overview, recent trends, challenges, and future research direction. *Sensors*, 20(10):2753, 2020.

[19] Shuaifei Chen, Jiayi Zhang, Emil Björnson, Jing Zhang, and Bo Ai. Structured massive access for scalable cell-free massive MIMO systems. *IEEE Journal on Selected Areas in Communications*, 39(4):1086–1100, 2020.

[20] Shuaifei Chen, Jiayi Zhang, Jing Zhang, Emil Björnson, and Bo Ai. A survey on user-centric cell-free massive MIMO systems. *Digital Communications and Networks*, 8(5):695–719, 2022.

[21] Zheng Chen and Emil Björnson. Channel hardening and favorable propagation in cell-free massive MIMO with stochastic geometry. *IEEE Transactions on Communications*, 66(11):5205–5219, 2018.

[22] Jinho Choi. Noma-based random access with multichannel aloha. *IEEE Journal on Selected Areas in Communications*, 35(12):2736–2743, 2017.

[23] Antonio Clemente, Melusine Pigeon, Lionel Rudant, and Christophe Delaveaud. Design of a super directive four-element compact antenna array using spherical wave expansion. *IEEE Transactions on Antennas and Propagation*, 63(11):4715–4722, 2015.

[24] Luiz F. da S Coelho, Marcele OK Mendonça, Paulo SR Diniz, and Fernando Cruz-Roldán. Optimal window design for intercarrier and intersymbol interference power minimization in w-ofdm. *IEEE Wireless Communications Letters*, 2023.

[25] Thomas Cover. Broadcast channels. *IEEE Transactions on Information Theory*, 18(1):2–14, 1972.

[26] Özlem Tugfe Demir, Emil Björnson, Luca Sanguinetti, et al. Foundations of user-centric cell-free massive MIMO. *Foundations and Trends® in Signal Processing*, 14(3-4):162–472, 2021.

[27] David Demmer, Robin Gerzaguet, Jean-Baptiste Doré, Didier Le Ruyet, and Dimitri Kténas. Block-filtered ofdm: A novel waveform for future wireless technologies. In *2017 IEEE International Conference on Communications (ICC)*, pages 1–6. IEEE, 2017.

[28] Marco Di Renzo, Alessio Zappone, Merouane Debbah, Mohamed-Slim Alouini, Chau Yuen, Julien de Rosny, and Sergei Tretyakov. Smart radio environments empowered by reconfigurable intelligent surfaces: How it works, state of research, and the road ahead. *IEEE Journal on Selected Areas in Communications*, 38(11):2450–2525, 2020.

[29] Ming Ding, Peng Wang, David López-Pérez, Guoqiang Mao, and Zihuai Lin. Performance impact of los and nlos transmissions in dense cellular networks. *IEEE Transactions on Wireless Communications*, 15(3):2365–2380, 2016.

[30] Zhiguo Ding, Fumiyuki Adachi, and H. Vincent Poor. Performance of MIMO-NOMA downlink transmissions. In *2015 IEEE Global Communications Conference (GLOBECOM)*, pages 1–6, 2015.

[31] Zhiguo Ding, Robert Schober, Pingzhi Fan, and H. Vincent Poor. Simple semi-grant-free transmission strategies assisted by non-orthogonal multiple access. *IEEE Transactions on Communications*, 67(6):4464–4478, 2019.

[32] Zhiguo Ding, Zheng Yang, Pingzhi Fan, and H. Vincent Poor. On the performance of non-orthogonal multiple access in 5G systems with randomly deployed users. *IEEE Signal Processing Letters*, 21(12):1501–1505, 2014.

[33] Zhiguo Ding, Zheng Yang, Pingzhi Fan, and H. Vincent Poor. On the performance of non-orthogonal multiple access in 5G systems with randomly deployed users. *IEEE Signal Process. Lett.*, 21(12):1501–1505, Dec. 2014.

[34] Michelle M. Do and J. Son Harrison. CoMP (1): CoMP Types- CS, CB, JT and DPS. www.netmanias.com/en/post/blog/6558/comp-lte-lte-a/comp- 1-comp-types-cs-cb-jt-and-dps, 2014.

[35] Charles Dumas, Lou Salaün, Iman Hmedoush, Cédric Adjih, and Chung Shue Chen. Design of coded slotted aloha with interference cancellation errors. *IEEE Transactions on Vehicular Technology*, 70(12):12742–12757, 2021.

[36] Joumana Farah, Eric Pierre Simon, Pierre Laly, and Gauthier Delbarre. Efficient combinations of NOMA with distributed antenna systems based on channel measurements for mitigating jamming attacks. *IEEE Systems Journal*, 15(2):2212–2221, 2021.

[37] Nusrat Fatema, Guang Hua, Yong Xiang, Dezhong Peng, and Iynkaran Natgunanathan. Massive MIMO linear precoding: A survey. *IEEE Systems Journal*, 12(4):3920–3931, 2018.

[38] Jose Flordelis, Fredrik Rusek, Xiang Gao, Ghassan Dahman, Ove Edfors, and Fredrik Tufvesson. Spatial separation of closely-located users in measured massive MIMO channels. *IEEE Access*, 6:40253–40266, 2018.

[39] Robert Kuku Fotock, Alessio Zappone, and Marco Di Renzo. Energy efficiency optimization in RIS-aided wireless networks: Active versus nearly-passive RIS with global reflection constraints. *IEEE Transactions on Communications*, 72(1):257–272, 2024.

[40] Iandra Galdino, Didier Le Ruyet, Marcello L. R. de Campos, and Rostom Zakaria. Per coefficient filter optimization for rectangular and quincunx qam-fbmc. *submitted to IEEE Access*, 2024.

[41] Seyyed Ali Hassani Gangaraj and Francesco Monticone. Molding light with metasurfaces: from far-field to near-field interactions. *Nanophotonics*, 7(6):1025–1040, 2018.

[42] Andres Garcia-Saavedra and Xavier Costa-Perez. O-RAN: Disrupting the virtualized RAN ecosystem. *IEEE Communications Standards Magazine*, 5(4):96–103, 2021.

[43] E. N. Gilbert and S. P. Morgan. Optimum design of directive antenna arrays subject to random variations. *The Bell System Technical Journal*, 34(3):637–663, 1955.

[44] Rafael Gonçalves Licursi de Mello. *Active and passive metasurfaces : methodology for the design of a low profile, beam-steerable, multiband, and wideband antenna*. Theses, Institut polytechnique de Paris, June 2022. Le texte intégral de cette thèse sera accessible librement à partir du 22-09-2024.

[45] Rafael Gonçalves Licursi de Mello, Anne Claire Lepage, and Xavier Begaud. Taming Fabry–Pérot resonances in a dual-metasurface multiband antenna with beam steering in one of the bands. *Scientific Reports*, 13(1):9871, June 2023.

[46] Shimin Gong, Xiao Lu, Dinh Thai Hoang, Dusit Niyato, Lei Shu, Dong In Kim, and Ying-Chang Liang. Toward smart wireless communications via intelligent reflecting surfaces: A contemporary survey. *IEEE Communications Surveys & Tutorials*, 22(4):2283–2314, 2020.

[47] Lov K. Grover. A fast quantum mechanical algorithm for database search, November 1996. arXiv:quant-ph/9605043.

[48] Muhammad Idham Habibie, Jihad Hamie, and Claire Goursaud. A Performance Comparison of Classical and Quantum Algorithm for Active User Detection. In *SPAWC 2022 - The 23rd IEEE International Workshop on Signal Processing Advances in Wireless Communications*, Oulu, Finland, July 2022.

[49] Ronny Hadani, hlomo Rakib, Michail Tsatsanis, Anton Monk, Andrea J. Goldsmith, Andreas F. Molisch, and Robert Calderbank. Orthogonal time frequency space modulation. In *2017 IEEE Wireless Communications and Networking Conference (WCNC)*, pages 1–6, 2017.

[50] Roger Harrington. On the gain and beamwidth of directional antennas. *IRE Transactions on Antennas and Propagation*, 6(3):219–225, 1958.

[51] Abdullah Haskou, Ala Sharaiha, and Sylvain Collardey. Design of small parasitic loaded superdirective endfire antenna arrays. *IEEE Transactions on Antennas and Propagation*, 63(12):5456–5464, 2015.

[52] Hajar El Hassani, Xuewen Qian, Sumin Jeong, Nemanja S. Perović, Marco Di Renzo, Placido Mursia, Vincenzo Sciancalepore, and Xavier Costa-Pérez. Optimization of RIS-Aided MIMO – a mutually coupled loaded wire dipole model. *IEEE Wireless Communications Letters*, pages 1–1, 2023.

[53] Hirosaki, B. An Orthogonally Multiplexed QAM System Using the Discrete Fourier Transform. *IEEE Transactions on Communications*, 29(7):982–989, 1981.

[54] Iman Hmedoush, Pengwenlong Gu, Cédric Adjih, Paul Mühlethaler, and Ahmed Serhrouchni. DS-IRSA: A deep reinforcement learning and sensing based IRSA. In *GLOBECOM 2023 - IEEE Global Communications Conference*, Kuala Lumpur, Malaysia, December 2023.

[55] Shaocheng Huang, Yu Ye, Ming Xiao, H Vincent Poor, and Mikael Skoglund. Decentralized beamforming design for intelligent reflecting surface-enhanced cell-free networks. *IEEE Wireless Communications Letters*, 10(3):673–677, 2020.

[56] Taewon Hwang, Chenyang Yang, Gang Wu, Shaoqian Li, and Geoffrey Ye Li. OFDM and Its Wireless Applications: A Survey. *IEEE Transactions on Vehicular Technology*, 58(4):1673–1694, 2009.

[57] Giovanni Interdonato, Emil Björnson, Hien Quoc Ngo, Pål Frenger, and Erik G Larsson. Ubiquitous cell-free massive MIMO communications. *EURASIP Journal on Wireless Communications and Networking*, 2019(1):1–13, 2019.

[58] Giovanni Interdonato, Emil Björnson, Hien Quoc Ngo, Pål Frenger, and Erik G. Larsson. Ubiquitous cell-free massive MIMO communications. *EURASIP Journal on Wireless Communications and Networking*, 2019(1), August 2019.

[59] Giovanni Interdonato, Marcus Karlsson, Emil Bjornson, and Erik G. Larsson. Downlink spectral efficiency of cell-free massive MIMO with full-pilot zero-forcing. In *2018 IEEE Global Conference on Signal and Information Processing (GlobalSIP)*, 2018.

[60] Giovanni Interdonato, Marcus Karlsson, Emil Björnson, and Erik G Larsson. Local partial zero-forcing precoding for cell-free massive MIMO. *IEEE Transactions on Wireless Communications*, 19(7):4758–4774, 2020.

[61] Giovanni Interdonato, Marcus Karlsson, Emil Björnson, and Erik G. Larsson. Local partial zero-forcing precoding for cell-free massive MIMO. *IEEE Transactions on Wireless Communications*, 19(7):4758–4774, 2020.

[62] S. M. Riazul Islam, Nurilla Avazov, Octavia A. Dobre, and Kyung-sup Kwak. Power-domain non-orthogonal multiple access (NOMA) in 5G systems: Potentials and challenges. *IEEE Communications Surveys & Tutorials*, 19(2):721–742, 2017.

[63] Hussein Jaafar, Sylvain Collardey, and Ala Sharaiha. Characteristic modes approach to design compact superdirective array with enhanced bandwidth. *IEEE Transactions on Antennas and Propagation*, 66(12):6986–6996, 2018.

[64] Sumin Jeong, Arman Farhang, Nemanja Stefan Perović, and Mark F. Flanagan. Low-complexity joint cfo and channel estimation for ris-aided ofdm systems. *IEEE Wireless Communications Letters*, 11(1):203–207, 2022.

[65] Sumin Jeong, Arman Farhang, Nemanja Stefan Perović, and Mark F. Flanagan. Joint CFO and channel estimation for RIS-aided multi-user massive MIMO systems. *IEEE Transactions on Vehicular Technology*, 72(9):11800–11813, 2023.

[66] Hui Jiang, Qimei Cui, Yu Gu, Xiaoqi Qin, Xuefei Zhang, and Xiaofeng Tao. Distributed layered grant-free non-orthogonal multiple access for massive mtc. In *2018 IEEE 29th Annual International Symposium on Personal, Indoor and Mobile Radio Communications (PIMRC)*, pages 1–7, 2018.

[67] Wei Jiang and Hans Dieter Schotten. Cell-free massive MIMO-OFDM transmission over frequency-selective fading channels. *IEEE Communications Letters*, 25(8):2718–2722, 2021.

[68] Rogério Pereira Junior, Carlos Aurélio Faria Da Rocha, Bruno S. Chang, and Didier Le Ruyet. A generalized two-dimensional fft precoded filter bank scheme with low complexity equalizers in time-frequency domain. *IEEE Access*, 11:112414–112428, 2023.

[69] Rogério Pereira Junior, Carlos Aurélio Faria da Rocha, Bruno S. Chang, and Didier Le Ruyet. A two-dimensional fft precoded filter bank scheme. *IEEE Transactions on Wireless Communications*, 22(11):8366–8377, 2023.

[70] Beomju Kim, Sungmook Lim, Hyungjong Kim, Sangwook Suh, Jonghyung Kwun, Sooyong Choi, Chungyong Lee, Sanghoon Lee, and Daesik Hong. Non-orthogonal multiple access in a downlink multiuser beamforming system. In *Military Communications Conference, MILCOM*, pages 1278–1283. IEEE, 2013.

[71] Joon-Hong Kim and Sangwook Nam. A compact quasi-isotropic antenna based on folded split-ring resonators. *IEEE Antennas and Wireless Propagation Letters*, 16:294–297, 2017.

[72] Akshit Kumar, Parikshit Hegde, Rahul Vaze, Amira Alloum, and Cédric Adjih. Breaking the unit throughput barrier in random access protocol based distributed systems. In *2023 National Conference on Communications (NCC)*, pages 1–6. IEEE, 2023.

[73] Pierre Laly, Davy Gaillot, Martine Lienard, Pierre Degauque, Emmeric Tanghe, Wout Joseph, and Luc Martens. Flexible real-time MIMO channel sounder for multidimensional polarimetric parameter estimation. In *2015 IEEE Conference on Antenna Measurements & Applications, CAMA 2015*, Proceedings of 2015 IEEE Conference on Antenna Measurements & Applications, CAMA 2015, Chiang Mai, Thailand, November 2015.

[74] Mai T. P. Le, Luca Sanguinetti, Emil Björnson, and Maria-Gabriella Di Benedetto. Code-domain noma in massive mimo: When is it needed? *IEEE Transactions on Vehicular Technology*, 70(5):4709–4723, 2021.

[75] Xiaohua Li and Juite Hwu. A frequency hopping spread spectrum transmission scheme for uncoordinated cognitive radios. In *2009 IEEE International Conference on Acoustics, Speech and Signal Processing*, pages 2345–2348, 2009.

[76] Yiqing Li, Miao Jiang, Qi Zhang, and Jiayin Qin. Joint beamforming design in multi-cluster MISO NOMA reconfigurable intelligent surface-aided downlink communication networks. *IEEE Transactions on Communications*, 69(1):664–674, 2020.

[77] Wei Liang, Zhiguo Ding, Yonghui Li, and Lingyang Song. User pairing for downlink non-orthogonal multiple access networks using matching algorithm. *IEEE Transactions on Communications*, 65(12):5319–5332, 2017.

[78] Fei Liu, Petri Mähönen, and Marina Petrova. Proportional fairness-based power allocation and user set selection for downlink noma systems. In *2016 IEEE International Conference on Communications (ICC)*, pages 1–6, 2016.

[79] Keqin Liu and Qing Zhao. Distributed learning in multi-armed bandit with multiple players. *IEEE Transactions on Signal Processing*, 58(11):5667–5681, 2010.

[80] Yang Liu, Gaofeng Pan, Hongtao Zhang, and Mei Song. On the capacity comparison between MIMO-NOMA and MIMO-OMA. *IEEE Access*, 4:2123–2129, 2016.

[81] Yuanwei Liu, Xiao Liu, Xidong Mu, Tianwei Hou, Jiaqi Xu, Marco Di Renzo, and Naofal Al-Dhahir. Reconfigurable intelligent surfaces: Principles and opportunities. *IEEE Communications Surveys & Tutorials*, 23(3):1546–1577, 2021.

[82] Yuanwei Liu, Zhijin Qin, Maged Elkashlan, Zhiguo Ding, Arumugam Nallanathan, and Lajos Hanzo. Non-orthogonal multiple access for 5G and beyond. *Proceedings of the IEEE*, 105(12):2347–2381, 2017.

[83] Zehao Liu, Fang Yang, Shiyuan Sun, Jian Song, and Zhu Han. Sum rate maximization for NOMA-based VLC with optical intelligent reflecting surface. *IEEE Wireless Communications Letters*, 12(5):848–852, 2023.

[84] Gianluigi Liva. Graph-Based Analysis and Optimization of Contention Resolution Diversity Slotted ALOHA. *IEEE Transactions on Communications*, 59(2):477–487, 2011.

[85] Asma Mabrouk and Rafik Zayani. Energy-efficient uplink cell-free massive MIMO through distributed cancellation technique of HWIs. In *2023 IEEE Virtual Conference on Communications (VCC)*, 2023.

[86] Asma Mabrouk and Rafik Zayani. Toward energy-efficient 6G networks: Uplink cell-free massive MIMO with NLD cancellation technique of hardware impairments. *IEEE Access*, 11:105314–105329, 2023.

[87] Robert Margolies, Ashwin Sridharan, Vaneet Aggarwal, Rittwik Jana, N. K. Shankaranarayanan, Vinay A. Vaishampayan, and Gil Zussman. Exploiting mobility in proportional fair cellular scheduling: Measurements and algorithms. *IEEE/ACM Transactions on Networking*, 24(1):355–367, 2016.

[88] James Massey and Peter Mathys. The collision channel without feedback. *IEEE Transactions on Information Theory*, 31(2):192–204, 1985.

[89] Asim Mazin, Mohamed Elkourdi, and Richard D. Gitlin. Comparison of slotted aloha-noma and csma/ca for m2m communications in iot networks. In *2018 IEEE 88th Vehicular Technology Conference (VTC-Fall)*, pages 1–5, 2018.

[90] Placido Mursia, Sendy Phang, Vincenzo Sciancalepore, Gabriele Gradoni, and Marco Di Renzo. Saris: Scattering aware reconfigurable intelligent surface model and optimization for complex propagation channels. *IEEE Wireless Communications Letters*, 12(11):1921–1925, 2023.

[91] Krishna R. Narayanan and Henry D. Pfister. Iterative collision resolution for slotted ALOHA: An optimal uncoordinated transmission policy. In *Turbo Codes and Iterative Information Processing (ISTC), 7th International Symposium on*, 2012.

[92] Hien Q. Ngo, Alexei Ashikhmin, Hong Yang, Erik G. Larsson, and Thomas L. Marzetta. Cell-free massive MIMO versus small cells. *IEEE Transactions on Wireless Communications*, 16(3):1834–1850, 2017.

[93] Thi Thuy Nga Nguyen, Olivier Brun, and Balakrishna J. Prabhu. Using channel predictions for improved proportional-fair utility for vehicular users. *Computer Networks*, 208:108872, 2022.

[94] Ronald Nissel and Markus Rupp. Pruned DFT-spread FBMC: low PAPR, low latency, high spectral efficiency. *IEEE Transactions on Communications*, 66(10):4811–4825, 2018.

[95] José Armando Oviedo and Hamid R. Sadjadpour. Fundamentals of power allocation strategies for downlink multi-user noma with target rates. *IEEE Transactions on Wireless Communications*, 19(3):1906–1917, 2020.

[96] Cunhua Pan, Gui Zhou, Kangda Zhi, Sheng Hong, Tuo Wu, Yijin Pan, Hong Ren, Marco Di Renzo, A. Lee Swindlehurst, Rui Zhang, and Angela Yingjun Zhang. An overview of signal processing techniques for RIS/IRS-aided wireless systems. *IEEE Journal of Selected Topics in Signal Processing*, 16(5):883–917, 2022.

[97] Enrico Paolini, Cedomir Stefanovic, Gianluigi Liva, and Petar Popovski. Coded Random Access: Applying Codes on Graphs to Design Random Access Protocols. *IEEE Communications Magazine*, 53(6):144–150, 2015.

[98] Emmanouil Pateromichelakis, Mehrdad Shariat, Atta ul Quddus, and Rahim Tafazolli. On the evolution of multi-cell scheduling in 3gpp lte / lte-a. *IEEE Communications Surveys and Tutorials*, 15(2):701–717, 2013.

[99] Zhangjie Peng, Zhibo Zhang, Cunhua Pan, Marco Di Renzo, Octavia A. Dobre, and Jiangzhou Wang. Beamforming optimization for active ris-aided multiuser communications with hardware impairments. *IEEE Transactions on Wireless Communications*, pages 1–1, 2024.

[100] Rogério Pereira, Carlos AF da Rocha, Bruno S Chang, and Didier Le Ruyet. A novel DFT precoded filter bank system with iterative equalization. *IEEE Wireless Communications Letters*, 2020.

[101] Ammar Rafique, Naveed Ul Hassan, Muhammad Zubair, Ijaz Haider Naqvi, Muhammad Qasim Mehmood, Marco Di Renzo, Mérouane Debbah, and Chau Yuen. Reconfigurable intelligent surfaces: Interplay of unit cell and surface-level design and performance under quantifiable benchmarks. *IEEE Open Journal of the Communications Society*, 4:1583–1599, 2023.

[102] Vida Ranjbar, Adam Girycki, Md Arifur Rahman, Sofie Pollin, Marc Moonen, and Evgenii Vinogradov. Cell-free mMIMO support in the O-RAN architecture: A PHY layer perspective for 5G and beyond networks. *IEEE Communications Standards Magazine*, 6:28–34, 2022.

[103] Yuya Saito, Anass Benjebbour, Yoshihisa Kishiyama, and Takehiro Nakamura. System-level performance evaluation of downlink non-orthogonal multiple access (noma). In *2013 IEEE 24th Annual International Symposium on Personal, Indoor, and Mobile Radio Communications (PIMRC)*, pages 611–615, 2013.

[104] B. Saltzberg. Performance of an Efficient Parallel Data Transmission System. *IEEE Transactions on Communication Technology*, 15(6):805–811, 1967.

[105] Frank Schaich, Berna Sayrac, Salaheddine Elayoubi, Ioannis-Prodromos Belikaidis, Marco Caretti, Andreas Georgakopoulos, Xitao Gong, Evangelos Kosmatos, Hao Lin, Panagiotis Demestichas, Belkacem Mouhouche, Klaus Pedersen, Nuno Pratas, Malte Schellmann, Martin Schubert, Musbah Shaat, and Gerhard Wunder. FANTASTIC-5G: Flexible air interface for scalable service delivery within wireless communication networks of the 5th generation. *Transactions on Emerging Telecommunications Technologies*, 27(9):1216–1224, 2016.

[106] Philipp Schulz, Maximilian Matthe, Henrik Klessig, Meryem Simsek, Gerhard Fettweis, Junaid Ansari, Shehzad Ali Ashraf, Bjoern Almeroth, Jens Voigt, Ines Riedel, Andre Puschmann, Andreas Mitschele-Thiel, Michael Muller, Thomas Elste, and Marcus Windisch. Latency critical IoT applications in 5G: Perspective on the design of radio interface and network architecture. *IEEE Communications Magazine*, 55(2):70–78, February 2017.

[107] Muhammad Basit Shahab, Rana Abbas, Mahyar Shirvanimoghaddam, and Sarah J. Johnson. Grant-free non-orthogonal multiple access for iot: A survey. *IEEE Communications Surveys & Tutorials*, 22(3):1805–1838, 2020.

[108] Ting Shi, Ming-Chun Tang, Ruolei Chai, and Richard W. Ziolkowski. Multipole-based electrically small unidirectional antenna with exceptionally high realized gain. *IEEE Transactions on Antennas and Propagation*, 70(7):5288–5301, 2022.

[109] Mahyar Shirvanimoghaddam, Mischa Dohler, and Sarah Johnson. Massive Non-Orthogonal Multiple Access for Cellular IoT: Potentials and Limitations. *IEEE Communications Magazine*, 55(9):55–61, 2017. arXiv:1612.00552 [cs, math].

[110] Eric Pierre Simon, Joumana Farah, and Pierre Laly. Performance evaluation of massive MIMO with beamforming and non-orthogonal multiple access based on practical channel measurements. *IEEE Antennas and Wireless Propagation Letters*, 18(6):1263–1267, 2019.

[111] Eric Pierre Simon, Joumana Farah, and Pierre Laly. Resource allocation and pairing techniques in multiuser massive MIMO-NOMA. *IEEE Systems Journal*, 17(4):6312–6321, 2023.

[112] Eric Pierre Simon, Joumana Farah, Pierre Laly, and Gauthier Delbarre. A gradual resource allocation technique for massive MIMO-NOMA. *IEEE Antennas and Wireless Propagation Letters*, 21(3):476–480, 2021.

[113] Eric Pierre Simon, Pierre Laly, Joumana Farah, Emmeric Tanghe, Wout Joseph, and Davy Paul Gaillot. Measurement of the V2I channel in cell-free vehicular networks with the distributed MaMIMOSA channel sounder. In *2023 17th European Conference on Antennas and Propagation (EuCAP)*, pages 1–5, 2023.

[114] Chirag Ramesh Srivatsa and Chandra R. Murthy. Throughput analysis of PDMA/IRSA under practical channel estimation. In *2019 IEEE 20th International Workshop on Signal Processing Advances in Wireless Communications (SPAWC)*, pages 1–5. IEEE, 2019.

[115] Čedomir Stefanović, Miyu Momoda, and Petar Popovski. Exploiting capture effect in frameless aloha for massive wireless random access. In *2014 IEEE Wireless Communications and Networking Conference (WCNC)*, pages 1762–1767. IEEE, 2014.

[116] A. Lee Swindlehurst, Gui Zhou, Rang Liu, Cunhua Pan, and Ming Li. Channel estimation with reconfigurable intelligent surfaces—a general framework. *Proceedings of the IEEE*, 110(9):1312–1338, 2022.

[117] Alessio Tornese, Antonio Clemente, and Christophe Delaveaud. A new method for gain prediction of superdirective end-fire arrays. In *2022 16th European Conference on Antennas and Propagation (EuCAP)*, pages 1–4, 2022.

[118] Abdellah Touhami, Sylvain Collardey, and Ala Sharaiha. A multi-objective optimisation for compact wideband and efficient superdirective antenna arrays design using network characteristic modes. *IET Microwaves, Antennas & Propagation*, 17(3):223–236, 2023.

[119] Abdellah Touhami, Ala Sharaiha, and Sylvain Collardey. Artificial neural network synthesis based approach for superdirective antenna arrays design. In *2021 XXXIVth General Assembly and Scientific Symposium of the International Union of Radio Science (URSI GASS)*, pages 1–4, 2021.

[120] Trinh Van Chien, Lam-Thanh Tu, Waqas Khalid, Heejung Yu, Symeon Chatzinotas, and Marco Di Renzo. Ris-assisted wireless communications: Long-term versus short-term phase shift designs. *IEEE Transactions on Communications*, 72(2):1175–1190, 2024.

[121] Chin-Liang Wang, Cheng-Chun Hsieh, Yu-Cheng Ding, and Shih-Hsuan Huang. Power allocation for downlink noma systems with imperfect channel estimation. In *2021 IEEE Wireless Communications and Networking Conference (WCNC)*, pages 1–7, 2021.

[122] Tiejun Wang, J.G. Proakis, E. Masry, and J.R. Zeidler. Performance degradation of OFDM systems due to Doppler spreading. *IEEE Transactions on Wireless Communications*, 5(6):1422–1432, 2006.

[123] Chenyu Wu, Changsheng You, Yuanwei Liu, Shuai Han, and Marco Di Renzo. Two-timescale design for star-ris-aided noma systems. *IEEE Transactions on Communications*, 72(1):585–600, 2024.

[124] Jun Wu, Zhifeng Zhang, Yu Hong, and Yonggang Wen. Cloud radio access network (c-ran): a primer. *IEEE Network*, 29(1):35–41, 2015.

[125] Chiyang Xiao, Jie Zeng, Wei Ni, Xin Su, Ren Ping Liu, Tiejun Lv, and Jing Wang. Downlink MIMO-NOMA for ultra-reliable low-latency communications. *IEEE Journal on Selected Areas in Communications*, 37(4):780–794, 2019.

[126] Zheng Yang, Zhiguo Ding, Pingzhi Fan, and Naofal Al-Dhahir. A general power allocation scheme to guarantee quality of service in downlink and uplink noma systems. *IEEE Transactions on Wireless Communications*, 15(11):7244–7257, 2016.

[127] Xianghao Yao, Jiancheng An, Lu Gan, Marco Di Renzo, and Chau Yuen. Channel estimation for stacked intelligent metasurface-assisted wireless networks. *IEEE Wireless Communications Letters*, pages 1–1, 2024.

[128] Wenjing Ye, Wei Chen, Xin Guo, Chen Sun, and Lajos Hanzo. Quantum Search-Aided Multi-User Detection for Sparse Code Multiple Access. *IEEE Access*, 7:52804–52817, 2019.

[129] Liang Yin, Wasiu O. Popoola, Xiping Wu, and Harald Haas. Performance evaluation of non-orthogonal multiple access in visible light communication. *IEEE Transactions on Communications*, 64(12):5162–5175, 2016.

[130] Marie-Josepha Youssef, Joumana Farah, Charbel Abdel Nour, and Catherine Douillard. Full-duplex and backhaul-constrained UAV-enabled networks using NOMA. *IEEE Transactions on Vehicular Technology*, 69(9):9667–9681, 2020.

[131] Marie-Josepha Youssef, Joumana Farah, Charbel Abdel Nour, and Catherine Douillard. Full-duplex and backhaul-constrained uav-enabled networks using noma. *IEEE Transactions on Vehicular Technology*, 69(9):9667–9681, 2020.

[132] Marie-Josepha Youssef, Charbel Abdel Nour, Joumana Farah, and Catherine Douillard. Backhaul-constrained resource allocation and 3d placement for uav-enabled networks. In *2019 IEEE 90th Vehicular Technology Conference (VTC2019-Fall)*, pages 1–7, 2019.

[133] Marie-Josepha Youssef, Venugopal V. Veeravalli, Joumana Farah, and Charbel Abdel Nour. Stochastic multi-player multi-armed bandits with multiple plays for uncoordinated spectrum access. In *2020 IEEE 31st Annual International Symposium on Personal, Indoor and Mobile Radio Communications*, pages 1–7, 2020.

[134] Weijie Yuan, Zhiqiang Wei, Shuangyang Li, Jinhong Yuan, and Derrick Wing Kwan Ng. Integrated sensing and communication-assisted orthogonal time frequency space transmission for vehicular networks. *IEEE Journal of Selected Topics in Signal Processing*, 15(6):1515–1528, 2021.

[135] Yifei Yuan, Zhifeng Yuan, and Li Tian. 5G non-orthogonal multiple access study in 3GPP. *IEEE Communications Magazine*, 58(7):90–96, 2020.

[136] Marwan Yusuf, Emmeric Tanghe, Frédéric Challita, Pierre Laly, Davy P. Gaillot, Martine Liénard, Luc Martens, and Wout Joseph. Stationarity analysis of v2i radio channel in a suburban environment. *IEEE Transactions on Vehicular Technology*, 68(12):11532–11542, 2019.

[137] Rostom Zakaria and Didier Le Ruyet. A novel filter-bank multicarrier scheme to mitigate the intrinsic interference: Application to MIMO systems. *IEEE Transactions on Wireless Communications*, 11(3):1112–1123, 2012.

[138] Rafik Zayani, Jean-Baptiste Doré, Benoit Miscopein, and David Demmer. Local PAPR-aware precoding for energy-efficient cell-free massive MIMO-OFDM systems. *IEEE Transactions on Green Communications and Networking*, 7(3):1267–1284, 2023.

[139] Rafik Zayani and Daniel Roviras. Low-complexity linear precoding for low-PAPR massive MU-MIMO-OFDM downlink systems. *International Journal of Communication Systems*, 34(12):e4889, 2021.

[140] Rafik Zayani, Hmaied Shaiek, and Daniel Roviras. PAPR-aware massive MIMO-OFDM downlink. *IEEE Access*, 7:25474–25484, 2019.

[141] Ming Zeng, Animesh Yadav, Octavia A. Dobre, Georgios I. Tsiropoulos, and H. Vincent Poor. On the sum rate of MIMO-NOMA and MIMO-OMA systems. *IEEE Wireless Communications Letters*, 6(4):534–537, 2017.

[142] Wenbo Zeng, Yigang He, Bing Li, and Shudong Wang. Pilot assignment for cell free massive MIMO systems using a weighted graphic framework. *IEEE Transactions on Vehicular Technology*, 70(6):6190–6194, 2021.

[143] Jiayi Zhang, Emil Björnson, Michail Matthaiou, Derrick Wing Kwan Ng, Hong Yang, and David J Love. Prospective multiple antenna technologies for beyond 5G. *IEEE Journal on Selected Areas in Communications*, 38(8):1637–1660, 2020.

[144] Jiayi Zhang, Jing Zhang, Emil Björnson, and Bo Ai. Local partial zero-forcing combining for cell-free massive MIMO systems. *IEEE Transactions on Communications*, 69(12):8459–8473, 2021.

[145] Ningbo Zhang, Jing Wang, Guixia Kang, and Yang Liu. Uplink nonorthogonal multiple access in 5G systems. *IEEE Communications Letters*, 20(3):458–461, 2016.

[146] Yanbo Zhang, Zheng Yang, Jingjing Cui, Peng Xu, Gaojie Chen, Yi Wu, and Marco Di Renzo. STAR-RIS assisted secure transmission for downlink multi-carrier NOMA networks. *IEEE Transactions on Information Forensics and Security*, 18:5788–5803, 2023.

[147] Datong P. Zhou and Claire J. Tomlin. Budget-constrained multi-armed bandits with multiple plays, 2017.

[148] Shaoqing Zhou, Wei Xu, Kezhi Wang, Marco Di Renzo, and Mohamed-Slim Alouini. Spectral and energy efficiency of IRS-assisted MISO communication with hardware impairments. *IEEE Wireless Communications Letters*, 9(9):1366–1369, 2020.

[149] Özlem T. Demir, Meysam Masoudi, Emil Björnson, and Cicek Cavdar. Cell-free massive MIMO in O-RAN: Energy-aware joint orchestration of cloud, fronthaul, and radio resources. *arXiv preprint arXiv:2301.06166*, 2023.

[150] Serdar Özyurt, Eric Pierre Simon, and Joumana Farah. NOMA with zero-forcing V-BLAST. *IEEE Communications Letters*, 24(9):2070–2074, 2020.